Copy No. _____

Defence Research and Development Canada
Recherche et développement pour la défense Canada

DEFENCE R&D DÉFENSE

Structural Analysis and Design of Pressure Hulls: the State of the Art and Future Trends

John R. MacKay

Defence R&D Canada – Atlantic

Technical Memorandum
DRDC Atlantic TM 2007-188
October 2007

Canada

This page intentionally left blank.

Structural Analysis and Design of Pressure Hulls: the State of the Art and Future Trends

John R. MacKay

Defence R&D Canada – Atlantic

Technical Memorandum
DRDC Atlantic TM 2007-188
October 2007

Principal Author

Original signed by John R. MacKay

John R. MacKay

Approved by

Original signed by Neil G. Pegg

Neil G. Pegg

Head, Warship Performance

Approved for release by

Original signed by James L. Kennedy

James L. Kennedy

DRP Chair

© Her Majesty the Queen in Right of Canada, as represented by the Minister of National Defence, 2007

© Sa Majesté la Reine (en droit du Canada), telle que représentée par le ministre de la Défense nationale, 2007

Abstract

Pressure hulls are the main load bearing structures of naval submarines, commercial and research submersibles, and autonomous underwater vehicles (AUVs). The many similarities between pressure hull, offshore, aerospace and some civil engineering structures mean that advances in one group are often applicable to the others, and thus this document is sometimes concerned with the entire collection of thin-walled curved structures designed for instability, referred to hereafter as "buckling-critical shells." The state-of-the-art of pressure hull structural analysis and design is established in this document by: 1) explaining the nature of structural strength, and associated weaknesses, in pressure hulls; 2) summarizing traditional and contemporary structural analysis and design methods for pressure hulls; 3) identifying trends with respect to numerical modeling of buckling-critical shell structures; and 4) reviewing novel design procedures for buckling-critical shell structures. It is suggested that the layered conservatism of the traditional design approach could be improved by the use of nonlinear numerical methods for strength predictions, and a way forward is suggested that would allow pressure hull design procedures to incorporate these methods.

Résumé

Les coques épaisses sont les structures portantes principales des sous-marins de la force navale, des submersibles commerciaux et scientifiques, et des engins sous-marins autonomes (AUV). Les nombreuses similitudes que présentent les coques épaisses, les plates-formes offshore, les constructions aérospatiales et certains ouvrages de génie civil font que les progrès réalisés pour les uns sont souvent applicables aux autres, et c'est ainsi que le présent document peut parfois viser l'ensemble total des structures courbes à paroi mince calculées pour des conditions d'instabilité, ci-après dénommées globalement « coques critiques en flambage ». Le présent document présente l'état de la technique en matière d'analyse de structure et de conception des coques épaisses : 1) en expliquant la nature de la résistance de structure, et les faiblesses sur ce plan, des coques épaisses; 2) en résumant les méthodes traditionnelles et contemporaines d'analyse de structure et de calcul utilisées pour les coques épaisses; 3) en identifiant les tendances en faveur de la modélisation numérique des structures de coques critiques en flambage; et 4) en examinant les méthodes novatrices de calcul pour les structures de coques critiques en flambage. L'auteur avance l'idée que le conservatisme existant à plusieurs niveaux dans l'approche de calcul traditionnelle pourrait être amélioré par l'emploi de méthodes numériques non linéaires pour les prédictions de résistance, et qu'il y aurait avantage à incorporer ces méthodes dans les méthodes de calcul des coques épaisses.

This page intentionally left blank.

Executive summary

Structural Analysis and Design of Pressure Hulls: the State of the Art and Future Trends:

MacKay, J.R.; DRDC Atlantic TM 2007-188; Defence R&D Canada – Atlantic; October 2007.

Background: Pressure hulls are the main load bearing structures of naval submarines, commercial and research submersibles, and autonomous underwater vehicles (AUVs). The many similarities between pressure hull, offshore, aerospace and some civil engineering structures mean that advances in one group are often applicable to the others, and thus this document is sometimes concerned with the entire collection of thin-walled curved structures designed for instability, referred to hereafter as "buckling-critical shells."

Results: The state-of-the-art of pressure hull structural analysis and design is established in this document by: 1) explaining the nature of structural strength, and associated weaknesses, in pressure hulls; 2) summarizing traditional and contemporary structural analysis and design methods for pressure hulls; 3) identifying trends with respect to numerical modeling of buckling-critical shell structures; and 4) reviewing novel design procedures for buckling-critical shell structures. It is suggested that the layered conservatism of the traditional design approach could be improved by the use of nonlinear numerical methods for strength predictions, and a way forward is suggested that would allow pressure hull design procedures to incorporate these methods.

Significance: The numerical methods – i.e. nonlinear finite element analysis – allow pressure hull strength calculations to be based on the elasto-plastic limit state with full geometric complexity, and can also include the effects of fabrication-induced residual stresses and in-service damage. Incorporation of the numerical methods in the design procedure would result in more efficient and reliable structures, both at the design stage and through-life, and allow for innovation in structural configurations and materials. For in-service naval submarines, this could translate to a greater operational envelope (i.e. deep diving depth) than that achieved by using the traditional design methods, especially when considering the degrading effects of structural damage.

Future plans: The incorporation of nonlinear numerical methods in pressure hull design procedures will require the establishment of modeling and analysis guidelines, the population of a database of experimental results, and the determination of the modeling error and uncertainty associated with the numerical modeling through a structured program of analysis. Additional research is required to address fabrication-induced residual stresses, appropriate inelastic material models, the treatment of shell eccentricities and the prescription of characteristic design imperfections. This work is being undertaken by DRDC Atlantic, in cooperation with the Netherlands Ministry of Defence and Delft University of Technology. This paper, in conjunction with an ongoing Netherlands-Canada collaborative pressure hull experimental collapse program, represents the first stage of this task, with modeling guidelines, an experimental database and numerical modeling to follow in the coming months and years.

Sommaire

Analyse de structure et calcul des coques épaisses : état de la technique et tendances à venir

MacKay, J.R.; DRDC Atlantic TM 2007-188; R & D pour la défense Canada – Atlantique; Octobre 2007.

Contexte : Les coques épaisses sont les structures portantes principales des sous-marins de la force navale, des submersibles commerciaux et scientifiques, et des engins sous-marins autonomes (AUV). Les nombreuses similitudes que présentent les coques épaisses, les plates-formes offshore, les constructions aérospatiales et certains ouvrages de génie civil font que les progrès réalisés pour les uns sont souvent applicables aux autres, et c'est ainsi que le présent document peut parfois viser tout l'ensemble des structures courbes à paroi mince calculées pour des conditions d'instabilité, ci-après dénommées globalement « coques critiques en flambage ».

Résultats : Le présent document présente l'état de la technique en matière d'analyse de structure et de conception des coques épaisses : 1) en expliquant la nature de la résistance de structure, et les faiblesses connexes, des coques épaisses; 2) en résumant les méthodes traditionnelles et contemporaines d'analyse de structure et de calcul utilisées pour les coques épaisses; 3) en identifiant les tendances en faveur de la modélisation numérique des structures de coques critiques en flambage; et 4) en examinant les méthodes novatrices de calcul pour les structures de coques critiques en flambage. L'auteur avance l'idée que le conservatisme existant à plusieurs niveaux dans l'approche de calcul traditionnelle pourrait être amélioré par l'emploi de méthodes numériques non linéaires pour les prédictions de la résistance, et qu'il y aurait avantage à incorporer ces méthodes dans les méthodes de calcul des coques épaisses.

Portée : Les méthodes numériques – par exemple, l'analyse par éléments finis non linéaire – permettent de baser les calculs de la résistance des coques épaisses sur l'état limite élastoplastique avec complexité géométrique totale, et d'inclure aussi les effets des contraintes résiduelles de fabrication et des dommages subis en service. L'incorporation de méthodes numériques dans la méthode de conception produirait des structures plus robustes et plus fiables, tant au stade de la conception que dans l'ensemble du cycle de vie, et cela permettrait d'innover dans les configurations et les matériaux des structures. Pour les sous-marins de la force navale déjà en service, cela pourrait se traduire par une enveloppe d'exploitation plus grande (par exemple, en termes de capacité de plongée profonde) que celle qu'on obtient en utilisant les méthodes de calcul traditionnelles, surtout si l'on tient compte des détériorations découlant des dommages de structure.

Recherches futures : Pour incorporer des méthodes numériques non linéaires dans les méthodes de calcul des coques épaisses, il faudra d'abord établir des lignes directrices de modélisation et d'analyse, populer une base de données de résultats expérimentaux, et déterminer les erreurs et incertitudes issues de la modélisation numérique en recourant à un programme d'analyse structuré. Des travaux supplémentaires de recherche sont nécessaires en ce qui concerne les contraintes résiduelles de fabrication, les modèles de matériaux inélastiques appropriés, le traitement des excentricités de coque et la prescription des imperfections caractéristiques de conception. Ce travail est en train d'être lancé par RDDC Atlantique, en coopération avec le

ministère de la Défense des Pays-Bas et l'université de technologie de Delft. Ce document, en conjonction avec un programme collaboratif entre les Pays-Bas et le Canada actuellement en cours en matière de recherche expérimentale sur l'écrasement des coques épaisses représente la première étape de cette tâche, après quoi les lignes directrices de modélisation, une base de données expérimentale et la modélisation numérique suivront dans les prochains mois et années.

This page intentionally left blank.

Table of contents

List of figures

List of tables

1 Introduction

Pressure hulls are the main load bearing structures of naval submarines, commercial and research submersibles, and autonomous underwater vehicles (AUVs). Pressure hulls are closely related to many structures in the offshore oil and gas industry that withstand hydrostatic pressure, and axially-compressed shell structures used in the aerospace industry. The many similarities between pressure hull, offshore, aerospace and some civil engineering structures mean that advances in one group are often applicable to the others, and thus this document is sometimes concerned with the entire collection of thin-walled curved structures designed for instability, referred to hereafter as "buckling-critical shells."

This document aims to identify the state-of-the-art of pressure hull analysis. The traditional analysis and design methods – empirically-derived knock-down factors on classical buckling pressures and first yield criteria for the most pessimistic geometry – are well-established and room for improvement is limited. This document will therefore dedicate large sections to analysis methods and design procedures that will likely be of increasing importance in the future, either because they provide more accurate (i.e. less erroneous and variable, i.e. more reliable) strength predictions, which can translate into increased structural efficiency, and/or because they are more flexible than existing design methods, allowing novel and innovative use of structural configurations and materials.

A conspicuous example of a sophisticated and flexible tool that is widely used for structural analysis in general and for buckling-critical shells specifically, but has not been implemented in pressure hull design codes, is nonlinear numerical analysis, or more specifically nonlinear finite element analysis (NLFEA). Future design codes may also reach beyond the traditional empirical and working stress approaches by establishing hierarchical design procedures that include levels of analytical rigor, from classical buckling pressures to nonlinear numerical collapse predictions.

This document concentrates on the main structural component of pressure hulls – the ring-stiffened cylinder – for the well-established classical design methods, while a more general examination of buckling-critical shells will be undertaken for more recent or novel developments in analysis and design. The state-of-the-art of pressure hull structural analysis and design is established in this document by:

- explaining the nature of structural strength, and associated weaknesses, in pressure hulls (Section 2);
- summarizing traditional and contemporary structural analysis and design methods for pressure hulls (Section 3);
- identifying trends with respect to numerical modeling of buckling-critical shell structures (Section 4); and
- reviewing novel design procedures for buckling-critical shell structures (Section 5).

This document concludes by suggesting a way forward (Section 5.4) that would allow pressure hull design procedures to incorporate nonlinear numerical strength predictions.

2 Pressure Hull Design Considerations

2.1 Buckling-Critical Shell Structures

Pressure hulls fall within the realm of general buckling-critical shell structures, for which design is governed by instability considerations. Research on such shell structures has focused on: 1) developing analytical predictions of buckling and post-buckling strength, and 2) relating these strengths to experimental values. It has been found that even for seemingly simple cases, such as a cylindrical tube under uniform axial compression, experimentally determined elastic buckling loads are consistently lower than classical buckling predictions (Schmidt, 2000). "Classical" buckling predictions refer to closed-form direct solutions of the governing differential equations of equilibrium for the shell structure, or the indirect solution using energy methods, typically based on a simplified (e.g. linear, membrane) pre-buckling solution.

The discrepancy between the classical shell theory and observed experimental buckling loads has been attributed to the effect of several factors (Teng, 1996; Schmidt, 2000): boundary conditions, nonlinear pre-buckling deformations, load eccentricities, anisotropies, residual stresses and geometric imperfections. Various analytical procedures have been developed in the attempt to account for these strength-reducing factors, particularly geometric imperfections, in the shell buckling theory. These include strength predictions based on post-buckling minima, minimum perturbation energy and membrane-reduced theories (Schmidt, 2000) – all of which are extensions of the basic shell theory.

The most common method of dealing with the strength-reducing factors in design has been the use of empirical curve-fitting (Arbocz and Starnes Jr, 2002). Traditional design methods for buckling-critical shells involve the calculation of the buckling load for the perfect structure – i.e. the classical elastic buckling load. The buckling strength of the real structure, i.e. the structure with imperfections, is taken by applying a "knock-down factor" to the classical buckling load. The knock-down factor is an empirically derived variable, often related to geometric or material parameters, which describes the classical-experimental buckling relationship. The empirical curve may be associated with the "lower bound" or the mean of the experimental data. The former is more common – the "lower-bound knock-down factor" approach for buckling-critical shells.

The complexity of shell buckling theory and the reliance on empirical methods has resulted in design codes for buckling-critical shells that are limited to basic geometry and loading (Teng, 1996). It will be shown in the following sections that pressure hulls incorporate many features of general buckling-critical shells, such as imperfection sensitivity and an empirically based knock-down factor design approach, as well as a further complexity due to the importance of material plasticity in pressure hull collapse behaviour.

2.2 The Typical Pressure Hull Structure

A pressure hull is a structure whose primary load-bearing responsibility is to withstand the compressive forces associated with hydrostatic pressure. The most efficient geometries for resisting these compressive forces are circular thin-walled cross-sections that transfer the normal

pressure load to in-plane compressive forces. Thus, pressure hulls are typically composed of a combination of ring-stiffened cylinders and cones, with spherical or torispherical domes at either end. The ring-stiffeners prevent elastic buckling from occurring before yielding of the material, further increasing structural efficiency (Ross, 1990). Load bearing, or "watertight", bulkheads divide longer pressure hulls into more-or-less isolated compartments. Figure 1 and Figure 2 show a complete pressure hull structure and single compartment, respectively.

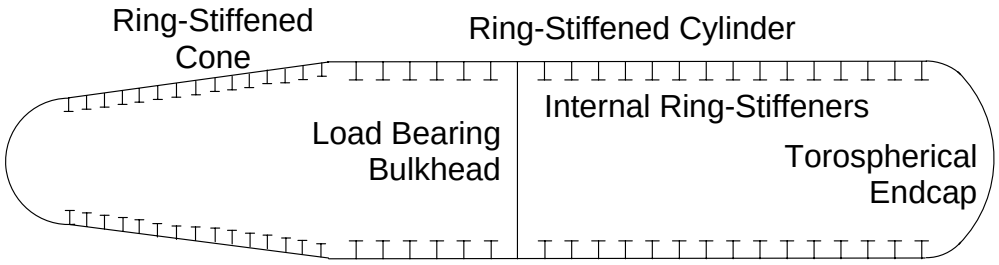

Figure 1: Typical pressure hull structure

Traditional design of pressure hulls is based on the assumption that a compartment, which may consist of cylindrical, conical and torispherical sections (Figure 1), can be approximated as a uniformly ring-stiffened cylinder terminated by rigid bulkheads. Conservatism is ensured by the incorporation of the most pessimistic dimensions in the idealized cylinder. This document focuses on the analysis and design of ring-stiffened cylinders as they are the critical component for pressure hull strength. This is because it is cheaper to design domes and bulkheads conservatively, as they make up a smaller portion of the pressure hull. Ring-stiffened cones are directly related to ring-stiffened cylinders, and are designed in a similar manner.

The hydrostatic pressure acting on the pressure hull is simplified as a uniform external pressure for design, but in reality it varies linearly with depth of submergence, and hence, over the height of the structure. Pressure hulls are designed so that the resulting upward load (i.e. buoyancy) is very nearly balanced by the weight of the structure plus that of the "secondary" internal and external structure, equipment, fuel, etc. Greater structural efficiency, in the form of higher strength to weight ratios, can mean larger payloads and greater operational ranges in operational submarines, submersibles and AUVs.

This document is concerned with pressure hulls that are constructed of ductile metals, especially steel, which have been the preferred construction material for pressure hulls in the past, and will likely remain so for future structures designed for moderate operating pressures (up to 20 MPa) (Morandi *et al.*, 1996A). Buoyancy concerns in deep-diving submersibles may require their pressure hulls to be constructed of a material with a greater strength to weight ratio than can be provided by traditional high-strength steel construction (e.g. composites).

The pressure hull structure converts the hydrostatic design load to compressive shell membrane stresses, and thus failure due to instability is paramount. Instability is associated with, and often analogous to, buckling, which is the occurrence of large deflections of a structure under a constant load (Wullschleger and Meyer-Peining, 2002). In general, the external pressure causing

elastic buckling or elasto-plastic collapse governs the ultimate strength of the pressure hull's ring-stiffened cylinder (Kendrick, 1985).

Pressure hull collapse pressures have traditionally been evaluated using a combination of analytical theory and empirical data. The analytical formulae resulting from the work of many researchers were collected (e.g. Bresse, 1859; von Mises, 1929; Bryant, 1954; Wilson, 1956A/B/C; and Kendrick, 1953A, 1965, 1970, 1979, 1982, 1985) and are used in most design codes – e.g. British Standard Specification for Unfired Fusion Welded Pressure Vessels: BS5500 (BSI, 1980), Buckling of Steel Shells: European Recommendations (ECCS, 1988) and Design of Submarine Structures: SSP74 (DPA, 2001).

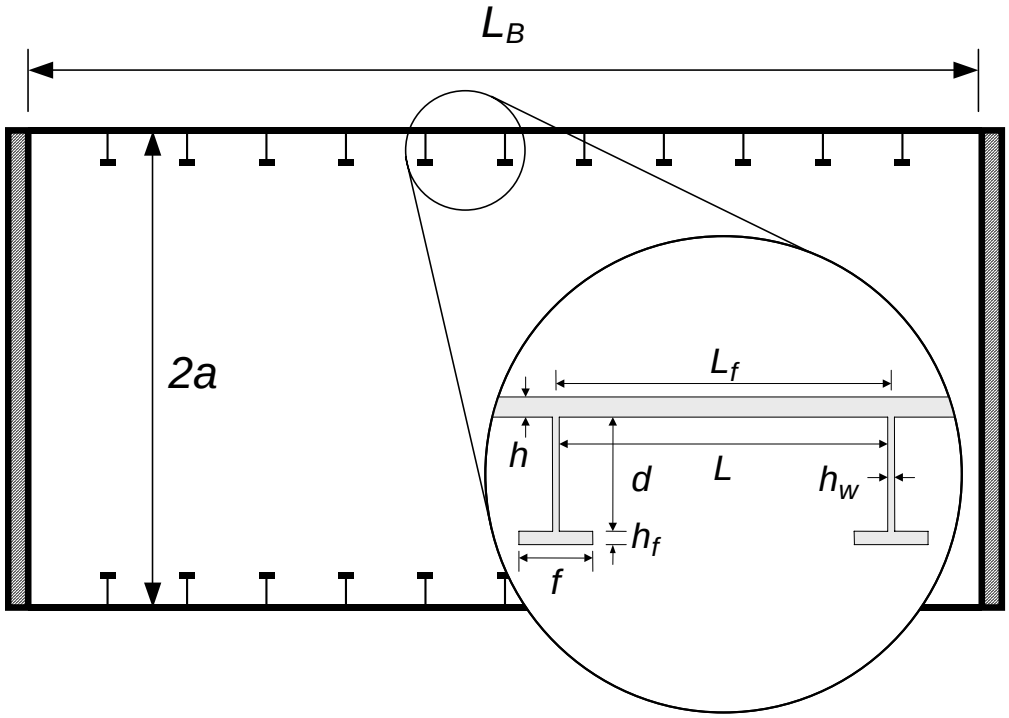

Figure 2: Pressure hull compartment with notation

The structural behaviour of a pressure hull is, by-and-large, characterized by that of its basic structural component: the ring-stiffened cylinder. For the static analysis of perfect cylinders, there are two behaviours referred to as 'buckling': 1) bifurcation buckling, and 2) collapse at the maximum or "limit" point in a load-deflection curve (Bushnell, 1981). Bifurcation buckling (i.e. classical elastic buckling) is associated with deformations that are orthogonal to the pre-buckling displacements, while limit-point, or "snap-through", buckling is characterized by large deformations that are in essentially the same configuration as the pre-buckling deformations (Wullschleger and Meyer-Peining, 2002). Analytically, the bifurcation buckling pressure is derived from elastic stability theory, and more specifically, the small deflection buckling behaviour.

2.3 Elastic Buckling of Ideal Pressure Hulls

A perfectly circular ring-stiffened cylinder subject to uniform external pressure will undergo axisymmetric deformation. The radial deflection, *w* (see Figure 3), is initially linearly proportional to applied pressure, but becomes increasingly non-linear as the pressure is increased. Eventually the external pressure will approach a limiting value, where a small increase in pressure results in large radial deflection. This collapse-type buckling is both axisymmetric, as it is associated with a uniform radial displacement of the shell, and asymptotic (Kendrick, 1970).

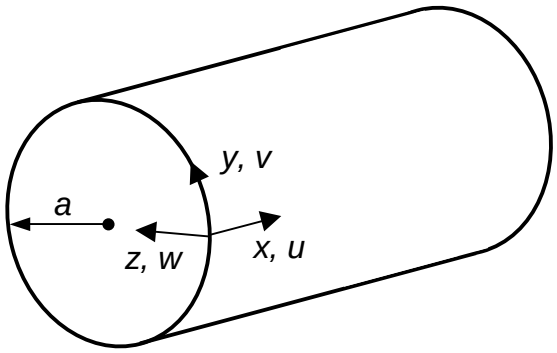

Figure 3:Cylindrical coordinates and associated displacements

In practice, as well as in theory, the axisymmetric buckling pressure is rarely attained before bifurcation buckling occurs (Kendrick, 1985). Figure 4 shows the theoretical load-deflection behaviour of a cylinder under external pressure. The curve OAB, representing axisymmetric collapse, is only theoretically possible because, for typical pressure hull geometries, the bifurcation buckling pressure is reached first.

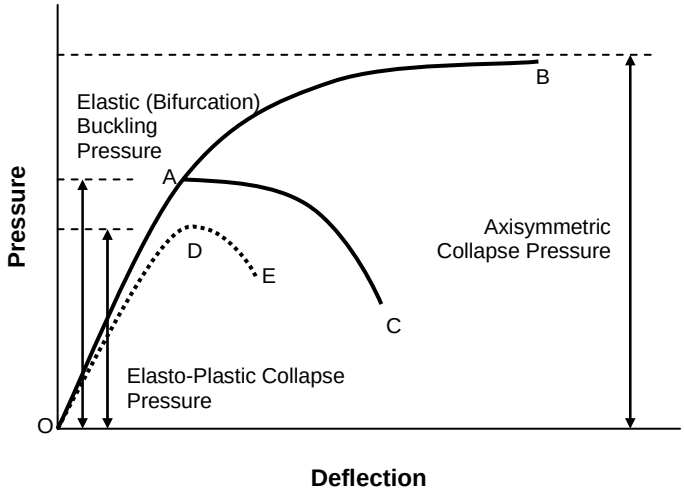

Figure 4: Theoretical load-deflection behaviour of a cylinder under external pressure

At the bifurcation load, the cylinder becomes unstable, and any small disturbance from axial symmetry will cause large deflections. Bifurcation buckling is so-called because, at the bifurcation buckling pressure, the load-deflection curve can follow either of two branches: 1) the pre-buckling, or fundamental, solution (curve OAB in Figure 4), or 2) the post-buckling solution (curve OAC in Figure 4).

Bifurcation buckling deformation occurs in a non-axisymmetric fashion, with the radial deflection following a sinusoidal pattern about the shell circumference. The number of complete circumferential lobes is denoted *n*, while the number of half-waves along the length of the cylinder is typically denoted *m*. An infinite number of combinations of circumferential and longitudinal buckling modes exist for a given cylinder geometry, with a buckling pressure associated with each combination of *n* and *m*. It is the lowest of these values that is of importance, and this is known as the buckling pressure in mode *n*.

For typical geometries, the lowest elastic buckling mode occurs for values of *n* between 2 and 20. For small values of *n* (approximately 2 to 4) the longitudinal buckling mode tends to be a half sine wave between bulkheads (*m*=1). This type of failure is termed overall collapse, because the stiffeners experience nearly as much deformation as the shell. For large values of *n* (approximately 10 and higher) the longitudinal buckling mode tends to be a half sine wave between each stiffener (*m*=*N*+1, where *N* is the number of ring-stiffeners). This is called interframe buckling, as the frames experience small deformations relative to the shell. Overall and interframe buckling mode shapes can be seen in Figure 5.

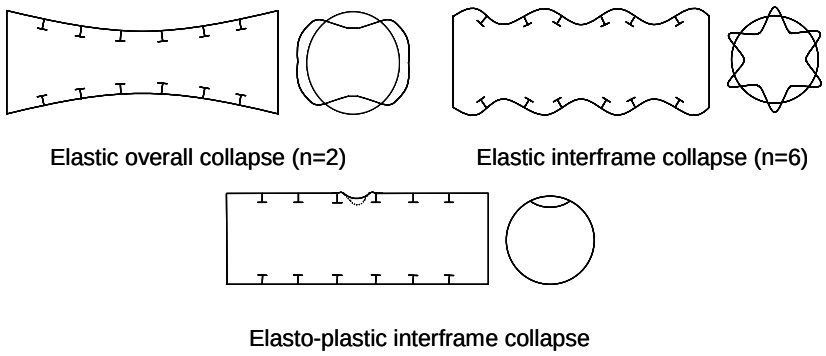

Figure 5: Collapse modes of ring-stiffened cylinders

For moderate values of *n* (approximately 5 to 9) the longitudinal buckling mode is such that the mode is somewhere between overall and interframe in nature. The distinction between overall and interframe buckling is quite arbitrary (Morandi *et al.*, 1996B; DPA, 2001); they are actually different forms of the same type of failure – namely, bifurcation buckling failure – but the terms are useful for traditional design, whereby the ring-stiffeners and shell are designed separately.

A further source of pressure hull instability is frame tripping, or stiffener tripping, which refers to the occurrence of local instability of the ring-stiffener. Stiffener tripping can occur in any of three manifestations: 1) lateral-torsional buckling of the ring-stiffener, 2) local buckling of the stiffener web normal to the shell, or 3) local buckling of the stiffener flange. Lateral-torsional buckling

can occur in various modes. If the web-shell connection provides little or no rotational restraint, the entire frame will buckle in the same direction (n=0 mode). As support to the web is increased the frame will trip in an alternating fashion, with mode number increasing with connection rigidity (DPA, 2001). The other two forms of stiffener tripping involve local buckling.

Stiffener tripping is important because it occurs without loss of circularity at the web-shell connection (Kendrick, 1970; DPA, 2001). When stiffener tripping occurs, in any form, the result is a loss of stiffening capability, which consequently leads to another form of instability, generally overall collapse. Traditionally designed pressure hulls require relatively stocky stiffeners in order to resist bending stresses, prevent web buckling and to allow for internal space constraints; such stiffeners are not prone to tripping, and design procedures focus on avoiding, rather than predicting this mode of failure (Kendrick, 1982; Morandi *et al.*, 1996B).

2.4 Collapse of Real Pressure Hulls

Bifurcation buckling pressures are typically calculated for perfectly circular ring-stiffened cylinders made of linear-elastic material, and thus represent the upper bound, or maximum possible external pressure that can be resisted by the perfect structure. The classical elastic buckling strengths must be used carefully in design, as the strengths of real buckling-critical shell structures are notoriously sensitive to deviations from the perfect structure (Schmidt, 2000). These strength-reducing factors can be fabrication-induced (e.g. geometric imperfections) or may stem from imperfect understanding and/or modeling of loading and support conditions. Each of these factors must be accounted for when determining the strength of buckling-critical shell structures.

Pressure hulls are no exception; however, they are unique in that their strength is typically influenced by the onset of material yielding, as opposed to pure elastic buckling, which governs the strength of many buckling-critical shells. As a result, pressure hulls are sensitive to both geometric imperfections and residual stresses, which are related to the early onset of yielding. These strength-reducing factors resulting from fabrication procedures must be accounted for in design, and are discussed in Section 2.5.

Typical pressure hulls fail via an elasto-plastic collapse mechanism, whereby the strength of the structure is limited by:

- material plasticity, including early onset of yield due to residual stresses;
- nonlinear geometric behaviour associated with geometric imperfections, beam-column behaviour due to the axial load, and follower force effects of the pressure load; and
- instability associated with elastic buckling.

Elasto-plastic collapse is represented in Figure 4 by curve ODE, with point D marking the limit point associated with the collapse pressure. For representative pressure hull geometries and materials, the value of external pressure to cause elasto-plastic collapse is significantly less than the classical critical elastic buckling pressure (Kendrick, 1970). This type of failure has been characterized under controlled experimental conditions (MacKay, 2007A) by:

- an increasingly nonlinear strain-pressure (or displacement-pressure) relationship as the applied load is increased (see also Kendrick, 1970);
- ultimate collapse at a load only slightly greater than the load causing the onset of yield in critical areas of the structure (for structures with no residual stresses); and
- a collapse shape associated with a critical elastic buckling mode (see also Bushnell, 1981).

These criteria, which were based on the collapse of machined model pressure hulls with no significant residual stresses, may not hold true for all pressure hulls, but can serve as a general guide.

2.5 Strength-Reducing Factors in Pressure Hulls

A typical pressure hull is constructed of metal plating (e.g. high-strength rolled steel), which is cold bent into a circular shape to form the pressure hull. The ring-stiffeners are usually either cold-bent T-sections, or built up T-sections composed of cold bent flanges and cut webs. The pressure hull shell is composed of several bent plate sections about the circumference and along the length. Butt welds form longitudinal and circumferential seams between plate sections and at the ring-stiffener connection to the shell.

The fabrication process – cold bending and welding – introduces imperfections in the form of locked-in, or residual, stresses, as well as local and global distortion of the structural geometry (Faulkner, 1977). The nature and impact of residual stresses and geometric imperfections resulting from construction is considered in the following sections.

2.5.1 Residual Stresses

Residual stresses are those stresses which remain "locked into" a structure that has been plastically deformed, and are naturally in an equilibrium state. The investigation of residual stresses in buckling-critical shells can be divided into two broad areas: 1) simulation (experimental, analytical, or numerical) of the fabrication procedures in order to determine the location and magnitude of residual stresses, and 2) determination of the effect of the resulting residual stress field on the strength and stiffness of the structure. Residual stresses are often accompanied by associated geometric imperfections that can additionally reduce strength (Rotter, 1998).

Residual stresses in pressure hulls are primarily the result of two processes (Faulkner, 1977): 1) cold bending of the hull plating and possibly the ring-stiffeners, and 2) welding of the pressure hull plating and ring-stiffeners.

Residual Stresses due to Cold Bending

Cold forming is the general term used to describe the plastic deformation of a material that results in a desired shape. Cold forming produces residual stresses and, typically, anisotropy in the deformed region (Sarawit *et al.*, 2003). The effect of cold forming on the "effective" yield strength of a structure is dependent on the combination of material, section geometry and final

configuration. In different circumstances, cold forming has been found to increase (Sarawit *et al.*, 2003) or decrease (Fukuda *et al.* (2003) yield strength.

In the construction of pressure hulls, the deformation of straight plate or beam sections into circular forms is referred to as cold bending. Cold bending proceeds by plastically deforming the section to a curvature greater than the desired radius of curvature (overbend), after which the overbend moment is released and the section undergoes springback, resulting in the final section curvature (Mitchell, 1986). In real situations, this process is undertaken piecemeal by successively crimping and/or rolling the section.

The springback moment is opposite in sign to the overbend moment and is typically in the elastic range of the material; however, plasticity can occur for some sections (e.g. T-section stiffeners). Residual stresses are the sum of the stresses due to overbend and springback. The stresses throughout the cold-bending process are shown in Figure 6 for a plate section. The zigzag pattern of residual stresses, with $\sigma_{r1}>\sigma_{r2}$, is typical (Faulkner, 1977). Cold-bending of internal T-section ring-stiffeners results in compressive residual stresses in much of the flange and at the toe of the web (Figure 7).

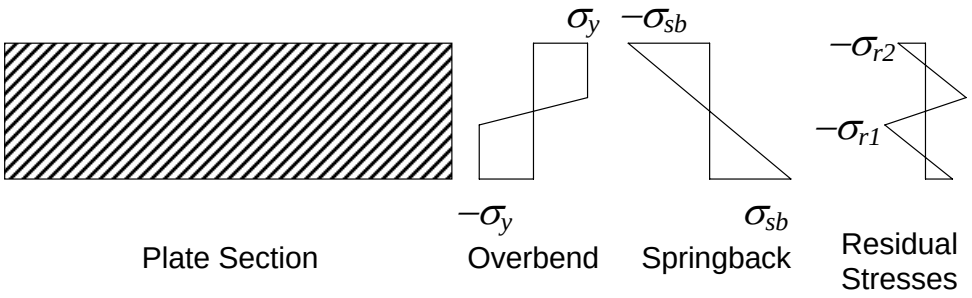

Figure 6: Overbend, springback and residual stresses in a cold bent plate

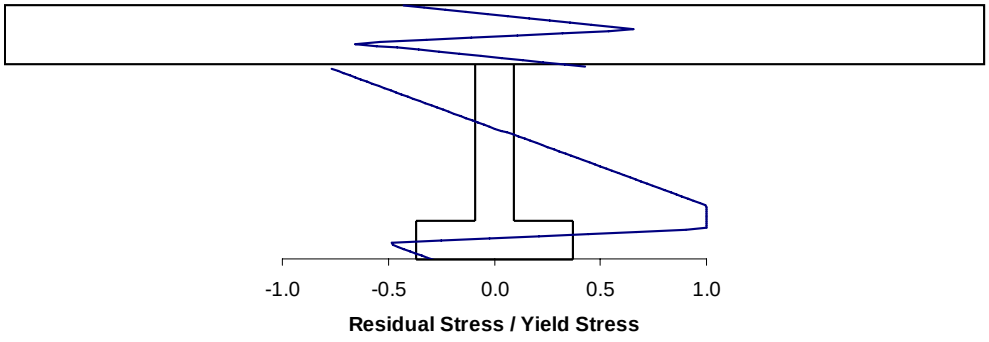

Figure 7: Typical residual stress distribution due to cold bending of the shell and ring-stiffener

Residual Stresses due to Welding

Residual stresses are formed in welded structures upon cooling and contraction of the welded region, which is restrained by other areas of the structure. This results in high tensile stresses in the welded region balanced by compressive residual stresses elsewhere in the structure.

The distribution of welding residual stresses in a pressure hull cross-section is shown in Figure 8. Welding of the ring-stiffeners to the shell plating results in tensile circumferential stresses in the shell at the stiffeners. The breadth of the tensile stress zone, $2\eta h$, is a characteristic of the welding procedure and structural configuration, and η ranges from 1.5 to 6 for marine structures (Faulkner, 1977).

Compressive residual stresses in the shell result from the equilibrium balance with tensile stresses, σ_{rc1}, and stresses associated with the distortion of the shell due to longitudinal weld stresses, σ_{rc2}. The maximum compressive residual stress in the shell due to welding, σ_{rc}, has been measured as $0.17\sigma_y$ in a real pressure hull (Faulkner, 1977). The shell distortion is in the form of a half sine wave between stiffeners (see Figure 8) and is balanced by a tensile stress in the stiffeners, σ_{rf}. The maximum interframe displacement, δ_p, is typically around 10% of the shell thickness (Faulkner, 1977).

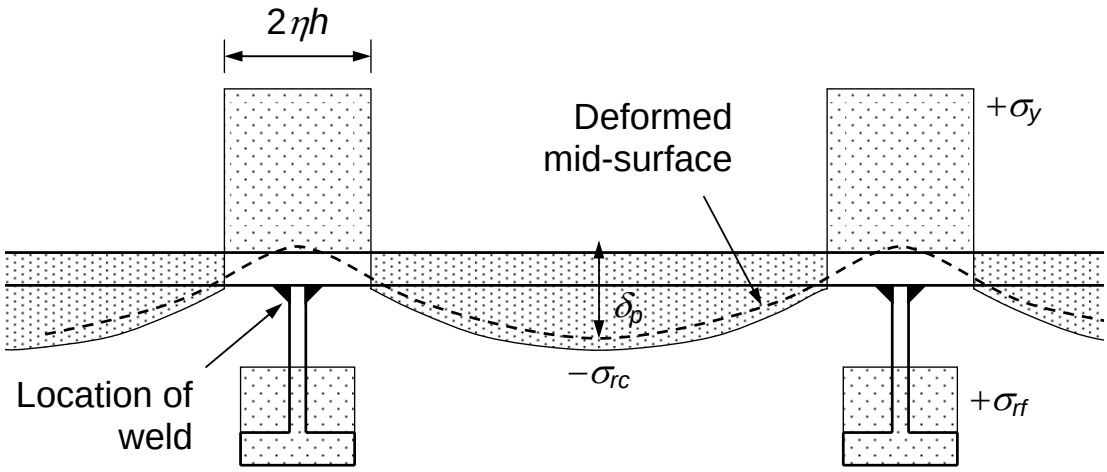

Figure 8: Typical residual stress distribution due to welding of the ring-stiffener and shell plating (Faulkner, 1977)

The following relationships, presented by Faulkner (1977), can be used to determine the maximum values of tensile and compressive residual stresses in the shell and ring-stiffeners.

$$\sigma_{rc} = \sigma_{rc1} + \sigma_{rc2} \tag{1}$$

$$\sigma_{rc1} = \frac{2\eta\sigma_y h}{L_f - 2\eta h} \tag{2}$$

$$\sigma_{rc2} = \sigma_{rf} - \delta_p E / r \tag{3}$$

$$\sigma_{rf} = \frac{2\delta_p E L_f h}{\pi r\left(L_f h + A\right)} \tag{4}$$

where:

$$A = A_f \left(r / a_{gc}\right)^2 \tag{5}$$

Effect of Residual Stresses on Pressure Hull Strength

Residual stresses reduce both stiffness and strength by causing the early onset of yielding under the applied loads. Compressive residual stresses in the critical circumferential direction are the main concern for pressure hulls. Residual stresses also change the structural behaviour of a pressure hull from one that fails almost immediately after yielding (MacKay, 2007A) to one where yielding occurs at loads significantly less than the ultimate strength (Faulkner, 1977).

The degradation of the section material can be quantified by examining the effective stress-strain relationship in the section with residual stresses. The inelastic behaviour of sections with residual stresses is described by an effective stress-strain curve (Figure 9), which is determined by experiments or analytically (see below).

The effect of residual stresses on interframe collapse pressure has not been extensively studied because the empirical design process for interframe collapse inherently includes fabrication effects. However, it is generally accepted that, due to the dominance of bending and shear actions over direct compression, cold-bending of the shell plating does not significantly reduce interframe collapse strength (Kendrick, 1970). Despite this, numerical studies have shown a decrease in interframe collapse pressure of approximately 10% when cold bending residual stresses are accounted for (Creswell and Dow, 1986). Welding-induced stresses in the shell may be significantly detrimental to strength, via early yielding, but this has not been studied to a significant extent (Faulkner, 1977).

Compressive residual stresses in the ring-stiffener due to cold bending may be somewhat lessened by tensile weld-induced stresses; however, this is counteracted by the transfer of load from the shell, which has a reduced stiffness due to cold bending and welding, to the stiffeners at higher loads. A secondary effect of welding is the global distortion (non-axisymmetric) of the pressure hull due primarily to longitudinal welding of the shell sections (Faulkner, 1977). Cold-bending, combined with an overall n=2 geometric imperfection, has been found to decrease overall collapse strength by up to 30% (Faulkner, 1977; Creswell and Dow, 1986); the effect of cold bending stresses on n=3 overall collapse is less severe (Faulkner, 1977).

Numerical simulations conducted by Lennon and Das (1997) confirmed that welding strains are (locally, at least) much greater than cold bending strains (11.5ε_y and 3.5ε_y, respectively), as well as the tendency of welding to induce “hungry horse” inter-stiffener shell deformation (see Figure 8). Those authors found that the initial buckling strength of ring- and stringer-stiffened cylinders

under external pressure was reduced by 23-27.5% due to welding and cold bending residual stresses, compared to similar “stress-relieved” cylinders.

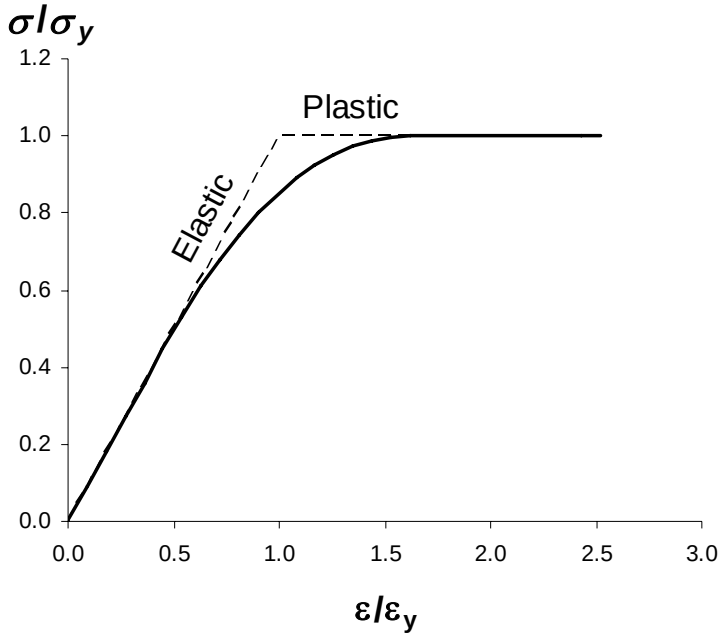

Figure 9: Effective stress-strain curve for a cold-bent section

Effective Stress-Strain Curves

Effective stress-strain curves, sometimes referred to as cold bend curves if the welding induced stresses are ignored, can be used for strength calculations for structures with residual stresses (e.g. Creswell and Dow, 1986). While the creation of curves for cold bent sections is described here, the same method could be used to create effective stress-strain curves for welded or welded and cold bent sections.

The residual stresses due to the cold bending process must first be estimated; e.g. using Mitchell’s algorithm that employs a finite strip method (Mitchell, 1986; Smith and MacKay, 2005). Once the residual stress pattern is determined, a uniaxial compressive strain is numerically applied to the ring section. The stress in the i^{th} fibre, for a particular value of ε_i, is given by:

$$\sigma_i = \max\left\{(\sigma_r)_i + E_i\varepsilon_i, -(\sigma_y)_i\right\} \text{ for } \varepsilon_i < 0 \tag{6}$$

where $(\sigma_r)_i$ and $(\sigma_y)_i$ are the residual stress in the fibre and the yield stress of the fibre, respectively. The average stress in a subset of fibres (for example, the shell plating, or an entire frame) is given by:

$$\overline{\sigma} = \frac{\sum \sigma_i A_i}{\sum A_i} \tag{7}$$

where A_i is the cross-sectional area of the fibre.

A stress-strain curve for each structural component (shell plating, frame) is built up by applying compressive strains until the entire section yields. The effective stress-strain relationship differs in compression and tension for cold bent T-section ring-stiffeners; however, the compressive curve is typically used when assessing strength. A typical effective stress-strain relationship for a cold bent plate section, determined by this method, is shown in Figure 9.

2.5.2 Geometric Imperfections

Geometric imperfections are detrimental to the strength of buckling-critical shells through their contribution to the nonlinear geometric behaviour, especially through bending and subsequent beam-column behaviour. Initial imperfections are not entirely random; it has been shown that their general distribution is a characteristic of the fabrication process (Arbocz and Hol, 1991), which is important when assuming the initial shape for design. Fabrication processes could lead to imperfections in the critical buckling mode, which can have severe consequences to the buckling strength of the structure (Berry *et al.*, 2000). Imperfection databases for shells, such as the one compiled at the Delft University of Technology in the Netherlands (Arbocz and Abramovich, 1979), provide a resource of realistic shapes and amplitudes for designers.

When analyzing in-service structures or experimental specimens, a survey to determine the maximum initial imperfection is not adequate because imperfection sensitivity is related to both the magnitude *and* shape of the initial imperfections (Arbocz and Starnes Jr, 2002). As such, considerable research has been undertaken on the measurement of shell structure geometry (e.g. Kendrick, 1977).

Initial geometric imperfections in pressure hulls can be in the form of:

- global non-axisymmetric deviations of the ring-stiffened cylinder or cone from the perfect circular form, referred to as out-of-circularity (OOC);
- additional distortion of the shell plating between stiffeners;
- out-of-plane orientation of the ring-stiffeners (frame tilt); and
- deviations of the dome ends from the perfect spherical or torispherical shape.

The collapse mode of a typical pressure hull is often determined by the magnitude and shape of OOC: interframe collapse governs when initial imperfections are small, while overall collapse is dominant when imperfections are large and in the critical mode. “Interactive” effects have been reported for moderate magnitudes of OOC, whereby the collapse pressure may be up to 14% lower than either the interframe or overall collapse pressure (Creswell and Dow, 1986; Graham *et al.*, 1992).

A convenient scalar description of the magnitude of OOC is the maximum eccentricity, which refers to the maximum absolute value of the deviation from the mean radius, reported in units of distance or as a percentage of the mean radius. Pressure hulls are typically designed to accommodate a maximum eccentricity of 0.5% of the mean shell radius and are built to a tolerance of one-third of this value (DPA, 2001).

Experimental investigations on ring-stiffened cylinders have shown that OOC in the form of the critical overall elastic buckling mode, and at the maximum allowable amplitude of 0.005*a*, results in a 15% reduction in the elasto-plastic overall collapse pressure (Bosman *et al.*, 1993). Numerical studies have shown similar decreases in overall collapse pressure due to OOC, and also indicate that n=2 overall collapse is less sensitive to imperfection amplitude than are n=3 and n=4 modes (Smith and MacKay, 2004).

Geometric imperfections in the form of the critical elastic interframe buckling mode (i.e. a large number of circumferential lobes and a half sine wave between stiffeners – "interframe nucleators") and at a small amplitude (0.0005*a*) have been shown to reduce the collapse pressure with respect to the perfect structure, and may be as detrimental to strength as global OOC imperfections (Creswell and Dow, 1986). Interframe imperfections are inherently addressed by the empirical interframe design method (see Section 3.2.3), and the greater emphasis has been placed on the measurement and modeling of OOC, which is associated with a reduction in overall collapse pressures.

Measurement of Out-of-Circularity

Out-of-circularity in a ring-stiffened cylinder of finite length, expressed in terms of the initial radial deviation from the perfect circle, w_0, can be defined by the following Fourier series (Kendrick, 1970), which allows the imperfect geometry to be converted into an easily understood quantity:

$$w_0 = \sum_{m=1}^{\infty}\sum_{n=1}^{\infty} C_{0mn} \cos n\theta \sin\left(m\pi x / L_B \right) \tag{8}$$

w_0 is the imperfection at cylindrical coordinates θ and x (where $\theta=y/a$ in Figure 3), and C_{0mn} is the amplitude of the imperfection corresponding with the axial and circumferential wave numbers, m and n, respectively. Implicit in the definition of OOC by equation (8) is the assumption that the ring-stiffeners have initial imperfections equal to those of the shell at the same axial location. Similar "double" Fourier series, accounting for discrete measurements of the pressure hull, are useful for representing the true shape of a ring-stiffened cylinder in numerical calculations (see Section 4.2.1).

It is often simpler to characterize the OOC of a pressure hull at discrete axial locations by use of a "one-dimensional" Fourier series, rather than the "double" Fourier series in equation (8). For example, the pressure hull radius, $R(\theta)$, at a particular angle, θ, is defined by the Fourier series expression (Kendrick, 1977):

$$R(\theta) = b_0 + a_1 \sin\theta + b_1 \cos\theta + \sum_{n=2}^{\infty} \left(a_n \sin n\theta + b_n \cos n\theta \right) \tag{9}$$

where b_0 is the average radius, a_1 and b_1 represent the offset from the true centre of the data, and a_n and b_n are the Fourier coefficients for a particular circumferential wave number, n. The Fourier amplitude, A_n, is taken as:

$$A_n = \sqrt{a_n{}^2 + b_n{}^2} \tag{10}$$

and is an indication of the contribution to OOC by the mode, n.

The Fourier coefficients can be calculated from evenly spaced discrete data using the following expressions:

$$b_0 = \frac{1}{N} \sum_{i=0}^{N-1} R(\theta_i) \tag{11}$$

$$a_1 = \frac{2}{N} \sum_{i=0}^{N-1} R(\theta_i) \sin\theta_i \,,\; a_n = \frac{2}{N} \sum_{i=0}^{N-1} R(\theta_i) \sin n\theta_i \tag{12}$$

$$b_1 = \frac{2}{N} \sum_{i=0}^{N-1} R(\theta_i) \cos\theta_i \,,\; b_n = \frac{2}{N} \sum_{i=0}^{N-1} R(\theta_i) \cos n\theta_i \tag{13}$$

where $\theta_i = \left(2\pi i / N \right)$. A minimum of two points are required to identify the peak and trough of a single sine or cosine wave, and thus the calculation of Fourier coefficients is limited to values of $n < N/2$ (Kendrick, 1977).

Direct measurements of the pressure hull radius are seldom practical for real pressure hulls that have internal structure, such as decks and bulkheads. A common method of measuring OOC in real pressure hulls is the use of a chord gauge (Figure 10). Kendrick (1977) described the use of a chord gauge and the mathematical interpretation of the measurement data.

The chord gauge length is based on the nominal circumference of the cylinder and the desired number of measurements. Displacement gauge readings, taken at equal intervals about the circumference, are subtracted from the zero gauge reading, taken on a flat surface, giving the chord height at each location. The chord heights are then converted to radial eccentricities, based on the average reading. Fourier analysis is then undertaken to determine the contribution of each circumferential mode, n, to the overall imperfection shape.

The chord gauge in Figure 10 was constructed specifically for the experimental models described in Section 3.3. The gauge length was specified to allow 18 evenly spaced measurements to be

taken about the circumference, which means that imperfection modes up to n=9 can be detected using Fourier analysis.

Figure 10: A small chord gauge device for measuring OOC in experimental pressure hull models (MacKay, 2007B)

2.5.3 Boundary Conditions

For certain structural shells (e.g. axially compressed cylinders), the effects of elastic supports are as important as initial imperfections in explaining experimental scatter (Arbocz and Starnes Jr., 2002). Ideal simply supported or clamped boundary conditions are difficult to achieve – experimental supports typically fall somewhere in the middle. Cylindrical specimens are also prone to out-of-flatness and non-parallel alignment of the end supports, which may be detrimental to strength.

Unstiffened cylindrical shells under external pressure failing by elastic buckling have been found to be more sensitive to boundary conditions than axially compressed cylinders (Schneider and Brede, 2005). For ring-stiffened cylinders under external pressure, overall collapse is more greatly affected by boundary conditions than interframe collapse, which tends to occur (by design) in the bays away from the end supports. It has been found that rotational constraints are less important than axial constraints at the cylinder ends, as the resistance to out-of-plane bending of thin shells is small compared to their resistance to in-plane warping (Ross, 1990). Prevention of 'end warping' has a particularly great influence on overall failure, increasing the overall elastic buckling pressure by up to 80% for the n=2 critical mode (Morandi *et al.*, 1996A). The boundary conditions in real pressure hulls are likely closer to being unrestrained in the axial direction, while end-warping tends to be significantly restricted in experimental specimens (Morandi *et al.*, 1996A).

3 Analytical Theory and Design Methods for Pressure Hulls

Contemporary pressure hull design codes (e.g. BSI, 1980; ECCS, 1988; DPA, 2001) are based on a combination of analytical methods, which include design formulae, empirical curves, and numerical calculations. Most design codes use a conventional deterministic working stress approach, undertaking an analysis for each mode of failure. A single safety factor, or several partial safety factors (PSF), accounting for uncertainties in the loading, fabrication, and strength of the pressure hull, are applied to the characteristic strength in order to determine the allowable working pressure. The analytical methods rely on many simplifying assumptions and require the safety factors to account for non-addressed design issues such as interactive collapse, local deformations, variable material properties and geometry, and the effect of penetrations and secondary structure on collapse.

3.1 Classical Elastic Buckling and Stresses in Pressure Hulls

The following sections present the basic analytical quantities used in pressure hull design codes: the classical elastic buckling solutions (Section 3.1.1), linear stress formulae (Section 3.1.2), and some analytical/semi-analytical methods for dealing with imperfect pressure hulls (Section 3.1.3).

3.1.1 Classical Elastic Buckling of Pressure Hulls

The classical elastic buckling pressures for ring-stiffened cylinders were primarily derived by the solution of the governing equilibrium equations or by using energy methods. Solutions began to emerge, beginning with the simplest cases of pressure loaded rings and tubes, continuing to the critical elastic buckling pressure for uniformly ring-stiffened cylinders, and finally to more advanced solutions for cylinders with non-uniform features such as variable frame spacing. Refer to Figure 2 and Figure 3 for notation of pressure hull geometry and cylindrical coordinate conventions, respectively.

Elastic Buckling of a Circular Ring under External Pressure

The simplest case, a circular ring under uniform external pressure, was treated by Bresse (1859). The governing differential equation for the radial displacement, w, of thin bar with a circular centre line (i.e. a ring), is taken as (Timoshenko and Gere, 1961):

$$\frac{d^2 w}{d\theta^2} + w = -\frac{MR^2}{EI} \tag{14}$$

where θ is the angular coordinate, M is the applied bending moment, R is the radius of the ring at the neutral axis, E is Young's modulus and I is the moment of inertia of the ring. Bresse determined the critical buckling pressure for a ring, q_{cr} (units of force/length), by assuming a slightly non-circular (n=2) post-buckling displacement and finding the exact solution to equation (14) for the resulting bending moment in terms of the applied pressure, and boundary conditions.

$$q_{cr} = \frac{3EI}{R^3} \tag{15}$$

Bresse's solution, equation (15), can be extended to the overall elastic buckling of a ring-stiffened cylinder of infinite length by assuming that the frame and associated bay of shell plating act as a unit, undergoing the same radial deflection. The result is the classical form of the Bresse pressure, P_B (units of force/area), for overall buckling of an infinitely long ring-stiffened cylinder (DPA, 2001):

$$P_B = \frac{(n^2 - 1)EI_c}{aa_{gc}{}^2 L_f} \tag{16}$$

where I_c and a_{gc} are the moment of inertia and radius to the centre of gravity, respectively, of the combined frame and shell plating, n is the complete number of circumferential buckling waves, a is the mean shell radius and L_f is the frame spacing. The Bresse pressure will always be a minimum for n=2 (implicit in equation (15)), however it is convenient to include the mode number in equation (16) as it is used in more rigorous calculations of overall collapse that are not necessarily minimized at n=2.

Elastic Buckling of a Cylindrical Shell under External Pressure

Von Mises (1929) extended the stability analysis of circular structures under external pressure to two-dimensional structures: cylindrical shells or tubes. As with Bresse, von Mises approached the derivation of the critical buckling pressure by direct solution of the equilibrium equations. The three degrees of freedom (u, v, w – see Figure 3) of the shell result in a set of three differential equations of equilibrium. The equilibrium equations are expressed in terms of the in-plane normal (N_x, N_y) and shear forces (N_{xy}, N_{yx}), and the bending moments (M_x, M_y, M_{xy}, M_{yx}), and can take into account both shell bending and stretching at the mid-surface (see Timoshenko and Gere, 1961).

The equilibrium equations were then expressed purely in terms of the displacements via the constitutive equations (relating forces and moments to strains and curvatures) and the kinematic relations (relating the strains and curvatures to the displacements). Trigonometric functions for the post-buckling displacements were assumed such that they satisfied simply supported boundary conditions at the shell ends. The critical pressure was determined by equating the determinant of the resulting set of homogenous equations to zero. This resulted in the classical elastic buckling pressure for a simply supported cylindrical shell under uniform external pressure, commonly referred to as the von Mises pressure.

The von Mises pressure has become a standard tool for design of the pressure hull shell between frames, providing an approximation of the elastic interframe buckling pressure. Kendrick (1965) proposed a slight modification to the von Mises pressure – P_{m1}, defined in equation (17) – that has been incorporated into many pressure hull design codes (e.g. BSI, 1980; ECCS, 1988; DPA, 2001).

$$P_{m1} = \frac{Eh}{a}\left[n^2 - 1 + \frac{1}{2}\left(\frac{\pi a}{L}\right)^2\right]^{-1}\left\{\left[n^2\left(\frac{L}{\pi a}\right)^2 + 1\right]^{-2} + \frac{h^2}{12a^2\left(1-\mu^2\right)}\left[n^2 - 1 + \left(\frac{\pi a}{L}\right)^2\right]^2\right\} \quad (17)$$

Kendrick's version of the von Mises pressure assumes a buckled shape in the form of a half sine wave in the axial direction, and must be minimized with respect to the number of circumferential waves, *n*. The von Mises pressure is generally assumed to be conservative for predicting the *elastic* interframe buckling pressure due to the assumption of simple support at the frames. The adjacent frames and shell plating may provide out-of-plane (bending) and in-plane (warping) flexural support, which could significantly increase the critical pressure.

It should be noted that von Mises was not alone in studying the critical buckling pressure for cylindrical shells under external pressure. He was closely followed by Flügge (1932), among others, in the solution of the equilibrium equations, and other authors have offered simplified versions of his solution that do not require iteration over *n* (Windenburg and Trilling, 1934). However, the full iterated von Mises solution remains the preferred form for many pressure hull design codes.

Elastic Buckling of a Ring-Stiffened Cylinder under External Pressure

The critical elastic buckling pressure of a cylindrical shell was soon extended to include the effects of equidistant circumferential rings (see, for example, Flügge,1932). Calculation of the buckling pressure proceeded in a similar manner as that for unstiffened cylindrical shells, with additional terms to account for the flexural stiffness of the rings. Flügge's solution was appropriate for prismatic ring-stiffeners and did not account for additional displacement of the shell between frames.

Kendrick (1953A) significantly extended the capability to predict the elastic buckling pressure of ring-stiffened cylinders, considering both overall and interframe modes, by employing energy methods (specifically, the method of Ritz). Kendrick's work was based on a similar solution presented by Salerno and Levine (1951), which, according to Kendrick (1953A) and later Bryant (1954), used some incorrect expressions in the energy formulation.

The solutions presented by Kendrick (1953A), and Salerno and Levine (1951), rely on the minimization of the total potential energy of the ring-stiffened cylinder just after buckling occurs. The total potential energy of the system is the sum of the internal strain energy stored in the shell and rings, and the work done by the applied external pressure. The energy expressions were developed in terms of the component displacements, assuming that the total displacement is the displacement just prior to buckling plus the additional displacement due to buckling. Kendrick (1953A) assumed a buckled shape for each displacement component and evaluated the total potential energy using the assumed displacement functions, which involve the use of arbitrary constants (generalized coordinates). The total potential energy must be a minimum in order for the system to be in equilibrium. This was enforced by taking the first derivative of the potential energy expression with respect to each generalized coordinate, leading to a system of three homogeneous simultaneous equations, which can be expressed in matrix form. In order for a

non-trivial solution to these equations to exist, the determinant of the coefficient matrix must vanish, thus allowing the critical buckling pressure to be calculated.

Kendrick (1953A) assumed a membrane-type pre-buckling solution (i.e. uniform radial displacement and longitudinal contraction of the cylinder). Post-buckling displacements were trigonometric in form, and based on simple supports at the ends of the cylinder. The critical buckling pressure of the cylinder is determined by minimizing the solution with respect to the circumferential and axial buckling modes (i.e. n and m, respectively). The buckled shape functions can describe a wide range of buckled shapes, particularly the governing overall and interframe cases. The main drawback of the allowable buckling shapes is that two or more mode shapes cannot be superimposed, negating the possibility of modelling "interactive" buckling mechanisms. Kendrick addressed this deficiency in later updates of this method (Kendrick, 1953B and 1953C).

Kendrick (1953A) presented the first generally accepted solution for the elastic buckling of a ring-stiffened cylinder that considered both overall and interframe modes. The resulting critical buckling pressure, P_{cr}, is shown in equations (18) to (20), where λ (a function of the axial buckling mode, m) and the coefficients a_{ij}, are defined in Kendrick's original report (1953A). The solution is quite intricate and was not incorporated into most pressure hull design codes.

$$P_{cr} = \frac{N}{D}\frac{Eh}{a(1-\mu^2)} \tag{18}$$

$$N = (a_{11}a_{22} - a_{12}{}^2)a_{33} + (a_{12}a_{13} - a_{11}a_{23})a_{23} + (a_{12}a_{23} - a_{22}a_{13})a_{13} \tag{19}$$

$$\begin{aligned} D = {} & (a_{11}a_2 2 - a_{12}{}^2)(n^2 - 1) + 2\lambda(a_{13}a_{22} - a_{12}a_{23}) + n\lambda(a_{13}a_{23} - a_{12}a_{33}) \\ & + n^2(a_{22}a_{23} - a_{23}{}^2) + \frac{\lambda^2}{2}\left[a_{11}(a_{22} + a_{33}) - a_{12}{}^2 - a_{13}{}^2\right] \end{aligned} \tag{20}$$

Bryant (1954) improved upon the Bresse pressure for overall elastic buckling pressure prediction by including the effects of finite cylinder length. Bryant used energy methods to show that the principal of conservation of energy is satisfied if the buckling pressure of a simply supported ring-stiffened cylinder is taken as the sum of the critical buckling pressures for: 1) a single ring-stiffener and associated shell plating, and 2) a cylindrical shell of finite length. Bryant used a modified version of the Bresse pressure, P_B, and a simplified von Mises pressure for the ring and shell buckling pressures, respectively, resulting in an overall elastic buckling pressure known as the Bryant pressure, P_N.

$$P_N = \frac{Eh\lambda^4}{a}\left[n^2 - 1 + \frac{\lambda^2}{2}\right]^{-1}\left[n^2 + \lambda^2\right]^{-2} + \left(n^2 - 1\right)\frac{EI_c}{aa_{gc}{}^2 L_f} \tag{21}$$

Equation (21) is in the form presented in a recent design code (DPA, 2001), where $\lambda = \pi a/L_B$, the axial buckling mode is fixed to be a half sine wave, and the critical pressure is found by

minimizing with respect to the circumferential wave number, *n*. Bryant found his solution to be within 5% of Kendrick's (1953A) more rigorous treatment of the overall buckling of ring-stiffened cylinders. This also served to validate Kendrick's (1953A) solution, which was derived from energy principals, by comparison with the Bryant pressure, based on two well-established equilibrium-derived buckling pressures. The simplicity of Bryant's solution, as well as its separation of stiffener and shell terms in the buckling solution, have led to its incorporation into many pressure hull design codes (e.g. BSI, 1980; ECCS, 1988; DPA, 2001).

Overall elastic buckling pressures calculated using the Bresse or Bryant equation vary with the moment of inertia of the combined stiffener and shell plating, I_c, which, in turn, depends on the value chosen for the effective breadth of shell plating (i.e. the length of shell between stiffeners that contributes to the overall flexural stiffness of the cylinder). There are several accepted methods of determining effective breadth or length. The simplest method, as suggested by Faulkner (1983), is to consider 75 percent of the shell length between stiffeners.

Values of effective length can also be interpolated from tables based on the geometric properties of the ring-stiffened cylinder and the wave number, *n*, under consideration. This approach is used in BS5500 (BSI, 1980) and SSP74 (DPA, 2001). Bijlaard (1957) presented a simple equation, which is also dependent on geometric properties and wave number, for determining the effective length (equation (22)).

$$L_e = 1.556\sqrt{ah}N\left[\sqrt{1+\frac{n^4h^2}{2a^2}}+\frac{n^2h}{\sqrt{3}a}\right]^{-\frac{1}{2}} \tag{22}$$

N and α are defined in the notation.

Elastic Tripping of Ring-Stiffeners

Tripping of ring-stiffeners is analogous to lateral-torsional buckling of columns under compression, the main differences being the radial load in ring-stiffeners that is in addition to the hoop stress, and the rotational constraint provided by the shell. The compressive radial load could lead to local buckling of the stiffener web, but it is small in comparison to the hoop load and is typically ignored for tripping calculations.

Tripping is resisted by the torsional and warping stiffness of the ring-stiffener, in addition to rotational constraint at the web-shell intersection. The degree of rotational constraint provided by the shell depends on the buckling mode being examined: for n=2 or n=3, the shell experiences little local interframe deformation and the stiffener is essentially clamped; for n>10, interframe buckling is dominant, the shell provides little rotational constraint, and the stiffener can be treated as pinned; and for intermediate values of n, the rotational constraint is somewhere between clamped and pinned (Morandi *et al.*, 1996B). Only the latter case will result in a stiffener tripping failure, as the former circumstances lead to overall and interframe buckling, respectively, with some associated out-of-plane deformation of the stiffeners. An isolated ring-stiffener would buckle with a wave number that increases with the degree of rotational constraint provided at the web toe (DPA, 2001).

Kendrick (1970) presented an energy-derived tripping stress for ring-stiffeners. Equation (23) is based on zero rotational constraint at the stiffener-shell intersection (i.e. a pinned stiffener). The minimum tripping stress is obtained using an axisymmetric buckling mode (n=0) for the assumed pinned boundary conditions.

$$\sigma_t = \frac{EI_z}{A_f a_1 x_f} \tag{23}$$

Faulkner (1991) also used an energy approach to determine the elastic tripping stress, but he included the effects of interaction with shell buckling via a rotational spring. Equation (24) includes terms associated with torsion, warping and the spring restraint, and must be minimized with respect to the circumferential mode, n.

$$\sigma_t = \frac{GJ + E\Gamma\left(\frac{n}{a}\right)^2 + k_{0n}\left(\frac{a}{n}\right)^2}{I_0 + \frac{k_{0n}}{\xi P_{m1}}\left(\frac{a}{n}\right)^2} \tag{24}$$

Morandi *et al.* (1996B) compared tripping stresses calculated according to equation (24) to those determined by linearized buckling analyses of three-dimensional numerical shell models. The authors found that Faulkner's equation is accurate for small values of n ($\leq$4), but inappropriate assumptions regarding the centre of rotation and web deformation result in inaccurate predictions for intermediate and large values of n.

Morandi *et al.* (1996B) used energy methods to derive a solution for the tripping stress including the effects of web deformation. The resulting system requires numerical solution; however, the authors have presented a simplified closed form solution in the form of a quadratic equation, the coefficients of which can be found in the reference. These authors have also presented knock-down factors for the inelastic tripping of stiffeners, which include the effects of residual stresses due to cold-bending and welding.

3.1.2 Classical Stress Analysis of Pressure Hulls

The geometries of ring-stiffened cylinders used in the construction of pressure hulls are typically proportioned such that yielding of the material occurs at a lower load than the critical elastic buckling pressure. It is therefore desirable to estimate the state of stress in critical regions of the pressure hull in order to predict the pressure causing yield to occur in these areas.

A simple approximation of the yield pressure is obtained by assuming the shell is not stiffened and is infinitely long. The so-called "boiler" pressure (equation (25)), sometimes referred to as P_{c2} in pressure hull analysis, is reached when the circumferential stress in the shell reaches the yield stress. The pressure causing the axial stress to reach yield in the same infinitely long cylindrical shell is twice the boiler pressure.

$$P_{c2} = \frac{\sigma_{yp} h}{a} \tag{25}$$

The deformation of a perfectly circular, uniformly stiffened cylinder is described by the following fourth order differential equation (Kendrick, 1970):

$$\frac{d^4 w}{dx^4} + \left(\frac{Pa}{2EI_c} \right) \frac{d^2 w}{dx^2} + \left(\frac{h}{I_c a^2} \right) w = \frac{P}{EI_c} \left(1 - \frac{\mu}{2} \right) \tag{26}$$

The second term in equation (26) is due to the axial load and causes the shell plating to act in a beam-column like fashion. At low pressures, the inclusion of this term results in expressions for deflection and stresses that are basically linear. However, when the applied pressure begins to approach the axisymmetric buckling pressure, including this term leads to increasingly non-linear expressions for deflection and stresses (see curve OAB in Figure 4). For most pressure hull geometries, axisymmetric stresses reach the yield stress at pressures significantly lower than the axisymmetric buckling pressure. Thus, the second term of the differential equation is often omitted when calculating elastic stresses.

Wilson (1956A/B/C; see also Kendrick, 1970) derived expressions, approximating the effect of the axial load term using a truncated Taylor series, for the external pressure causing the following stresses to reach the yield stress: 1) the stress in the circumferential direction on the outside of the plating midway between stiffeners (P_{c3}), 2) the stress in the circumferential direction at the mid-surface of the plating midway between stiffeners (P_{c5}), and 3) the stress in the longitudinal direction on the inside of the plating, adjacent to the stiffener (P_{c7}). The external pressure causing the mean stress in the plating at midbay to reach the von Mises yield criterion is called P_{c6}.

$$P_{c3} = \frac{h\sigma_{yp}}{a(1 + \gamma H)} \tag{27}$$

$$P_{c5} = \frac{h\sigma_{yp}}{a(1 + \gamma G)} \tag{28}$$

$$P_{c6} = \frac{h\sigma_{yp}}{a\sqrt{\gamma^2 G^2 + 1.5\gamma G + 0.75}} \tag{29}$$

$$P_{c7} = \frac{2h\sigma_{yp}}{a\left[1 + \gamma R\sqrt{\frac{12}{1 - \mu^2}}\right]} \tag{30}$$

γ, H, G, and R are defined in the notation.

Before the development of empirical design curves (see Section 3.2.3), which was only possible after a large amount of experimental data was produced and collected, axisymmetric yield pressures similar to those defined by the following equations were used in working stress design of pressure hulls. The observation that shell failures, even those occurring after the onset of yielding, resembled the classical (i.e. von Mises) elastic buckling shape led to the development of a semi-empirical knock-down factor on the shell yield pressure, P_{c3}. The resulting collapse pressure, P_{c4}, recognized the influence of low elastic buckling pressures on the actual elasto-plastic collapse pressure, and was the basis for many early pressure hull designs (Kendrick, 1955).

$$P_{c4} = \frac{P_{c3}}{1 + \left(P_{c2} \Big/ 2P_{m1} \right)^2} \tag{31}$$

The expression for the external pressure causing yield in the stiffener flange, P_{fy}, was developed in a similar manner to the shell yield pressures (Kendrick, 1970).

$$P_{fy} = \frac{h\sigma_{yf} a_f}{a^2 \left(1 - \frac{\mu}{2} - \gamma \right)} \tag{32}$$

Salerno and Pulos (1951) developed numerical, iterative solutions for the governing differential equation, including the full axial load term, arriving at more accurate solutions to the various shell and stiffener yield pressures given by Wilson.

3.1.3 Analytical Methods for Pressure Hulls with Imperfections

Geometric imperfections in the form of out-of-circularity are detrimental to pressure hull strength in two ways: 1) they introduce bending stresses that are in addition to the axisymmetric stresses, thus reducing the pressure causing yield to occur; and 2) they contribute to the nonlinear large-displacement behaviour of the structure, thereby decreasing the strength of structures failing in the elastic range as well. The standard methods used in design codes to account for the effect of OOC on overall collapse are summarized below.

The initial OOC of a pressure hull, w_0, can be described by a single term of the Fourier series in equation (8); i.e. in a form described by a single axial and circumferential wave number (Kendrick, 1985).

$$w_0 = C_0 \cos n\theta \sin\left(m\pi x \Big/ L_B \right) \tag{33}$$

The initial imperfection of equation (33) has been shown to be magnified under an applied pressure (Kendrick, 1953D), producing a normal displacement, w:

$$w = \left(\frac{P}{P_{cr,o} - P} \right) w_0 \tag{34}$$

where P is the applied pressure and $P_{cr,o}$ is the overall elastic buckling pressure, which can be taken as P_N (equation (21)), P_{cr} (equation (18)), or from a linearized numerical buckling analysis. Equation (34) results in displacements that become increasingly large as the elastic buckling pressure is approached. Kendrick related the displacement due to bending to a change in curvature, and finally to the bending stress in the stiffener flange, σ_{fb}.

$$\sigma_{fb} = \frac{\left(n^2 - 1\right) E e_f}{a^2} \left(\frac{P}{P_{cr,0} - P} \right) C_0 \cos n\theta \sin\left(m\pi x / L_B \right) \tag{35}$$

The total stress in the stiffener flange, σ_{fT}, is the sum of the bending stress, σ_{fb}, and the axisymmetric stress, σ_f, derived from equation (32).

$$\sigma_{fT} = \sigma_f + \sigma_{fb} = \frac{P}{P_{fy}} \sigma_{yf} + \frac{\left(n^2 - 1\right) E e_f}{a^2} \left(\frac{P}{P_{cr,0} - P} \right) C_0 \cos n\theta \sin\left(m\pi x / L_B \right) \tag{36}$$

Replacing σ_{fT} with σ_{yf} in Equation (36), and rearranging the terms to solve for the applied pressure leads to a quadratic equation, sometimes referred to as the Kendrick equation. The Kendrick equation is used to estimate overall collapse based on the applied pressure causing first yield of the frame flange, $P_{y(n)}$. The solution is minimized by computing values over a range of circumferential modes.

The form of the Kendrick equation presented below is a modified version of the SSP74 formulation (DPA, 2001). Equation (37) includes a simple method to account for the effects of residual stress. The early onset of stiffener yielding due to residual stress is simulated by multiplying the design pressure by a so-called residual stress factor, R_{sf}, which is essentially a safety factor accounting for residual stress. An accepted value of the residual stress factor is 1.333 (Pegg and Smith, 1987; BSI, 1980).

$$P_{y(n)} = \frac{Q - \sqrt{Q^2 - \dfrac{4\sigma_{yf}{}^2 P_{cr,o}}{P_{fy}}}}{2R_{sf} \dfrac{\sigma_{yf}}{P_{fy}}} \tag{37}$$

where:

$$Q = \left(n^2 - 1\right)\frac{EC_0 e_f}{a^2} + \sigma_{yf}\left[1 + \frac{P_{cr,o}}{P_{fy}}\right] \tag{38}$$

Under certain conditions, such as external frames and small values of OOC, overall collapse can be precipitated by yielding of the shell at the toe of the frame (MacKay, 2007A; MacKay, 2007B). The bending stress in the shell plating due to initial OOC can be found by replacing the distance from the combined section neutral axis to the frame flange, e_f, with the equivalent distance to the plating, e_p. Adding the bending stress to the average direct stress in the plating, and rearranging the terms, yields a solution for the pressure causing first yield in the plating, P_P (DPA, 2001):

$$P_P = \frac{-b' - \sqrt{b'^2 - 4a'c'}}{2a'} \tag{39}$$

where a', b', and c' are defined in the notation.

The treatment of overall collapse in Kendrick's equation is limited to first-yield failure criteria. The full elasto-plastic response of the structure must be handled by an incremental approach. Kendrick (1979) developed such a numerical procedure for determining the overall elasto-plastic collapse pressure of pressure hulls, which is included in at least one recent pressure hull design code (DPA, 2001).

Kendrick's (1979) analysis begins with a non-linear differential equation for a single ring frame and a single bay of shell plating, in which a harmonic out-of-circularity shape and residual stresses due to cold bending of the frame and plating are included. The equation can be solved for a given external pressure by finite differences. The pressure is increased until a solution can no longer be found; the last converged solution provides the collapse pressure of the ring frame and its plating, P_{co}. For a complete description of the elasto-plastic method for determining overall collapse, see Kendrick (1979), Smith and MacKay (2005), or SSP74 (DPA, 2001).

3.2 Traditional Design Methods for Pressure Hulls

3.2.1 General Design Approach

Traditional pressure hull design methods are deterministic in nature, and are based on classical elastic buckling and stress calculations. The strength-reducing effects – geometric imperfections, residual stresses, boundary conditions, etc. – are dealt with differently for interframe and overall collapse. Interframe collapse is predicted using empirical design curves, which inherently take the collapse mechanisms and fabrication processes of real pressure hulls into account. Analytical methods that account for geometric imperfections and residual stresses are used to calculate overall collapse pressures, based on the occurrence of first yield ($P_{y(n)}$) or by using the full elasto-plastic strength of the structure (P_{co}).

Kendrick (1982) presented an overview of externally loaded pressure vessel design criteria based on the BS5500 design code (BSI, 1980). The design methods outlined by Kendrick (or a slightly modified version) were used in many contemporary codes (e.g. ECCS, 1988) and are still standard practice today (e.g. DPA, 2001).

The BS5500 approach to design of pressure hulls is to proportion the structure such that: 1) interframe collapse is the critical failure mode, and 2) it is over-designed for overall collapse, which is difficult and computationally costly to predict accurately. Kendrick (1982) noted that the structural cost of avoiding failure by overall collapse is relatively small, and it is more economical to focus on predicting, and minimizing structural costs associated with, interframe failure of the shell.

The implementation of more rigorous overall elasto-plastic collapse methods (i.e. Kendrick's finite difference solution, P_{co}) has allowed at least one contemporary design code (DPA, 2001) to place roughly equal weight on interframe and overall collapse. This presents its own problems, as pressure hulls having similar predicted interframe and overall collapse pressures may have real collapse pressures that are significantly less than either of the calculated values. This so-called "failure mode interaction," or FMI, has been observed experimentally in at least one instance (Graham *et al.*, 1992).

FMI is attributed to large shell stresses due to overall bending of the combined ring-stiffener and shell plating that lead to shell yielding with the growth of overall displacements, and ultimately failure of the shell – collapse is "interframe, with overall tendencies" (Graham *et al.*, 1992). Graham *et al.* (1992) suggest that FMI can be avoided by ensuring that $P_{co} \geq 1.2 P_{ci}$. FMI has been addressed in SSP74 (DPA, 2001) by the inclusion of an interaction term, which reduces the flexural rigidity of the combined stiffener-shell based on P_{ci}, in the calculation of the overall elasto-plastic collapse pressure, P_{co}.

3.2.2 Design Safety Factors

The collapse predictions discussed in the following sections are related to the allowable working pressure of a pressure hull through deterministic safety factors that were developed through a combination of experiments and past experience with pressure hull design. Some design codes use a single safety factor to account for all uncertainties (e.g. BS5500), while other codes use a partial safety factor (PSF) approach (e.g. SSP74). Typical PSFs account for uncertainty in:

- design – i.e. uncertainties associated with the "strength model", including approximations in the analysis methods and uncertainties due to correlation of experimental data with analysis results (this PSF is unique to the type of failure being considered);
- construction – i.e. departures from specified design parameters and discrepancies between the as-built structure and the model; and
- operation – i.e. uncertainties in the loads, including accidental overloading and other discrepancies in the load estimation.

Safety factors are also required to account for other factors such as in-service damage (due to collision, corrosion, grounding, docking, etc.), high local stresses (at cone-cylinder intersections,

penetrations, secondary structure, etc.) and, for naval submarines, pressure loading from underwater explosions (Morandi *et al.*, 1998).

For the pressure hull structure, collapse pressures are typically determined for each of four failure modes: interframe collapse, overall collapse, dome-end collapse, and stiffener tripping. The allowable working pressure is determined by dividing the calculated collapse pressures by the appropriate factor(s), and minimizing with respect to the various failure modes.

3.2.3 Design for Interframe Collapse

Design for interframe failure is based on the use of an empirical curve for cylinders and cones, which was derived from a database of experiments (Kendrick, 1970) on uniformly ring-stiffened and plain cylinders with a maximum deviation from circularity of 0.5% of the mean shell radius. Interframe collapse is calculated for a single bay of shell plating, which is assumed to be simply supported at the ring-stiffeners. Conical shells are idealized as cylindrical shells.

The interframe design curve in BS5500 is associated with the lower bound of the experimental collapse pressures plotted against the elastic interframe buckling pressure (typically P_{m1}), with both axes normalized with respect to the shell yielding pressure for the perfect structure (typically P_{c5}). The lower bound curve is offset from the mean curve by 15%. This value was chosen to coincide with $P_{ci}=P_{m1}/2$ in the elastic region of the lower bound curve (i.e. $P_{m1}/P_{c5}<1$), which has been shown to be a good lower bound for elastic buckling of fabricated shells (Kendrick, 1970). The lower bound curve was found to be safe for all known experimental results at the time of its derivation.

The following expressions may be used to represent the lower bound empirical interframe design curve (see Figure 11), and are accurate to within 1% of the lower bound curve used in BS5500 (Pegg and Smith, 1987). The interframe collapse pressure used for design, P_{ci}, is determined using equation (40) or Figure 11.

$$\frac{P_{ci}}{P_{c5}} \cong \frac{P_{m1}}{2P_{c5}} \quad \text{for} \quad \frac{P_{m1}}{P_{c5}} < 1.0$$
$$\frac{P_{ci}}{P_{c5}} \cong 1 - \frac{P_{c5}}{2P_{m1}} \quad \text{for} \quad \frac{P_{m1}}{P_{c5}} \geq 1.0 \tag{40}$$

Interframe design undertaken following SSP74 is similar to the BS5500 procedure, except that the mean, rather than the lower bound, empirical curve is used (see Figure 11). SSP74 uses an updated mean curve (DPA, 2001), as additional experimental data has become available since the derivation of the BS5500 lower bound curve. There is significant scatter in the experimental data due to the broad range of geometries, materials and geometric imperfections; the interaction between elastic buckling and plastic collapse; and experimental error. As such, the lower bound of the interframe empirical collapse curve is offset from the updated mean curve by approximately 15-40% over the range of interest for typical pressure hulls. A PSF accounting for the experimental scatter has been adopted for use with the SSP74 mean curve.

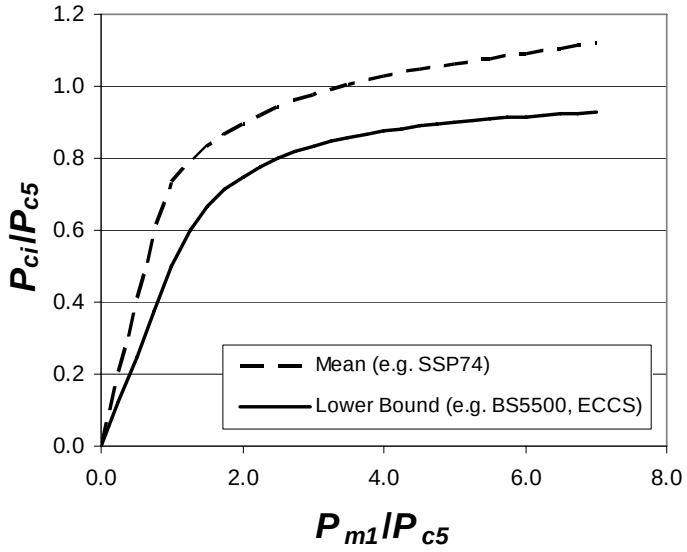

Figure 11: Empirical design curves for interframe collapse

The empirical methods used for prediction of interframe collapse and dome collapse, which follows a similar procedure, are examples of knock-down factor approaches. BS5500 prescribes a single safety factor of 1.5, which accounts for uncertainties in pressure hull construction and operation, in addition to the lower-bound knock-down factor, which can be regarded as an inherent safety factor on the strength model.

3.2.4 Design for Overall Collapse

The overall elastic buckling pressures, as presented by Bresse (1859) and Bryant (1954), are non-conservative estimates of the overall collapse pressure. In order to more conservatively calculate the actual collapse pressure, OOC and residual stresses due to fabrication procedures must be accounted for, as well as material plasticity. The requirement for design in BS5500 (BSI, 1980) is that the maximum stress in the ring-stiffener, σ_{fT}, must not exceed the yield stress at twice the design pressure (i.e. a safety factor of 2.0), with OOC at the maximum allowable amplitude and in the critical overall mode. This ensures that interframe failure occurs well before overall collapse, and takes into account the sensitivity of overall collapse to OOC. The safety factor for overall collapse of 2.0 applies to cold formed vessels, and can be reduced to 1.8 for hot formed, heat treated, or fabricated structures (BSI, 1980).

SSP74 (DPA, 2001) requires that both elastic overall yield pressures (i.e. the lower of $P_{y(n)}$ and P_P) and the elasto-plastic overall collapse pressure (P_{co}), divided by the appropriate PSF, exceed the design pressure. Compared with BS5500, this is a somewhat less conservative method of design for overall collapse, and is more likely to produce pressure hull designs with similar overall and interframe collapse pressures. Any detrimental effects associated with FMI are avoided in SSP74 by the use of an "interaction" knock-down term in the calculation of P_{co}.

3.2.5 Design for Stiffener Tripping

SSP74 (DPA, 2001) suggests criteria that typically result in conservative stiffener designs with regards to local stiffener failure. The criteria to prevent web buckling, f_1, flange buckling, f_2 and sideways tripping, f_3, are given by equation (41), (42) and (43), respectively. These formulae are based on past pressure hull design experience.

$$f_1 = \frac{d}{h_w}\sqrt{\frac{\sigma_{yf}}{E}} < 1.1 \tag{41}$$

$$f_2 = \frac{f}{2h_f}\sqrt{\frac{\sigma_{yf}}{E}} < 0.5 \tag{42}$$

$$f_3 = \frac{\sigma_{yf} A_f x_f a_1}{EI_z} = \frac{\sigma_{yf}}{\sigma_t} < 2.0 \tag{43}$$

Following traditional BS5500 (BSI, 1980) practice, the minimum tripping pressure is calculated according to equation (23), which assumes zero rotational support at the stiffener-shell intersection, and is required to exceed the yield stress:

$$\sigma_t > \sigma_{yf} \tag{44}$$

This requirement, which is twice as conservative as equation (43), is assumed to result in a tripping pressure that is greater than three times the allowable working pressure, ensuring this mode of failure does not govern the design (Kendrick, 1982).

More recent versions of BS5500 are less conservative (Morandi *et al.*, 1996B), requiring the tripping stress calculated according equation (23) to exceed the axisymmetric stress in the frame flange at the design pressure rather than the yield stress:

$$\sigma_t > \frac{P_d \sigma_{yf}}{P_{fy}} \tag{45}$$

SSP74 (DPA, 2001) requires a more rigorous assessment of the elastic tripping pressure for design, which includes the effects of web deformation and rotational constraint at the shell-stiffener intersection; i.e. similar to the method described by Morandi *et al.* (1996B).

3.3 Example Pressure Hull Analysis

The use of the analytical methods discussed in Sections 3.1 and 3.2 is demonstrated by application to real pressure hull structures with known collapse pressures. Two small-scale experimental pressure hull models (Figure 12) were considered: 1) model L300-No1, designed to

fail by interframe collapse, and 2) model L510-No1, designed to fail by overall collapse. The cylinders were constructed of extruded aluminium alloy tubing, with external T-section ring-stiffeners.

Figure 12: Experimental pressure hull models L300-No1 (left) and L510-No1 (right)

These cylinders form part of a larger testing program, which includes cylinders with various combinations of structural configuration (long and short cylinders, internal an external stiffeners), shell thinning (i.e. simulated damage due to corrosion and subsequent grinding), geometric imperfections and residual stresses. The goals of the experimental program are to establish a database of experimental collapse pressures to validate analytical and numerical methods for structural analysis, and to develop guidelines for corrosion tolerance on submarine pressure hulls (MacKay, 2007A; MacKay, 2007B).

Geometric and material parameters that were used in the calculation of analytical buckling pressures, stresses, etc, are summarized in Table 1. The cylinders were machined from extruded aluminium tubing. Tensile coupon tests have shown that significant anisotropy in the plastic region exists, with a yield strength that is greater in the axial direction (306 MPa) than the circumferential direction (272 MPa). The circumferential yield strength was used in the analytical calculations, the results of which are summarized in Table 2 and Table 3.

The cylinders after collapse testing are shown in Figure 13. Specimen L300-No1 displayed a ‘classical’ interframe buckling mode, with lobes alternating between adjacent bays. Specimen L510-No1 has clearly failed by overall collapse. The final deformed configuration makes it

difficult to assess the mode number, but strain gauge data indicate a dominant n=3 shape at the collapse pressure.

Table 1: Geometric and material properties for experimental cylinders

Parameter	**L300-No1**	**L510-No1**
h (mm)	2.5	3.0
a (mm)	111.25	111.5
L_B (mm)[1]	260 (250 for P_{cr})	470 (450 for P_{cr})
L_f (mm)	50	50
d (mm)	10.0	8.0
h_w (mm)	3.0	2.0
f (mm)	16.0	8.0
h_f (mm)	2.0	2.0
C_0 *(%a)*	0.07	0.07
E (MPa)	71350	71350
μ	0.3	0.3
σ_y (MPa)	272	272
R_{sf}	1.0	1.0

1. The bulkhead length of each cylinder for buckling calculations was taken as the overall length less the width of the thick end rings. This value was further modified for P_{cr} calculations to conform to the requirement of uniform stiffener spacing.

Table 2: Comparison of predicted and measured stresses for experimental cylinders

Stress[1] (MPa)	**L300-No1**		**L510-No1**	
	Predicted[2]	*Measured*	*Predicted*[2]	*Measured*
σ_3	40.0 - 48.0	43.3	34.9 - 37.8	33.8
σ_5	36.9 - 44.2	40.6	33.4 - 36.2	32.6
σ_6	32.0 - 38.3	36.4	28.9 - 31.3	28.6
σ_f	18.3 - 21.9	17.7	21.4 - 23.2	20.3

1. Indicated stresses were calculated for an applied pressure, and derived from strains measured at, 1±0.09 and 1±0.04 MPa for specimens L300-No1 and L510-No2, respectively.

2. Stresses are based on the corresponding linear yield pressures – P_{c3}, P_{c5}, etc.

These experimental specimens are ideal for comparing with the analytical linear stress and yield pressure predictions, as they are largely free of residual stresses (i.e. due to cold bending or welding) and have very little geometric imperfections (maximum OOC is less than 1/6th of the standard design value of 0.005a). The available strain gauge data were converted to stresses, and

compared to analytical stress predictions (Table 2). For the short specimen, the average measured stresses fell within the range of predicted stresses (based on the accuracy of pressure measurement) for all but one case. The average measured stresses for the longer cylinder fell slightly below the predicted ranges for all cases.

Table 3: Results of analytical calculations for experimental cylinders

	L300-No1		**L510-No1**	
	P (MPa)	*n*	*P* (MPa)	*n*
P_B	10.69	2	5.57	2
P_{m1}	15.06	9	23.61	8
P_{cr}	13.71	9	14.84	2
P_N	32.74	3	14.28	2
P_{c3}	6.18	N/A	7.47	N/A
P_{c5}	6.71	N/A	7.82	N/A
P_{c6}	7.73	N/A	9.03	N/A
P_{c7}	5.28	N/A	8.60	N/A
P_{fy}	13.54	N/A	12.18	N/A
$P_{y(n)}$	12.57	3	9.64	3
P_P	7.61	6	7.88	3
P_{co}	7.92	4	8.25	3
P_{ci} *(lower)*	5.21	9	6.53	8
P_{ci} *(mean)*	6.16	9	7.65	8
$\boldsymbol{P_{c,exp}}$[1]	**7.11**	**6-8**	**9.05**	**3**

1. Experimental collapse pressures are accurate to within ±0.09 and ±0.04 MPa for specimens L300-No1 and L510-No2, respectively.

The analytically calculated buckling, collapse and yield pressures, along with the experimental collapse pressures, for the two specimens are summarized in Table 3. Considering the typical design collapse pressures (i.e. P_{ci}, $P_{y(n)}$, P_P and P_{co}), the analytical calculations successfully predicted an interframe collapse for the short cylinder, while incorrectly predicting the same type of failure for the long cylinder.

Large shell stresses in the long cylinder led to overall collapse by way of shell yielding at the stiffeners, rather than interframe collapse. This speculation is supported by both elastic buckling ($P_N<P_{m1}$) and first yield ($P_P<P_{y(n)}$) calculations. The inaccurate prediction of the failure mode for the long cylinder is due to pessimistic empirical predictions for interframe collapse ($P_{ci(lower)}$, $P_{ci(mean)}$), which are based on a large body of tests with up to 0.5% OOC, compared to the overall predictions ($P_{y(n)}$, P_P, P_{co}), which have used the measured geometric imperfections (<0.1% OOC).

Figure 14 shows a comparison of the experimental collapse pressure for the short cylinder with the relevant interframe predictions. This chart clearly demonstrates the importance of shell yielding in interframe collapse, as well as the unconservative nature of the elastic buckling pressures, P_{m1} and P_{cr}. Figure 15 presents a similar chart for overall collapse of the long cylinder. The elastic buckling predictions, P_N and P_{cr}, overpredict the strength of the long cylinder, as do predictions based on stiffener yielding (P_{fy}, $P_{y(n)}$). The most pessimistic overall collapse predictions are the Bresse pressure, which is based on an infinitely long cylinder, and those accounting for yielding of the shell at the stiffener (P_P, P_{co}). The importance of shell yielding in this case of overall collapse is due to both the external location of the stiffeners and the small amount of initial OOC.

Figure 13: Experimental models L300-No1 (left) and L510-No1 (right) after collapse

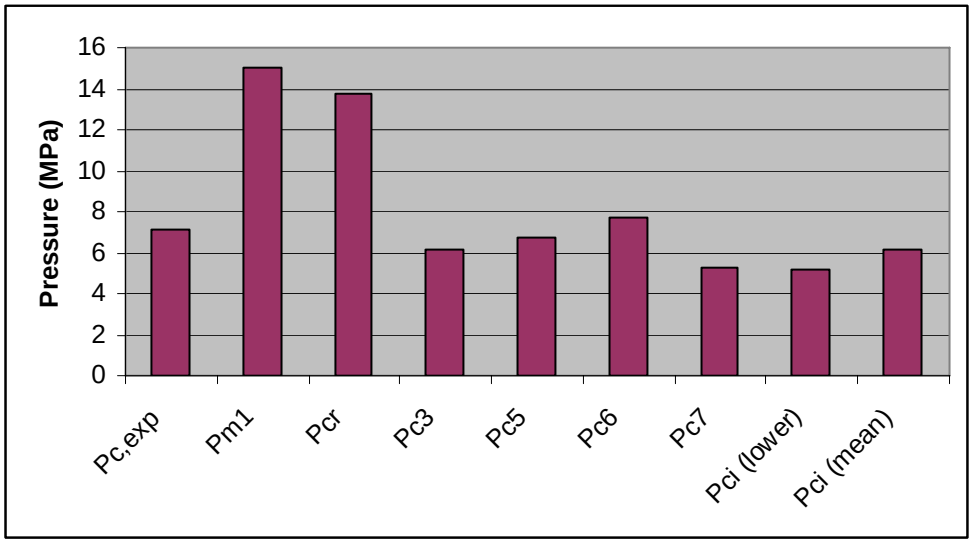

Figure 14: Comparison of predicted and experimental failure pressures for L300-No1

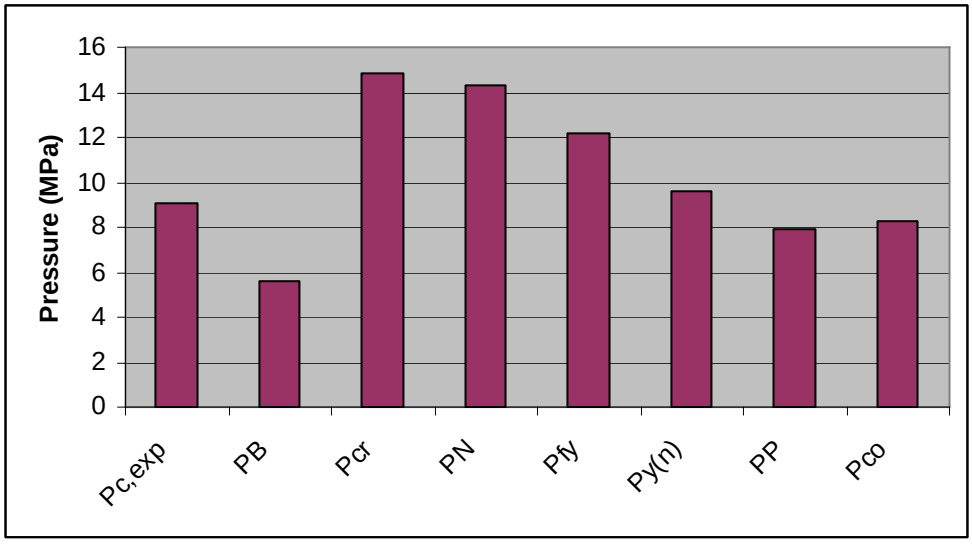

Figure 15: Comparison of predicted and experimental failure pressures for L510-No1

3.4 Discussion of Analytical Methods

The traditional pressure vessel design methods, as described in Sections 3.1 and 3.2, are conservative in many respects. For example, using the BS5500 (BSI, 1980) design rules, the allowable working pressures for the short and long cylinders described in Section 3.3 are 3.5 and 3.2 MPa, respectively. These values are based on the maximum allowable OOC (0.5%), and safety factors on interframe collapse and stiffener yielding equal to 1.5 and 1.8 (i.e. not cold formed), respectively. The experimental collapse pressures are approximately 2 and 3 times the allowable pressures for the short and long cylinders, respectively. This reflects both the general conservativeness of the BS5500 design methods, as well as the relative caution used when predicting overall as opposed to interframe collapse.

The experimental specimens considered in Section 3.3 tend to amplify the inherent conservativeness of the traditional design methods because they are relatively free of the geometric imperfections and residual stresses that exist in full-scale pressure hulls. Nonetheless, these examples serve to highlight the deficiencies of the traditional methods in dealing with real pressure hull structures, which often deviate from the ideal ring-stiffened cylinder (e.g. non-uniform frame spacing, dome bulkheads, conical sections, etc). These discrepancies are dealt with by idealizing the structure as a uniformly ring-stiffened cylinder with the most pessimistic geometry.

A layered conservativeness is built up throughout the traditional pressure hull design process, which has its roots in the necessity to analyze the simplest and most pessimistic geometry, which is, in turn, required due to the complexity of shell stability theory and the reliance on empirical design methods. The desire for more realistic estimates of the strength of real (i.e. complex) shell structures is the motivation for the inclusion of numerical methods in the shell design procedures (Teng, 1996; Schmidt, 2000; Arbocz and Starnes Jr, 2002; MacKay, 2005). These methods will be the focus of Section 4.

4 Computational Modeling of Buckling-Critical Shells

Computational modeling, synonymous with "numerical methods," is often used to predict the stability behaviour of buckling-critical shells. In fact, owing to advances in digital technology, computational modeling, particularly the finite element method, has become a standard tool for the analysis of structures in general (Moaveni, 2003). The complexity of the numerical stability analysis can range from a simple two-dimensional axisymmetric linearized buckling analysis to a full nonlinear collapse analysis of the three-dimensional structure, considering both large-deflection theory and material plasticity (i.e. nonlinear finite element analysis, or NLFEA).

Numerical methods are currently implemented in certain pressure hull design procedures. For example, linearized numerical buckling analyses are sometimes used in design to obtain a better estimate of the elastic buckling load for use in traditional design methods (e.g. Kendrick, 1982). Kendrick's (1979) elasto-plastic overall collapse method, which is based on a finite difference numerical solution, has been incorporated in SSP74 (DPA, 2001). Also, the BOSOR series of finite difference codes for axisymmetric shell structures (Bushnell, 1970, 1974, 1975) have been widely used to determine buckling loads and stresses in pressure hulls (e.g. Moradi and Parsons, 1993).

However, for most buckling-critical shell structures a comprehensive study of the accuracy of the more complex numerical methods (i.e. NLFEA) has not been undertaken (Schmidt, 2000). As such, these numerical methods are typically left out of design codes, and, indeed, the standardization of numerical modeling methods for reliably predicting the strength of buckling-critical shells is seen as a pressing need (Teng, 1996). Nonetheless, NLFEA is commonly used to predict and understand the behaviour of buckling-critical shells, and something of a consensus on appropriate modeling and solution procedures is emerging.

In general, three different types of static finite element analyses can be performed: 1) small deflection linear-elastic stress analysis, 2) linearized elastic buckling (i.e. eigenvalue) analyses, and 3) large deflection non-linear elasto-plastic collapse analysis. For shell structures, the linear-elastic stress and buckling analyses are typically performed on the perfect structure, allowing comparison with the classical buckling analyses. Non-linear collapse analyses are usually performed on more realistic models with either assumed or measured geometric imperfections and, if necessary, a nonlinear material model and allowance for the presence of fabrication-induced residual stresses.

The following sections provide an overview of the numerical methods for linear stress, linearized buckling and nonlinear collapse analyses, in general (Section 4.1) and in application to buckling-critical shell structures reported in the literature (Section 4.2). Various modeling and analysis techniques will be reviewed, and trends will be identified for buckling-critical shells.

4.1 The Finite Element Method

The finite element method is a technique used to solve boundary- and initial-value problems by dividing a domain into discrete sub-domains (i.e. elements) within which the unknown, or "state", variables are approximately defined. The function defining the state variables within an element

must match those of the adjacent elements at the shared nodes, which also define the element boundaries and shape. For structural mechanics problems, the domain is the structure, or portion of the structure, being studied and the state variables are typically the nodal displacements. The basic steps undertaken to formulate and solve a finite element problem are as follows (Kardestuncer, 1987), with specific reference to structural mechanics problems:

1. *Define the problem and its domain*: establish the physical and geometric extent of the problem, as well as the global coordinate system.

2. *Discretize the domain*: divide the structure into finite elements.

3. *Identify the state variables*: these are typically displacements for structural problems, but may also be forces. The state variables are related to the so-called flux (i.e. stress or strain, depending on the state variable) via the constitutive equation (e.g. Hooke's law for linear elastic behaviour), and the kinematic relationship between strains and displacements.

4. *Formulate the problem:* typically, the structural problem is defined by an integral equation (i.e. a functional) at the element level, for which approximate trial solutions are suggested (i.e. shape functions). The functional is minimized with respect to the state variables (i.e. displacements) at the element level, and the resulting relationships are summed up over the entire domain yielding a set of simultaneous equations. Dirichlet (displacement) and Neumann (force) boundary conditions are defined at this stage.

5. *Solve the set of simultaneous equations:* solution techniques may be direct (e.g. Gaussian elimination, Cholesky decomposition) or iterative (e.g. preconditioned conjugate gradient, Gauss-Seidel or Jacobi iterations). Linear systems may be solved in a single step using any of the aforementioned methods, while nonlinear systems require an iterative solution procedure (e.g. Newton-Raphson method).

6. *Interpret the results:* calculate stress and strain, estimate solution error, mesh convergence, etc.

The formulation of the structural problem in step 4 results in the following system of equations (Moaveni, 2003):

$$[K]\{u\} = \{f\} \tag{46}$$

[K] is referred to as the stiffness matrix, and is expressed in terms of the shape functions and their derivatives, {u} is the vector of displacements to be solved for, and {f} is composed of terms associated with the external load. This global relationship is built up by the addition of stiffness and force terms derived at the element level. The system of equations is solved for the unknown nodal displacements (and rotations for some structural elements – i.e. beams, plates and shells).

4.1.1 Linear Finite Element Analysis

Linear Stress Analysis

A linear static finite element stress analysis proceeds as described in the preceding section, with the formulation and solution of equation (46). For buckling-critical shells, linear stress analysis serves a dual purpose: 1) to examine the stress distribution under a static load – identifies regions of high stress and allows comparison to analytically calculated stresses; and 2) to calculate the geometric stiffness matrix for a subsequent linearized elastic buckling analysis (see below).

Linearized Buckling Analysis

The critical elastic buckling load of a structure can be estimated by a linearized finite element buckling analysis, which is performed in two stages. Initially, some unit or typical value of external load is applied to the structure and a linear-elastic small deflection analysis is undertaken. The second stage of the buckling analysis is the solution of the eigenproblem.

Elastic buckling is a variation of the standard eigenproblem analysis, which determines the stability of a system by investigating the possibility of bifurcation behaviour occurring at a critical load due to a small perturbation to the system. For an elastic buckling analysis, the eigenproblem is defined with respect to the tangent stiffness matrix, $[K_T]$, which is analogous to the second variation of the potential energy. Critical points, either bifurcation or limit points, are indicated by zero eigenvalues:

$$[K_T]\{\phi\} - \lambda\{\phi\} = 0 \tag{47}$$

The vector, $\{\phi\}$, and coefficient, λ, are called the eigenvector and eigenvalue, and are analogous to the buckling mode shape and the buckling load factor, respectively. Equation (48) shows that the tangent stiffness matrix is composed of the linear-elastic stiffness matrix, $[K_0]$, which is load-independent, and the initial displacement and stress matrices, $[K_L]$ and $[K_\sigma]$, respectively, which are both related to the applied load (Moradi and Parsons, 1993)).

$$[K_T] = [K_0] + [K_L] + [K_\sigma] \tag{48}$$

The tangent stiffness matrix can be "linearized" by assuming a linear relationship for the initial displacement and stress matrices, with respect to a small pre-load, δp, and the load under consideration, p:

$$[K_T] = [K_0] + \frac{p}{\delta p}\left([K_L] + [K_\sigma]\right) \tag{49}$$

Thus, the "linearized" eigenproblem takes the form of equation (50):

$$[K_0]\{\phi\} + \lambda\left([K_L] + [K_\sigma]\right)\{\phi\} = 0 \tag{50}$$

where $[K_L]$ and $[K_\sigma]$ are evaluated at the pre-load step, δp. The eigenvalue, λ, is the factor by which the preloading condition, δp, must be multiplied in order to satisfy equation (50) (i.e. for buckling to occur in the particular mode shape defined by $\{\phi\}$).

An alternative linearization of the eigenproblem involves the assumption that the displacements at the pre-load step are small, and thus $[K_L]$ can be neglected. This results in the eigenproblem defined by equation (51).

$$[K_0]\{\phi\} + \lambda[K_\sigma]\{\phi\} = 0 \tag{51}$$

For a single discretized eigenproblem, there exists N eigenvalues, where N is the order of the linear stiffness matrix (Bathe, 1982). The lowest (or group of clustered lowest) of these eigenvalues is of primary interest, as this value represents the critical elastic buckling load factor for the structure. This value is approximately equivalent to the classical elastic buckling pressure.

It should be noted that the linearization of the tangent stiffness matrix is not restricted to linear analyses, and can be undertaken after any static analysis – i.e. after a nonlinear incremental analysis as described in the following section. A linearized buckling analysis performed after each increment of a nonlinear analysis can be used to identify the approach of a limit point or the occurrence of bifurcation of the equilibrium path (Shi, 1996).

4.1.2 Nonlinear Finite Element Analysis

Linearized buckling analyses, as described in Section 4.1.1, are suitable for predicting the critical load of structures that fail in the linear load-displacement range and before material plasticity or large deflections occur. However, for pressure hulls and many other buckling-critical structures, nonlinear behaviour occurs as a combination of large deflections/rotations and material plasticity; the structural behaviour may also be further complicated by bifurcation buckling instability. Static non-linear finite element analysis is performed in order to determine the maximum magnitude of loading such a structure can sustain before the occurrence of instability or collapse (Bathe, 1982).

The nonlinear solution is typically arrived at by:

- accounting for the effects of large displacements and/or nonlinear material, via the nonlinear formulation and material model, respectively;
- incremental application of the load; and
- iterative solution of the nonlinear system for each increment via equilibrium of the internal and external forces.

Common approaches for dealing with these nonlinear considerations are reviewed below.

Nonlinear Geometry (Large Displacements)

Buckling-critical shells exhibit nonlinear load-displacement behaviour, even in the elastic range of the material, due to large displacements and rotations, which are the result of bending stresses associated with initial geometric imperfections and beam-column behaviour of the shell. Three common methods for including nonlinear geometric behaviour – associated with large displacements – in finite element analyses are (Ramm and Stegmüller, 1982; Knight Jr. *et al.*, 1995):

1. *Lagrangian approach*: the deformed configuration is defined with respect to the initial undeformed configuration. This approach requires the inclusion of the nonlinear strain-displacement relationships in the element formulation to account for large displacements.
2. *Updated Lagrangian approach*: the deformed configuration is defined with respect to an updated geometry (typically, the previous increment). Linear strain-displacement relationships can be used in combination with incremental application of the load to take account of large displacements, as well as to trace the full load-displacement history.
3. *Corotational* approach: the reference frame moves and rotates with the element, and rigid body motion is separated from strain-producing deformation. For small displacements and rotations, linear strain-displacement relationships may be used (low-order approach). Either nonlinear strain-displacement relationships, or a refined mesh, can be used if large displacements occur (high-order approach).

Nonlinear Material

Some buckling-critical shells, such as pressure hulls, fail by elasto-plastic collapse. For most materials, the modulus, and hence the stiffness of the structure, is significantly reduced after yielding. As such, the nonlinear material behaviour is an important factor in the determination of the ultimate load of structures failing inelastically. The nonlinear behaviour of a material is described by the plasticity theory (e.g. flow theory vs. deformation theory), yield criterion (i.e. yield surface) and hardening rule.

Plasticity Theories

The flow theory of plasticity differs from deformation theory in that it assumes that plastic strain rate, rather than plastic strain, is determined by the instantaneous stress. The former treatment of plasticity is generally accepted to be the most analytically correct; however, comparisons between experiment and numerical calculations for buckling-critical structures are in better agreement when calculations are based on the deformation theory (Teng, 1996). Nonetheless, flow theory is chosen over deformation theory for most numerical analyses of buckling-critical shells (see 4.2.2).

Yield Criteria

The yield criterion defines the allowable state of stress for a material. The yield surface is defined in the principal stress space, whereby combinations of principal stresses falling within the surface are allowable; yielding is indicated by a stress state on the surface itself. In general, a yield surface is defined by the function, f, taken equal to zero:

$$f = \sigma_e - \sigma_0 = 0 \tag{52}$$

σ_e is the equivalent stress, a function of the principal stresses, and σ_0 is the reference stress, typically taken as the yield stress of the material. A common yield criterion is associated with von Mises, and is represented by a cylinder in the 3-D principal stress space (Crisfield, 1997):

$$f_m = \sqrt{\frac{1}{2}\left[(\sigma_1 - \sigma_2)^2 + (\sigma_2 - \sigma_3)^2 + (\sigma_3 - \sigma_1)^2\right]} - \sigma_0 = \sqrt{3J_2} - \sigma_0 = 0 \tag{53}$$

σ_1, σ_2 and σ_3 are the principal stresses. J_2 is the second invariant of the deviatoric stresses, and thus flow theory using the von Mises yield criteria is also referred to as J_2 flow theory. The von Mises yield criteria is related to Tresca's yield criteria, which is based on the assumption that a metal yields when the maximum shear stress, τ_{max}, surpasses the shear stress associated with the uni-axial tensile strength; i.e. half the yield stress (Hibbeler, 1997):

$$f_t = \tau_{\max} - \sigma_0 / 2 = (\sigma_1 - \sigma_3) - \sigma_0 = 0 \tag{54}$$

The von Mises yield criteria is more popular than Tresca's, however, because it is a continuous function, rather than having corners, and is thus relatively simple to implement in numerical codes. The von Mises yield surface passes through the corner points of the Tresca surface, and, as such, the two criteria define yielding of metals in a similar manner.

The Von Mises and Tresca yield surfaces are for isotropic materials. Hill extended von Mises' yield criterion to anisotropic materials. Hill's yield criterion (equation (55)) is defined in terms of material constants (F, G, H, etc) related to the principal axis yield strengths (Crisfield, 1997).

$$\begin{aligned} f_h &= F(\sigma_{yy} - \sigma_{zz})^2 + G(\sigma_{zz} - \sigma_{xx})^2 + H(\sigma_{xx} - \sigma_{yy})^2 \\ &+ 2L\sigma_{yz}^2 + 2M\sigma_{xz}^2 + 2N\sigma_{xy}^2 - 1 = 0 \end{aligned} \tag{55}$$

Jansson *et al.* (2005) have found the use of Hill's yield criteria to be ineffective at predicting yield in some highly anisotropic materials, such as extruded or rolled metals, and have suggested that more rigorous treatment of anisotropy is required. They have suggested that an eight-parameter anisotropic yield model developed by Barlat *et al.* (2003) results in the best correlation with biaxial yielding in experimental shell specimens. For shells or plates, the eight material parameters are derived using three uniaxial tension tests (in the principal directions of anisotropy and at 45 degrees) and some type of biaxial stress test whereby the biaxial stresses are known.

The biaxial stress test is typically a balanced biaxial tension test (i.e. equal stresses in orthogonal directions) performed on a plate sample. This type of test is difficult to perform on a tube structure without damaging or otherwise affecting the material, and so Jansson *et al.* (2005) have suggested that the biaxial stress test for extruded tubes can be based on an internal pressure test –

the “hydro-bulge” test. Simulation of a hydro-bulge test on an extruded aluminium tube by nonlinear numerical analysis using the Barlat *et al.* (2003) yield function, in combination with the material parameters developed by Jansson *et al.* (2005), showed accurate prediction of yield onset; whereas, the Hill yield function over-predicted the yield pressure by nearly 50% (Jansson *et al.*, 2005).

For shell elements, the in-plane material plasticity is addressed via the numerical integration; however, the through-thickness plasticity due to bending must be accounted for by, either, multiple through-thickness integration (i.e. layered elements) or the use of stress resultants (Ramm and Stegmüller, 1982). When modeling shell structures using solid elements, multiple through-thickness elements are required to account for through-thickness stress and plasticity variation.

The layered approach to shell element plasticity is used in combination with yield functions of the form of equation (53), e.g. von Mises, Tresca, Hill yield functions. The alternative is to define the yield surface using stress resultants, as in the Ilyushin yield function (Crisfield, 1997):

$$f_i = \sqrt{\frac{\overline{N}}{t^2} + \frac{4s\overline{P}}{t^3\sqrt{3}} + \frac{16\overline{M}}{t^4}} - \sigma_0 = 0 \tag{56}$$

$\overline{N}$, $\overline{P}$, $\overline{M}$ and *s* are functions of the force and moment stress resultants (equation (57)), and *t* is the shell element thickness.

$$\begin{aligned}
\overline{N} &= N_x^2 + N_y^2 - N_x N_y + 3N_{xy}^2 \\
\overline{M} &= M_x^2 + M_y^2 - M_x M_y + 3M_{xy}^2 \\
\overline{P} &= N_x M_x + N_y M_y - 0.5N_x M_y - 0.5N_y M_x + 3N_{xy} M_{xy} \\
s &= \frac{\overline{P}}{\left|\overline{P}\right|} = \pm 1
\end{aligned} \tag{57}$$

The Ilyushin yield criterion described by equation (56), like Tresca’s criterion, has corners and is thus difficult to implement in numerical codes. It can be simplified as a hyperellipse, which avoids the corners but adds some inaccuracies due to the approximation (Skallerud *et al.*, 2001).

Stress resultant yield theories, such as Ilyushin’s, have the advantage of being less computationally expensive than through-thickness integration; however, they do not pick up first-fibre yield, and care must be taken when using multi-linear material models and for cases of combined bending and compression (Skallerud *et al.*, 2001).

Hardening Rules

Once plasticity has occurred, strain hardening theories allow stress to be further increased by permanently extending the yield surface. The two main types of hardening are referred to as isotropic and kinematic hardening, and are defined in relationship to the Bauschinger effect, illustrated in Figure 16. Isotropic hardening ignores the Bauschinger effect by allowing post-yield stress reversals up to twice the initial maximum stress, while kinematic hardening models limit the total stress reversal to twice the yield stress before yielding occurs in the opposite direction (Crisfield, 1997).

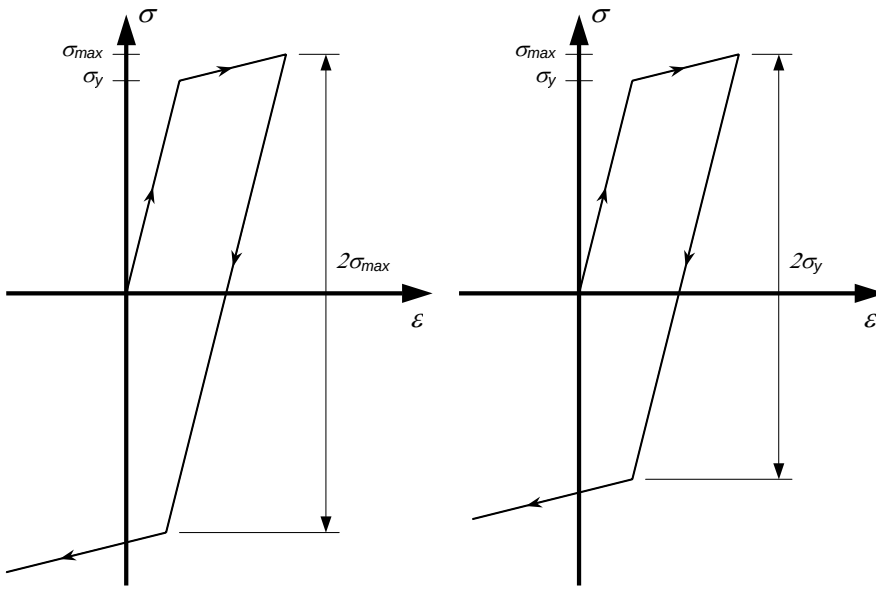

Figure 16: Isotropic (left) and kinematic (right) hardening for a bi-linear material

Figure 16 shows hardening models for bi-linear material behaviour, but multi-linear stress-strain relationships are also used in numerical models for particularly nonlinear material behaviour. Multi-linear stress-strain curves can be derived using the so-called 'overlay' or Besseling model. Overlay material models involve the superimposition of elastic and elastic-perfectly-plastic material curves; each of these overlays is weighted in order to achieve the desired nonlinear material behaviour (Crisfield, 1997). Overlay models intrinsically incorporate kinematic hardening, with the bi-linear version strictly adhering to the Bauschinger effect as shown in Figure 16.

Solution Path Following Schemes

While it is technically possible to solve the nonlinear system in a single load step, the load is typically applied incrementally, for one or more of the following reasons: 1) the nonlinear strain-displacement relationships have not been implemented, 2) yielding of the material is expected, or 3) the full load-displacement history is required. There are several common methods used to

follow the nonlinear solution path (i.e. the load-displacement relationship) (Ramm and Stegmüller, 1982; Knight Jr. *et al.*, 1995):

1. *Load control*: the applied load is specified and applied incrementally. This results in a singular tangent stiffness matrix at limit points (i.e. snap-through behaviour), and thus the post-collapse load-displacement relationship cannot be investigated.
2. *Displacement control*: a displacement component is controlled, with calculation of the corresponding load factor. Limit points are surmountable using this method, but not snap-back behaviour (i.e. displacement reversal). Displacement control requires pre-analysis knowledge of the appropriate displacement component to control.
3. *Arc length method*: an extension of displacement control, whereby the load factor is related to the generalized displacements via a constraint equation that requires convergence to occur within a specified load-displacement "arc". The arc length, or Riks (1979), method allows both snap-through and snap-back behaviour to be traversed.

Nonlinear solutions obtained through incremental application of the loads or displacements are called "pseudo-static" analyses due to the similarity with time-stepping procedures used in transient analyses.

Iterative Solution of the Nonlinear System

The nonlinear solution is achieved by balancing the internal and external forces at a given increment:

$$\{f^{in}\} = \{f^{ext}\} \tag{58}$$

$\{f^{in}\}$ is the internal force vector, which is a function of the displacement vector, $\{d\}$, and $\{f^{ext}\}$ is the external force vector, which is a function of the load factor, λ. The imbalance between the external and internal force vectors is referred to as the residual force vector, $\{r\}$.

A Newton-Raphson approach is typically employed to solve the nonlinear system described by equation (58) (Knight *et al.*, 1995). The Newton-Raphson method is based on a linearization of the system at each load increment, followed by iterative solution of the resulting system:

$$\begin{aligned} [K_T]\{\delta d\}_{i+1}^{k+1} &= \{r\}_{i+1}^{k} \\ \{d\}_{i+1}^{k+1} &= \{d\}_{i+1}^{k} + \{\delta d\}_{i+1}^{k+1} \end{aligned} \tag{59}$$

i and k are the load step or increment and iteration numbers, respectively. The tangent stiffness matrix, $[K_T]$, and the residual force vector, $\{r\}$, are used to compute the iterative displacement change, $\{\delta d\}$, which is then added to the displacement matrix from the previous iteration. The force balance is checked after each iteration with iteration continuing until a specified convergence criterion is met.

There are several options for updating the tangent stiffness matrix during the nonlinear solution procedure, the most common of which are listed below (Ramm and Stegmüller, 1982; Knight Jr. *et al.*, 1995):

1. *Full Newton-Raphson method*: the tangent stiffness matrix is updated before each iteration.
2. *Modified Newton-Raphson*: the tangent stiffness matrix is updated at the beginning of the load step only.
3. *Linear-elastic method*: the stiffness matrix is computed at the beginning of the first load step only.

The latter methods of updating the tangent stiffness save computations during the iterative solution, but may lead to the requirement for many additional iterations, compared to the full Newton-Raphson method, before convergence is achieved.

4.1.3 Finite Elements

In general, the behaviour of buckling-critical shell structures can be described assuming the occurrence of small to moderate strains, moderate to large rotations, and large displacements (Ramm and Stegmüller, 1982; Skallerud *et al.*, 2001). The effects of deformations are accounted for by the nonlinear formulation, as described above, and/or in the element-level strain-displacement relationships. The general types of finite elements available, rather than specific element formulations, will be covered in this section. Typically, and intuitively, finite elements derived from structural shell theory are used for modeling shell structures; however, solid (continuum) elements will also be briefly discussed.

Shell Elements

There are two general theories behind thin shell element formulations (Ramm and Stegmüller, 1982; Knight Jr. *et al.*, 1995):

1. *Classical concept (C^1 formulation)*: discretization of the thin structural shell theory, which idealizes a 3D structure as 2D, based on thin shell assumptions (Kirchhoff-Love hypothesis).
2. *Degeneration concept (C^0 formulation)*: direct discretization of the 3D continuum, while making shell assumptions in parallel. Shear deformations are allowed, and displacement and rotation are independent.

In nonlinear analyses, the classically derived shell elements have difficulty representing rigid body modes for large rotations and interelement compatibility is also an issue. The use of isoparametric degenerated elements addresses both of these problems; however, these types of elements are susceptible to “locking”, due to the numerical integration, which leads to an artificially stiff structure (Ramm and Stegmüller, 1982; Knight Jr. *et al.*, 1995). Element locking can be eliminated by the use of reduced integration schemes, which, in turn, present the problem of hour-glass or spurious deformation modes, but several methods of dealing with this issue are available (Reid, 1998).

In general, reduced integration schemes, in combination with a method of hour-glass control, are required for thin or curved shell elements, or elements with a small number of nodes – see Table 4 (Ramm and Stegmüller, 1982). Some higher order elements, for example the 16 node Lagrange

element, are not prone to locking and thus do not require reduced integration; however, such elements are computationally expensive and not considered practical for most applications.

Table 4: Integration requirements for various shell elements (Ramm and Stegmüller, 1982)

		Tendency of the fully integrated element to:		Reduced integration is required if:
		Shear locking	**Membrane locking (curved elements)**	
Serendipity elements	12-node 	High	Low	Thin
	8-node 	High	High	Curved, thin
Lagrange elements	16-node 	Low	Low	Unnecessary
	9-node 	Low	High	Curved
S/L	4-node 	Very high	Very high	Always

Solid Elements

An alternative to using structural shell elements is the use of solid, or continuum, elements. The requirement of maintaining reasonable element aspect ratios, combined with thin-shell geometry, results in a large number of elements for typical shell structures. This is especially pronounced if multiple through-thickness elements are required to model, for instance, bending-induced material yielding. In addition to being computationally expensive due to a relatively large number of elements, solid modeling of shell structures may also lead to ill-conditioned systems of equations due to small through-thickness shell deformation, leading to difficulties obtaining a solution (Ramm and Stegmüller, 1982).

4.2 Computational Modeling of Buckling-Critical Shells – Current Practice

Many papers that address the current and future trends of various aspects of buckling-critical shell analysis have been published since the use of computational methods has become widespread (e.g. Ramm and Stegmüller, 1982; Moradi and Parsons, 1993; Knight Jr *et al.*, 1995; Morandi *et al.*, 1996A; Shi, 1996; Teng, 1996; Choong and Ramm, 1998; Rotter, 1998; Schmidt, 2000; Arbocz and Starnes Jr, 2002). While many of these papers also report on general design methods and considerations for buckling-critical shells, each has the stated or unstated goal of accurate nonlinear numerical predictions for shell strength. In addition to these review papers, many nonlinear numerical analyses of specific buckling-critical shell structures have been reported (Table 14 in Annex A).

The studies listed in Table 14 cover a wide variety of shell structures and failure modes, thus allowing the general trends for nonlinear numerical analysis of buckling-critical shells to be identified. The following sections summarize the recommendations of previous reviewers and trends observed from practical analyses (Table 14).

4.2.1 Geometric Modeling

Structural Modeling

Not surprisingly, shell elements, rather than solid elements, are widely used to model shell structures. Three-dimensional structural modeling using quadrilateral shells or plates (either 4- or 8-node) is favoured over two-dimensional axisymmetric models (see Table 14 and Table 5). Element formulation is not always noted by the authors, but when it is, degenerative rather than classical formulations are most common.

Table 5: FE modeling methods for buckling-critical shell structures: trends

Topic	Trend or Recommendation	Sources
Structural modeling	1) 3-D modeling, 4- or 8-node shells 2) 2-D axisymmetric modeling with shells	1) Ramm and Stegmüller, 1982; Creswell and Dow, 1986; Guggenberger, 1995; Knight Jr *et al*., 1995; Morandi *et al.*, 1996A; Lennon and Das, 1997; Choong and Ramm, 1998; Bisagni, 2000; Holst *et al.*, 2000; Arbocz and Starnes Jr, 2002; Barlag and Rothert, 2002; Wullschleger and Meyer-Piening, 2002; Aghajari *et al.*, 2006 2) Ross and Johns, 1998; Berry *et al.*, 2000; Zhao and Teng, 2004
Characteristic geometric imperfections	1) Assumed (classical buckling mode, axisymmetric, etc.) 2) Eigenmode- or collapse-affine[1]	1) Creswell and Dow, 1986; Guggenberger, 1995; Berry *et al.*, 2000; Şanal, 2000; Barlag and Rothert, 2002 2) Zhao and Teng, 2004; Schneider and Brede, 2005
Measured geometric imperfections	1) Fourier series 2) Splines 3) Linear or no interpolation	1) Graham *et al.*, 1992; Arbocz and Starnes Jr, 2002; Arbocz and Starnes Jr, 2004 2) Keron et al, 1997 3) Wullschleger and Meyer-Piening, 2002; Zhao and Teng, 2004
Material model	Isotropic von Mises yield criterion, with associated flow rule	Ross and Johns, 1998; Barlag and Rother, 2002; Fukuda *et al.*, 2003; Zhao and Teng, 2004, Schneider and Brede, 2005

1. Eigenmode-affine refers to a characteristic imperfection based on a linearized buckling analysis of the perfect finite element model. Collapse-affine refers to a characteristic imperfection based on the post-peak shape from a nonlinear collapse analysis of the perfect finite element model.

Knight Jr *et al.* (1995) performed parametric studies on shell elements to determine their effectiveness for shell elastic buckling problems. The authors found that biquadratic (8- or 9-node) shell elements are superior to bilinear (4-node) elements for similar meshes; in addition, nonlinear strain-displacement relationships at the element level were recommended for problems that include large rotations.

Mesh Structure

The structure of the finite element mesh – density and pattern – has a significant influence on the subsequent prediction of buckling or collapse load and mode (Arbocz and Starnes Jr, 2004). The mesh should be able to accurately represent the shape of both the anticipated mode of failure and any geometric imperfections (Wullschleger and Meyer-Piening, 2002). Meshes from the literature were, whenever possible, arranged such that the shell element boundaries lined up with the orthogonal cylindrical axes – that is, highly structured "checkerboard" patterns were favoured.

Mesh convergence studies account for the discretization error in finite element models by successively reducing the element size until the solution is converged to a reasonable tolerance. Common practice for ensuring suitable mesh density is a convergence criterion of 1% after halving a characteristic dimension of the element (e.g. Berry *et al.*, 2000). Other studies have used convergence on a well-known analytical value as the criteria; for example, comparison of linearized buckling predictions with classical elastic buckling loads (Bisagni, 2000; Arbocz and Starnes Jr, 2004). Arbocz and Starnes Jr (2003) suggest that an accepted practice for good convergence for buckling problems is the use of five mesh points per buckling half-wave.

Sometimes other considerations affect the choice of element mesh; for example, Arbocz and Starnes Jr (2002) structured the shell element mesh such that the in-plane integration point spacing was on the order of the grid used to measure imperfections. This allowed the measured imperfections to be easily transferred to the model without interpolation. Conversely, Zhao and Teng (2004) based the measurement grid for imperfections on pre-analyzed FE models developed for a mesh convergence study, resulting in a one-to-one node-to-measurement correlation. The point of both methods was to ensure compatibility of the finite element mesh with the geometric imperfection measurement grid.

Modeling the Nominal Structure

Mid-plane representation of the shell is the obvious choice for cylindrical tubes, which make up a large portion of the numerical studies for buckling-critical shells. However, for the so-called "branched" shells (e.g. ring-stiffened cylinders), the treatment of the intersection or junction can be important. Sridharan and Alberts (1997) compared linearized and nonlinear elastic buckling predictions for axisymmetric shell and solid finite element models of ring-stiffened cylinders. Those authors found that: 1) the treatment of the shell-stiffener intersection is important for moderately thick and thick cylinders ($a/h<150$), and 2) connection of the mid-planes of the shell and stiffener was superior to connection of the stiffener to the inside/outside of the shell. The conclusions of Sridharan and Alberts (1997) are based on comparison to the solid element models, which were assumed to be the most accurate.

The connection of shell mid-planes results in a "double" area at the shell-stiffener intersection. This could be corrected by attaching the stiffeners to the appropriate inner/outer face of the shell,

which is possible by a modification to the basic element formulation. The effect of this offset on the shell behaviour is not well known, but it has been reported to have only a small influence on pressure hull buckling pressures (Morandi *et al.*, 1996B).

Offset shell elements may be useful in situations where eccentricities between adjacent shells exist, such as the case of one-sided thinning of pressure hulls due to corrosion damage and subsequent grinding (MacKay, 2007A, 2007B). An alternative method of modeling an abrupt eccentricity is the use of layered shell elements with zero stiffness in the layer representing the non-existent material.

Modeling Geometric Imperfections

The incorporation of geometric imperfections into numerical models of buckling-critical shells can be divided into two broad categories (see Table 5 and Figure 17): 1) characteristic imperfections, derived from typical or pessimistic configurations; and 2) measured imperfections, based on direct measurement of the structure being analyzed.

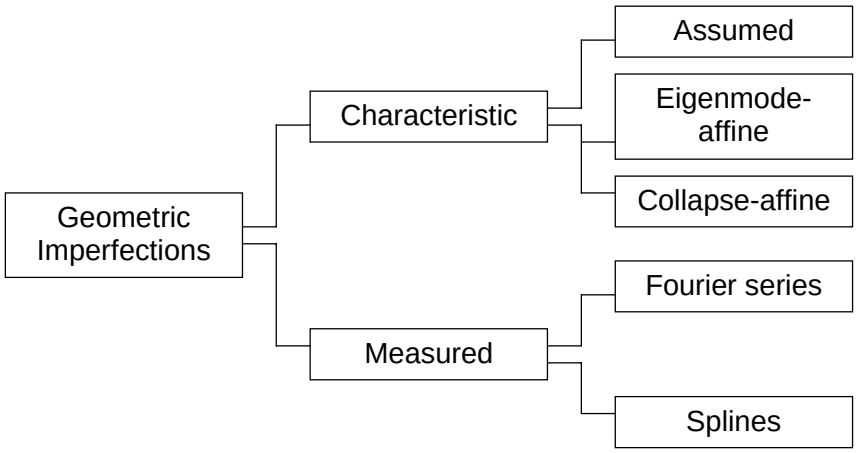

Figure 17: Numerical modeling of buckling-critical shells with geometric imperfections

Characteristic geometric imperfections are usually relatively simple to describe. They are sometimes assumed to be in the form of the critical buckling mode from a classical analysis; for cylindrical shells, these assumed imperfections tend to take the form of equation (8). Alternatively, the characteristic imperfection may be based on an initial analysis of the perfect finite element model by using either the critical mode from a linearized buckling analysis ("eigenmode-affine") or the post-peak shape from a nonlinear collapse analysis ("collapse-affine").

Eigenmode-affine imperfections, derived using either a linear or nonlinear prebuckling analysis, tend to be the worst case, especially if collapse is dominated by geometric, rather than material, nonlinearity (Schneider and Brede, 2005). There are several sources of caution that must be heeded when using eigenmode-affine (and collapse-affine) imperfections (Schmidt, 2000):

- the choice of imperfection shape may not be straightforward, as several eigenmodes sometimes cluster around a single eigenvalue;

- eigenmode-affine patterns tend to be multi-wave and continuous, but single dimple imperfections may be worse;
- eigenmode-affine imperfections may not be likely to occur in practice; and
- eigenmodes can only provide an imperfection shape, leaving the amplitude, which is just as important, to be prescribed by another method, such as the use of fabrication tolerances.

Another method of determining the characteristic imperfection was described by Schmidt (2000), in his state-of-the-art report for stability design of steel shell structures. This numerical technique inherently searches for and finds the "definitely worst" geometric imperfection shape by including extra degrees of freedom, associated with the imperfection, at the shell element nodes. The problem is thus defined by a variable reference geometry, and algorithms have been developed that lead to the most pessimistic, or "definitely worst", imperfection shape (i.e. the lowest possible limit load). The results of such an analysis would have to be studied carefully to ensure that the resulting imperfection mode is at least possible, if not probable.

Application of measured geometric imperfections (e.g. radii or eccentricities) can be undertaken by either: 1) enforcing the measured values at coinciding node-measurement locations, with some form of interpolation for intermediate nodes, or 2) positioning of nodes based on curve fitting of the measurement data. The first method is most common for cylindrical shells (e.g. Graham *et al.*, 1992; Arbocz and Starnes Jr, 2002; Arbocz and Starnes Jr, 2004; Wullschleger and Meyer-Piening, 2002; Zhao and Teng, 2004).

The simplest methods for incorporating measured geometric imperfections are to linearly interpolate for nodal positions between data points (Wullschleger and Meyer-Piening, 2002), or to base the nodal spacing (i.e. the mesh structure) on the measurement spacing such that no interpolation is required (Arbocz and Starnes Jr, 2002; Zhao and Teng, 2004). These methods may be sufficient for a fine grid of measurement locations; however, the mesh density of the finite element model is often greater than that of the measurement grid, and a nonlinear interpolation is preferred.

Arbocz and Starnes Jr (2002, 2004) and Graham *et al.* (1992) recommend interpolation of the measured imperfection data for cylindrical shells using a two-dimensional, or "double", Fourier series of the general form found in equation (60).

$$R(\theta) = \sum_{m=0}^{\infty}\sum_{n=0}^{\infty}\left\{\cos\left(\frac{m\pi x}{L_B}\right)\left[A_{mn}\cos n\theta + B_{mn}\sin n\theta\right]\right\} \tag{60}$$

Equation (60) is referred to as a half-wave cosine representation, due to the cosine term outside of the square brackets that operates over the length of the cylinder. Alternatively, a half-wave sine representation could be used, by replacing the cosine term with an identical sine term. However, both of these half-wave representations may idealize the actual geometry and a "full" double Fourier series may be more accurate. Equation (61) represents the expansion of a complete Fourier series in both the circumferential and longitudinal directions (Poularikas, 1999).

$$R(\theta) = \sum_{m=0}^{\infty}\sum_{n=0}^{\infty}\left\{\begin{array}{l} A_{mn}\cos\dfrac{m\pi x}{L_B}\cos n\theta + B_{mn}\sin\dfrac{m\pi x}{L_B}\cos n\theta \\ + C_{mn}\cos\dfrac{m\pi x}{L_B}\sin n\theta + D_{mn}\sin\dfrac{m\pi x}{L_B}\sin n\theta \end{array}\right\} \tag{61}$$

Evaluation of the Fourier coefficients in equations (9), (60) and (61) will be accurate only if the numerical integration is performed on evenly-spaced data in both measurement directions. In some practical cases, this may not be possible (e.g. variable stiffener spacing, the presence of penetrations, etc.), but can be overcome by the use of iterative methods. Lin and Teng (2003) described a method whereby a one-dimensional Fourier series (equation (9)) for non-uniform data was improved by performing successive iterations on the residuals until a desired convergence tolerance was met. This method can be easily adjusted for use with two-dimensional Fourier series (equations (60) and (61)).

An alternative to Fourier series approaches is the use of splining techniques, which involve fitting geometric data to a collection of polynomial, rather than trigonometric, functions. Keron *et al.* (1997) suggest that cubic splines may be more appropriate for describing geometric imperfections than Fourier series because evenly spaced data is not required and the assumption that the measured data is correct is not implicit (i.e. regression methods could be used to develop a best-fit curve). It should be noted that the first objection to the use of Fourier series, i.e. the requirement for evenly-spaced measurement data, can be overcome by the use of iterated analysis methods (Lin and Teng, 2003).

4.2.2 Material Modeling

Material Nonlinearities and Anisotropies

Extracting trends from the literature regarding the selection of material models for buckling-critical shells was difficult because: 1) the majority of numerical studies have been concerned with elastic buckling problems that do not require complex nonlinear material models, and 2) the specific material model chosen for buckling-critical shell problems involving plasticity frequently goes unreported.

For the limited available data, the isotropic von Mises yield function (implying through-thickness integration schemes) is the most common – see Table 5. The selection of a strain hardening rule is largely unreported, but both isotropic (Fukuda *et al.*, 2003) and kinematic hardening (Creswell and Dow, 1986) were used in the studies reviewed here. Measured material properties are used for simulations of buckling/collapse or cold bending experiments, whenever available (Berry *et al.*, 2000; Fukuda *et al.*, 2003; Aghajari *et al.*, 2006).

Isotropic material models are the standard for metallic shells. Recent work has suggested that the typical anisotropic models (i.e. Hill and related yield surfaces) are not sufficient to predict the onset of yield in extruded shells; as such, more rigorous anisotropic yield functions have been developed and validated (Barlat *et al.*, 2003; Jansson *et al.*, 2005). An alternative to using a more complex anisotropic yield surface in the numerical analysis is the use of an average yield stress,

taken from material tests in the principal directions of anisotropy, in an isotropic model (e.g. Berry *et al.*, 2000).

The choice of material model is particularly important for the collapse analysis of pressure hulls because they are governed by elasto-plastic collapse. Collapse can occur immediately following the onset of yield for pressure hulls without significant residual stresses, and so the accurate definition of the yield surface is essential. This may be further complicated if the pressure hull material has significant anisotropies due to the manufacture of the base material (e.g. rolled steel plates, extruded ring-stiffeners, etc.) or the fabrication process (i.e. cold bending). Pressure hulls with residual stresses undergo yielding well before collapse, and thus the proper definition of the nonlinear stress-strain curve is important. The hardening rule is significant for cases of load reversal, which may arise due to local buckling (e.g. MacKay, 2007A) or repeated loadings past the yield pressure (e.g. MacKay *et al.*, 2006).

Residual Stresses

As discussed in Section 2.5.1, residual stresses arise in pressure hulls due to fabrication procedures, especially cold bending and welding of the ring-stiffeners and shell plating. Representation of residual stresses in a numerical model represents one of the main advantages of, and challenges for, nonlinear numerical analysis of pressure hulls. Residual stresses are typically modeled by either of two methods: 1) calculation of residual stresses analytically or experimentally, which are then applied to the finite element model before the collapse analysis is undertaken, and 2) explicit numerical simulation of the fabrication process as a preliminary analysis before strength calculations.

Analytically determined residual stresses are applied to the numerical model either as an initial stress state before the collapse analysis is undertaken or by manipulation of the material properties (e.g. effective stress-strain curves). Morandi *et al.* (1996A) found that there is not always close agreement in the nonlinear collapse pressure of ring-stiffened cylinders for the same analytically determined residual stresses modelled using the initial stress and effective stress-strain curve methods, with the latter typically resulting in lower collapse pressures. Comparison with experiment or more rigorous simulation of the fabrication process was not available to suggest which method is more accurate.

Analyses incorporating residual stresses via initial stress conditions require preliminary nonlinear analyses in order to guarantee equilibrium (Morandi *et al.*, 1996A; Sarawit *et al.*, 2003). This initial analysis will involve deformation of the structure if the residual stresses are not perfectly balanced; this is not often desirable, especially if a specific pattern of geometric imperfections is being applied to the model. This can be avoided by either transferring the balanced residual stress configuration to the original model (Sarawit *et al.*, 2003), or by restraining the nodal displacements (but not rotations) during the initial balancing analysis and then releasing the nodes for the collapse analysis (Morandi *et al.*, 1996A).

The second method of modeling residual stresses is to explicitly simulate the fabrication process, using nonlinear numerical methods, in order to generate the residual stresses, followed by an analysis to determine the buckling or collapse strength of the structure. Welding residual stresses (Holst *et al.*, 2000) and cold bending (Fukuda *et al.*, 2003) have been simulated separately;

however, the greatest challenge is simulating the fabrication process sequentially such that a strength calculation can be performed for fabricated structures.

Lennon and Das (1997) performed such a fabrication simulation and subsequent strength analysis on a complicated structural configuration and loading regime. The construction of a ring- and stringer-stiffened steel cylinder, with a cold bent shell and welded T-stiffeners, was simulated using nonlinear finite element analysis in the following manner:

- the residual strain distribution required for the desired curvature of the cold bent shell was determined by applying successively greater rotations to one end of the clamped plate;
- the residual strain pattern was applied, in a nonlinear load step, to a stress- and strain-free plate by the use of thermal strains in order to achieve the desired curvature and stress state;
- nodes on the shell corresponding to ring- and stringer-stiffener nodes were coupled in all degrees of freedom (this allows the stiffeners to be initially stress-free, but later attached to the shell);
- welding was simulated in a second nonlinear load step by applying a temperature distribution to the nodes at the shell-stiffener intersection; and
- the pressure and axial loads were applied incrementally to determine the collapse pressure.

Notwithstanding the elaborate numerical simulations reported by Lennon and Das (1997), the simulation of fabrication processes for use in strength calculations still requires extensive research. This includes further work on the simulation of cold bending of ring-stiffeners, longitudinal and circumferential welding of pressure hull sections, and welding of built up ring-stiffeners (Morandi *et al.*, 1996A). Additional study is required to produce "consistent" residual stress fields that satisfy equilibrium and are geometrically compatible with observed imperfections (Holst *et al.*, 2000).

4.2.3 Modeling of Loads and Boundary Conditions

Boundary conditions either define the loads that act on the structure (force or Neumann boundary conditions), or describe the way in which the structure is supported (displacement or Dirichlet boundary conditions). Both types of boundary conditions often involve simplifications of the actual structural situation, either to reduce the model size by replacing structure with boundary conditions or because the real state of loading and support is known imperfectly. A consistent set of boundary conditions is required for a unique mathematical solution of the finite element equations.

Some typical boundary conditions for shell structures are listed in Table 6. The first six scenarios listed are associated with modeling the entire shell under investigation while simulating the supporting structure (e.g. bulkheads, end caps, domes, etc.) using prescribed displacements. The latter symmetry boundary conditions are associated with replacing sections of the shell by making informed assumptions on the structural behaviour.

The correlation of experimental and numerical results is significantly influenced by the accuracy of the assumed boundary conditions (Arbocz and Starnes Jr, 2002). Boundary conditions in real structures and experimental models are not typically identical to one of those listed in Table 6, but

rather fall somewhere in between the extreme cases of simply supported and clamped; Arbocz and Starnes Jr (2002) have used elastic supports at the boundaries to achieve better experimental-numerical correlation.

Table 6: Typical shell structure boundary conditions

Boundary Condition[1]	**Prescribed Displacements**[2]
Simply supported	$v=w=0$
Simply supported with axial restraint	$u=v=w=0$
Simply supported with constant axial displacement	$v=w=0$, u=constant
Clamped	$v=w=\theta_x=\theta_y=\theta_z=0$
Clamped with constant axial displacement	$v=w=\theta_x=\theta_y=\theta_z=0$, u=constant
Fixed	$u=v=w=\theta_x=\theta_y=\theta_z=0$
Axial symmetry	$u=\theta_y=\theta_z=0$
Tangential symmetry	$\theta_x=v=\theta_z=0$
Tangential anti-symmetry	$u=\theta_y=w=0$

1. Descriptions of boundary conditions are taken from Morandi *et al.* (1996A) except for clamped and fixed cases, which were added by the author.

2. The displacements u, v and w and rotations θ_x, θ_y and θ_z are associated with the cylindrical coordinate directions x (axial), y (tangential) and z (radial), respectively – see Figure 3.

Symmetry and anti-symmetry boundary conditions are used when only a portion of the shell is modeled under the assumption that the resulting displacements are repeated in a symmetric (or anti-symmetric) pattern (e.g. linearized buckling analyses, nonlinear analyses with a single-mode characteristic imperfection). Symmetry boundary conditions must be applied with caution in order to prevent critical modes from being disqualified (Ramm and Stegmüller, 1982), and are not appropriate for modeling structures without symmetry (e.g. real structures with random imperfections).

An important aspect of the solution for pressure loaded structures is the nature of the load. Pressure loads are referred to as 'live' loads, because they change direction as the structure deforms. This is in contrast to the associated 'dead' load: a radial load consistently directed towards the axis of symmetry.

Live loads (or follower forces, as they are sometimes called) have been shown to decrease the critical (n=2) elastic buckling pressure of rings by up to 50% compared to similar structures with dead loads (Jones Jr *et al.*, 1977). The discrepancy between live and dead loading is less for higher values of n (Jones Jr *et al.*, 1977), but the effects of follower forces must nonetheless be accounted for in the analysis if a high degree of accuracy is to be achieved. This is accomplished by updating the element geometry at each nonlinear load increment, thereby updating the shell normal and thus the direction of the pressure load.

4.2.4 Linearized Buckling Analyses

The ultimate strength of pressure hulls, unlike the majority of axially compressed cylinders, is highly influenced by material plasticity; that is, axially compressed cylinders typically fail by elastic buckling, while pressure hulls fail via elasto-plastic collapse. As such, linearized buckling analyses tend to over-predict the strength of collapse-critical pressure hulls, and have been found to over-predict the buckling pressure of ring-stiffened cylinders that fail elastically as well (Sridharan and Alberts, 1997). As such, the usefulness of linearized (elastic) buckling analyses for pressure hulls is much less than for other buckling-critical shells. However, pressure hull buckling pressures derived from linearized analyses can be used to:

- improve upon analytical collapse predictions (see Section 3.1.3),
- perform mesh convergence and sensitivity studies,
- provide an upper bound to the nonlinear collapse pressure, and
- determine an initial step size for a nonlinear collapse analysis.

In addition to the above-mentioned uses of linearized buckling analyses, a significant merit of eigenvalue buckling analyses for pressure hulls is their role in detecting bifurcation of the primary solution path during a nonlinear collapse analysis (see Section 4.2.5).

Buckling of ring-stiffened cylinders constructed of certain high-strength materials, such as fibre-reinforced plastics, may behave elastically up to collapse; considering this, and due to the benefits described above, several studies have been performed on linearized numerical elastic buckling analyses for ring-stiffened cylinders (e.g. Jones Jr *et al.*, 1977; Moradi and Parsons, 1993; Sridharan and Alberts, 1997).

4.2.5 Nonlinear Collapse Analyses

The nonlinear equilibrium path can be divided into two regions: 1) the pre-buckling solution, up to the point of buckling or collapse, and 2) the post-buckling solution, including the unstable buckling process itself and any possible stable post-buckling equilibrium states. For low loading rates, prediction of the pre-buckling behaviour has not been found to be improved by the use of transient analysis, as opposed to pseudo-static nonlinear analysis (Choong and Ramm, 1988; Bisagni, 2000; Arbocz and Starnes Jr, 2002). In fact, if only a single post-buckling equilibrium state exists, a pseudo-static analysis may be sufficient to describe the entire pre- and post-buckling behaviour (Choong and Ramm, 1998).

Transient analysis is only required if a rigorous simulation of the transition from one equilibrium state to another (i.e. buckling) is desired. The collapse load is often the main point of interest to designers of buckling-critical shells; thus, a meticulous post-buckling analysis is not required and a pseudo-static analysis is sufficient for most buckling-critical shells (see Table 7).

Bifurcation (elastic or plastic) may occur at any point along the nonlinear solution path, and should be checked for regularly while incrementing along the nonlinear load-displacement solution (Ramm and Stegmüller, 1982; Shi, 1996; Wullschleger and Meyer-Piening, 2002). A critical point, either a bifurcation point or limit point, is indicated by, for example, a zero or

negative eigenvalue, a zero or negative determinant of the tangent stiffness matrix, etc. (Shi, 1996). Branch-switching techniques are available to allow the secondary solution path to be followed if that is required (Ramm and Stegmüller, 1982; Shi, 1996).

Table 7: Nonlinear FE solution methods for buckling-critical shell structure: trends

Topic	Trend or Recommendation	Sources
Method for prediction of buckling or collapse load	1) Nonlinear (geometry and, if necessary, material) pseudo-static analysis 2) Frequent checks for bifurcation of the equilibrium solution	1) and 2) Ramm and Stegmüller, 1982; Moradi and Parsons, 1993; Morandi *et al.*, 1996A; Berry *et al.*, 2000; Wullschleger and Meyer-Piening, 2002; Zhao and Teng, 2004; 1) only: Creswell and Dow, 1986; Guggenberger, 1995; Knight Jr *et al.*, 1995; Shi, 1996; Lennon and Das, 1997; Choong and Ramm, 1998; Ross and Johns, 1998; Bisagni, 2000; Holst *et al.*, 2000; Şanal, 2000; Arbocz and Starnes Jr, 2002; Barlag and Rothert, 2002; Schneider and Brede, 2005; Aghajari *et al.*, 2006
Nonlinear formulation	Updated Lagrangian	Wullschleger and Meyer-Piening, 2002
Iterative procedure	Full or modified Newton-Raphson	Knight Jr *et al.*, 1995; Choong and Ramm, 1998; Barlag and Rothert, 2002
Nonlinear path following scheme	Arc length method	Ramm and Stegmüller, 1982; Creswell and Dow, 1986; Knight Jr *et al.*, 1995; Morandi *et al.*, 1996A; Lennon and Das, 1997; Bisagni, 2000; Holst *et al.*, 2000; Arbocz and Starnes Jr, 2002; Barlag and Rothert, 2002; Wullschleger and Meyer-Piening, 2002; Zhao and Teng, 2004; Aghajari *et al.*, 2006
Solution increments	Appropriately small step-size is emphasized (e.g. adaptive step size with initial step based on linearized buckling analysis; 30 to 50 steps up to buckling load)	Ramm and Stegmüller, 1982; Knight Jr *et al.*, 1995; Wullschleger and Meyer-Piening, 2002

The main trends from the reviewed literature (Table 7) are the use of: 1) pseudo-static analysis for determining the pre-buckling solution and the buckling/collapse load; 2) an arc length path-following scheme (Riks, 1979; Crisfield, 1981) to allow limit points to be passed; and 3) frequent checks for bifurcation of the equilibrium path. Holst *et al.* (2000) used an arc length method for tracing the complete load-displacement history of the structure. The structure was then re-analyzed using a load-control scheme with increment-size reduction near the limit point to produce a more precise prediction of the collapse load, which may be stepped over by the arc-length procedure.

The iteration scheme used within a load step (i.e. Newton-Raphson, modified Newton-Raphson, etc) and the nonlinear formulation used (i.e. total Lagrangian, updated Lagrangian, etc) was not typically reported. Knight Jr *et al.* (1995) used an arc length method combined with a modified Newton-Raphson iteration scheme while parametrically studying various aspects of element formulation. They found that the use of a corotational approach was helpful in predicting the

nonlinear behaviour of elastic shells, but also stressed that the inclusion of the nonlinear strain-displacement terms was of great importance regardless of the nonlinear formulation used.

4.3 Discussion of Computational Modeling

The tools available for computational modeling have reached a state of maturity whereby the parameters and mechanisms essential to understanding the strength of buckling-critical shells are well-addressed – this includes, for instance, the effects of large displacements, material plasticity and solution-path bifurcation. For the most part, the limitations on the numerical prediction of nonlinear collapse loads are related to computational expense and the accuracy of experimental data input in the numerical model (e.g. shell thickness, geometric imperfections, material properties, etc.) rather than to inaccuracies in the computational methods.

The limited sample of the literature for numerical modeling of buckling-critical shells reviewed here points to some outstanding trends, which have been discussed in this section. Based on this review, a typical numerical analysis of a buckling-critical shell, which is aimed at reproducing the critical buckling or collapse load and mode (i.e. the post-buckling behaviour is of less interest) of a real structure, would proceed as follows:

- Generation of the finite element model:
  - Modeling of the structure is undertaken in three dimensional space using 4- or 8-noded degenerated shell elements in a structured finite element mesh, refined until the critical load is more-or-less constant.
  - Geometric imperfections are included by applying a double Fourier series approximation of the measured radii/eccentricities to the nodal coordinates of the finite element model.
  - If applicable, material plasticity of metals is modeled using a von Mises yield surface and corresponding flow theory, in combination with a bi- or multi-linear stress-strain curve with kinematic or isotropic hardening.
  - Support structure (e.g. experimental apparatus, bulkheads, etc.) is implicitly modeled using prescribed displacements (i.e. boundary conditions). More advanced modeling of the boundary conditions using elastic (i.e. spring) supports is sometimes necessary.
- Solution of the nonlinear buckling/collapse problem:
  - A nonlinear pseudo-static analysis that includes the effects of large displacements and inelastic material is performed with updated Lagrangian and/or corotational nonlinear formulation. If applicable, the follower force effect of pressure loading is taken into account.
  - The load is applied in small increments – 30-50 steps up to the critical load – using the full or modified Newton-Raphson iteration scheme within each increment.
  - An arc-length path-following scheme is used to enable local limit points to be traversed.
  - Regular checks for bifurcation of the solution path are performed (typically by checking for zero or negative eigenvalues).

- The buckling or collapse load is taken as the lower of the load causing bifurcation or the maximum point on the load-deflection curve.

The procedure described above should result in a reasonably accurate prediction of the critical load for typical buckling-critical shell structures and load configurations (see Section 5.3). Transient or dynamic analysis has been shown to be unnecessary unless prediction of the post-buckling behaviour is of great interest; pseudo-static analysis has been found to predict the pre-critical behaviour, critical load, and for some specific cases even the post-critical path, as well as transient analysis.

It is important to make allowance for the strength-reducing effects of fabrication processes, other than initial geometric imperfections, for welded and cold formed shell structures. This can be achieved in a simple manner using effective stress-strain curves based on analytical predictions of the residual stresses, or can be more thoroughly treated by explicit simulation of the fabrication process itself. The treatment of these fabrication-induced residual stresses, along with appropriate inelastic and/or anisotropic material models, and the use of offset shell elements to model eccentricities are the main numerical modeling areas for buckling-critical shells requiring further investigation.

5 Trends in Design Procedures

The current major research thrusts dealing with design procedures for buckling-critical shells are the use, or proposed use, of: 1) a "hierarchical" design approach, 2) statistical methods (i.e. reliability and probabilistic design) and 3) nonlinear numerical methods (e.g. Faulkner *et al.*, 1987; CEN, 1994; Morandi *et al.*, 1996A; Teng, 1996; Das, 1998; Morandi *et al.*, 1998; Rotter, 1998; Schmidt, 2000; Arbocz and Starnes Jr, 2002, Arbocz and Starnes, 2003; Arbocz and Starnes, 2004; Radha and Rajagopalan, 2006B). These various methods are often presented in an interrelated manner, especially when considering the hierarchical design approach, which refers to a design procedure with increasing levels of analytical sophistication.

5.1 Hierarchical Design Approach

A typical hierarchical approach for buckling-critical shells begins with a classical elastic buckling analysis and progresses to a numerical analysis considering both geometric and material nonlinearities (Arbocz and Starnes Jr, 2002). In between, more rigorous analytical methods and/or less sophisticated numerical methods may be used. In a hierarchical design, the relatively simple and computationally inexpensive analytical methods are used to conduct parametric studies of design variables, and to determine the nominal dimensions of the structure. The structural reliability (see Section 5.2) of the design is then determined using a detailed nonlinear numerical analysis and an advanced reliability method (Arbocz and Starnes Jr, 2002). Thus, a full range of design variables can be studied economically using the lower-level analyses, leading to an efficient design, the strength and reliability of which may be accurately determined using nonlinear numerical analysis.

Model Reduction

Nonlinear numerical models may also be used in the initial parametric study of design variables by using model reduction techniques. Barlag and Rothert (2002) presented a method to reduce the size of numerical models of ring- and stinger-stiffened cylinders. The amount of model reduction depends on the failure mode predicted by a classical elastic buckling analysis. For example, ring-stiffened cylinders predicted to fail by interframe collapse are idealized as simply supported cylindrical shell panels with an axial length equal to one frame spacing and circumferential angle of $360°/n$. Ring-stiffened cylinders predicted to fail by overall collapse are reduced by modeling only a portion of the cylinder circumference (with an angle of $360°/n$), with symmetry boundary conditions along the length. For the nonlinear analysis, characteristic geometric imperfections can be applied in the shape of the classical buckling mode.

Eurocode for Shell Structures

An example of a modern design code that incorporates a hierarchical procedure is the new Eurocode 3 for shell structures (CEN, 1994), which is focused primarily on civil engineering shell structures, such as steel silos, tanks, pipelines, chimneys, towers, and masts. Specific design rules for these types of structures are found in other codes, so that the main goal of the new Eurocode is to provide rules for the analysis of a generic shell of unspecified geometric and loading configuration (Rotter, 1998).

The Eurocode may be considered hierarchical because it allows for a range of analysis sophistication, from simple membrane theory to a full geometrically and materially nonlinear finite element analysis (Rotter, 1998). The Eurocode is not hierarchical in the strictest sense, however, as the designer is not required to proceed from simple to sophisticated analysis, but rather can choose the level of analysis complexity.

The Eurocode prescribes a knock-down factor to each type of analysis to account for modeling uncertainties, regardless of the level of analysis sophistication; the reward for using a more complex method is a smaller knock-down factor. Codification of the more sophisticated analyses (i.e. nonlinear numerical methods) is required in order to ensure that the application-specific standards are conservative with respect to the generic (i.e. numerical) standards. Rules for the numerical methods are also warranted due to the complicating factor of geometric imperfections, which are handled by either an additional knock-down factor or through prescribed characteristic imperfections (Rotter, 1998).

Probably the most innovative feature of the Eurocode is the implementation of nonlinear numerical methods in the design procedure. The Eurocode allows design of buckling-critical shells by "global" numerical analysis, with various levels of sophistication within the computational methods themselves (Schmidt, 2000). Knock-down factors are defined for critical loads determined by numerical analyses ranging in complexity from linearized buckling of the perfect structure to nonlinear collapse of the imperfect shell. Numerical strength calculations must be calibrated by conducting an analysis of a similar benchmark model.

Unfortunately, the validation of the numerical methods for the Eurocode is based on comparisons with experimental data for axially compressed cylinders (Schmidt, 2000), and so the use of the derived knock-down factor for other structural shells is questionable. The use of the Eurocode's knock-down factor for pressure hulls is especially inappropriate as these structures often fail by mechanisms involving material plasticity, as opposed to the typical elastic buckling occurring with axially compressed cylinders.

Eurocode rules for the nonlinear numerical analysis of the imperfect structure are primarily concerned with the prescription of geometric imperfections (Schmidt, 2000), which must be assigned such that they result in the "most unfavourable effect on the buckling behaviour of the shell." Because the Eurocode is concerned with design, as opposed to in-service analysis, the application of measured imperfections is not covered. Characteristic imperfections can be either eigenmode- or collapse-affine (Schneider and Brede, 2000), with an amplitude that must account for the detrimental effects caused by fabrication tolerances (e.g. OOC, plate misalignment, etc.), as well as other strength-reducing factors that are not modeled (e.g. residual stresses). These "equivalent" geometric imperfections are intended to represent the detrimental effects of all strength-reducing factors in the shell (Schneider and Brede, 2000).

5.2 Reliability and Probabilistic Design

Reliability and probabilistic design methods are concerned with: 1) the statistical probability that a structure will survive or fail, and 2) quantifying and understanding the uncertainties associated with a given design and method of analysis (Thoft-Christensen and Baker, 1982). It has been suggested that the traditional deterministic method of design for buckling-critical shells could be

improved (i.e. made less conservative) if the knock-down factor approach was replaced by a safety factor based on reliability analysis (Morandi *et al.*, 1996A; Arbocz and Starnes Jr, 2002).

Reliability Basics

Failure of a structure will occur if the applied load, *S*, is greater than the load which can be resisted by the structure, *R*. Both loads and resistances contain random variables, and are thus random themselves. This randomness is characterized by their respective means (μ_S and μ_R), standard deviations (σ_S and σ_R) and probability density functions ($f_S(s)$ and $f_R(r)$), which describe the likelihood of occurrence for a particular level of loading or resistance – see Figure 18.

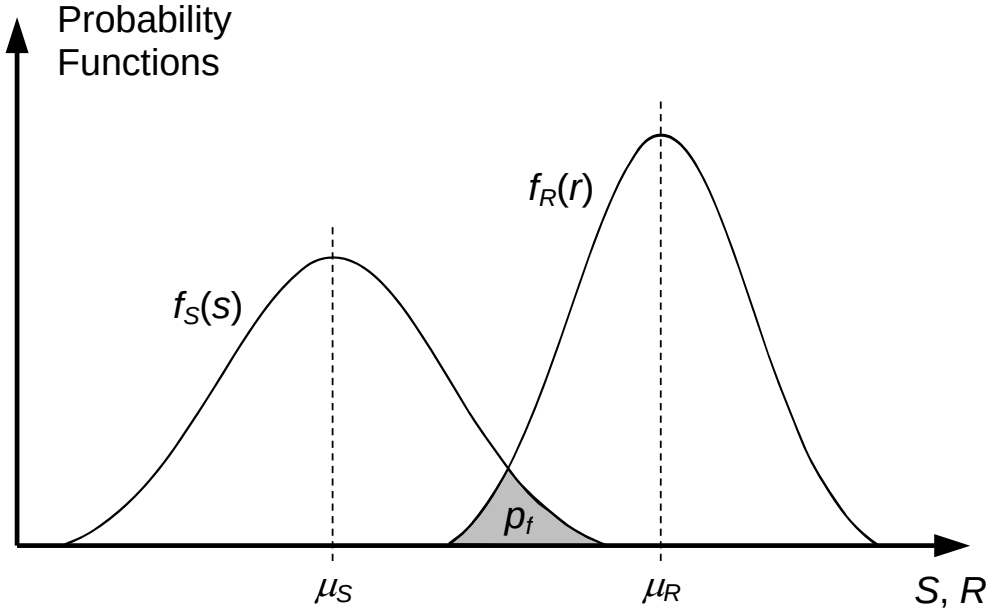

Figure 18: Probability density functions and probability of failure

The probability that a particular structure will fail, p_f, is taken as the probability that the resistances are less than the loads (Radha and Rajagopalan, 2006B):

$$p_f = p(R < S) = \int_0^\infty \left[\int_0^s f_R(r)dr \right] f_S(s)ds = \int_0^\infty F_R(s)\, f_S(s)ds \tag{62}$$

$F_R(s)$ is referred to as the cumulative distribution function (CDF) of *R* evaluated at *s*. Another value indicating the status of a structure is the performance function, *Z*:

$$Z = R - S = g(X_1, X_2, ..., X_n) \tag{63}$$

g is a functional relationship of the basic variables describing the load and resistance, X_i.

Reliability analysis is focused on generating the performance function for a given structural problem, based on measured or assumed probability functions for load and resistance variables. The failure surface, defined by Z=0, can be evaluated analytically (e.g. First Order Second Moment method) if $g(X_i)$ is simple; otherwise, a simulation technique such as Monte Carlo simulation is used to generate random data according to a specified distribution. Monte Carlo simulation is computationally expensive due to the large number of samples required to generate statistically meaningful and repeatable results. As such, several methods (e.g. point estimation, importance sampling, Latin hypercube, random polar sampling) have been developed to reduce the required sample size (e.g. Radha and Rajagopalan, 2006B).

Reliability analysis proceeds by first defining the failure function, Z, through the resistances and loads. For example, consider a pressure loaded ring, for which the critical load, q_{cr}, is given by equation (15) and is a function of bending stiffness, EI, and radius, R. If the applied load is taken as q, the failure function becomes:

$$Z = R - S = q_{cr}(E, I, R) - q \tag{64}$$

Z data is generated by a simulation technique (e.g. Monte Carlo simulation), which computes a sample of N points based on known or assumed distributions of the design variables (i.e. E, I and R). The mean, μ_Z, and standard deviation, σ_Z, of the generated failure function data are computed and the reliability index, β, is given by:

$$\beta = \frac{\mu_Z}{\sigma_Z} \tag{65}$$

The reliability index describes the tendency of the performance function to be concentrated around a certain value (the higher the reliability index, the more 'reliable' the structure).

The probability of failure (the lower the value of p_f, the more reliable the structure) is based on the cumulative standard normal distribution function, Φ (Thoft-Christensen and Baker, 1982):

$$p_f = \Phi(-\beta) = \int_{-\infty}^{-\beta} \frac{1}{\sqrt{2\pi}} \exp\left(-\frac{t^2}{2}\right) dt \tag{66}$$

The safety factor is given by the ratio of mean resistance to mean load:

$$SF = \frac{\mu_{q_{cr}}}{\mu_q} \tag{67}$$

Finally, the reliability, R, is taken as (higher R equals greater reliability):

$$R = 1 - p_f \tag{68}$$

Modeling Errors and Uncertainty

In reliability, the modeling error, or the modeling uncertainty factor, X_m, is defined as the ratio of the experimental value to the theoretical predicted value (Das, 1998; Faulkner *et al.*, 1987).

$$X_m = \frac{actual\_behaviour}{predicted\_behaviour} \tag{69}$$

The "behaviour" in equation (69) can be related to strength, loading, material properties, geometry, etc. The mean value of X_m for a sample is referred to as the *bias*, and is an indication of the systematic error, e.g. due to the inapplicability of the basic theory of the analysis method. The random component of the X_m is called the *modeling uncertainty*, and is defined by the coefficient of variation, V_{xm}, taken as the standard deviation divided by the bias (mean).

The bias differs from a safety factor for the modeling/analysis method in that it represents the mean error of the method, whereas a safety factor has to account for the mean error plus the random nature of the results (i.e. the modeling uncertainty). Many deterministic design codes overcome the systematic and random error by using knock-down factors or lower-bound design approaches; that is, the safety factor is based on the worst known experimental data. An alternative method is to determine the safety factor through reliability methods by letting the bias and modeling uncertainty become variables in the reliability analysis.

Morandi *et al.* (1998) used reliability methods to assess partial safety factors for pressure hulls designed using traditional analysis methods. A range of pressure hull designs that represent standard practice in industry were compiled, and these designs were used to determine the average reliability of current design processes. Partial safety factors were optimized by using constrained minimization whereby "the probabilities of failure of designs … [were] compared with the target reliability and the partial safety factors altered until the spread of reliabilities for a range of designs [was] minimized."

The reliability method of determining the partial safety factor differs from the so-called 'deterministic' approach whereby the safety factor would most likely be taken as the maximum discrepancy between the experimental and calculated collapse pressures (i.e. if the scatter in the strength model results was limited to ±10% of the experimental values, the safety factor would be taken as 1.10). The advantage of the reliability method is that it takes into account the nature of the scatter in the strength model predictions by using probability theory, and may therefore be less conservative than the deterministic approach. The disadvantages of using the reliability method to determine the safety factor are that it requires some knowledge of the desired (target) reliability, as well as assumptions regarding the definition of standard designs. In addition, the resulting safety factor would not be applicable to novel or non-standard designs.

Reliability analysis of pressure hulls using traditional analytical methods have also shown that the modeling uncertainty factor, as opposed to other variables such as frame spacing, yield stress, shell thickness, etc, dominates the analysis sensitivity (Morandi *et al.*, 1998; Das, 1998). Thus, the greatest uncertainty for the pressure hull designer is not variation of the material or geometry, but rather the suitability of the traditional design methods.

Table 8 summarizes modeling error (bias) and uncertainty (COV) for pressure hull design formulae and material data, when comparison with experiments was possible (taken from Morandi *et al.*, 1996A). This data illustrates that: 1) the analysis methods display greater error and variability than the available material data, thus resulting in the greater sensitivity to the analysis method than other parameters, and 2) the limited numerical buckling results represent an improvement in statistical properties over the classical methods.

Table 8: Modeling error and uncertainty for pressure hull design (Morandi et al., 1996A)

Model	Analysis Method	Experimental Sample	Bias	COV
Overall elastic buckling	Kendrick (1953A) [equation (18)]	72	1.25	15.2%
Overall elastic buckling[1]	Kendrick (1953A) [equation (18)]	20	1.05	4.5%
Overall elastic buckling	Linearized numerical buckling analyses of 3D shell models	72	1.02	11.8%
Interframe collapse	Mean empirical curve (e.g. DPA, 2001)	700	1.028-1.064	8.33-14.57%
Yield stress of shell plating	N/A	219	1.0	4.3%
Yield stress of stiffeners	N/A	448	1.0	4.6%

1. Statistical properties for overall elastic buckling by the classical method were improved by removing experimental data where the boundary conditions were thought to disagree with the analysis assumptions.

It is also interesting to note the implicit confidence placed by Morandi *et al.* (1996A) in numerical methods, which were, in lieu of experimental data, compared to analytical predictions of overall collapse due to stiffener yielding (similar to equation (37)) to calculate the bias and COV for the reliability analysis.

5.3 Numerical Strength Predictions for Buckling-Critical Shells

The accuracy of nonlinear computational modeling for predicting collapse loads of buckling-critical shell structures is generally associated with the level of detail and precision of the model. Table 9 summarizes a list of studies collected from the literature that consider both the experimentally- and numerically-derived critical load for the buckling-critical shell under investigation. A variety of structures (cylindrical shells, ring-stiffened cylinders, bulk solid tanks), materials (steel, aluminium, composite), and loading (axial compression, external pressure) are covered. Numerical results discussed below are those reported in the relevant sources, and are thus computed using a variety of analysis codes and methods.

Table 9: Nonlinear numerical-experimental studies for buckling-critical shells

Source	Type of Shell	Analysis	Level of Detail
Guggenberger, 1995	Polymer cylinders with dent under external pressure	NL G, static	Medium-Low (3D shells, idealized imperfections, symmetry boundary conditions)
Morandi *et al.*, 1996A	Ring-stiffened steel cylinders under external pressure	NL G+M, static (including checks for bifurcation)	Medium-High (3D shells, measured imperfections, relatively coarse mesh)
Ross and Johns, 1998	Plastic axisymmetric collapse of cylinders and cones under external pressure	NL G+M, static	Low (axisymmetric shells, no imperfections)
Berry *et al.*, 2000	Axially compressed steel cylinders with circumferential weld depressions	NL G+M, static (including checks for bifurcation)	Medium-Low (axisymmetric shells, idealized imperfections)
Bisagni, 2000	Axially compressed composite cylinders	NL G, static	Medium-High (3D shells, measured geometric imperfections and geometry, converged mesh, uncertainty regarding composite construction)
Arbocz and Starnes Jr, 2002	Axially compressed composite cylinders	NL G+M, static up to collapse, transient buckling response, static in post-buckling	High (3D shells, measured geometric imperfections and shell thickness, thickness-adjusted material properties, measured load variation, elastic radial support)
Wullschleger and Meyer-Piening, 2002	Axially compressed composite cylinders	NL G, static (including checks for bifurcation)	Medium-Low (3D shells, linearly interpolated measured geometric imperfections, uncertainty regarding experimental buckling load)
Zhao and Teng, 2004	Steel silo transition junctions	NL G+M, static	Medium-Low (3D shells, measured geometric imperfections, significant experimental loading uncertainty)
Aghajari *et al.*, 2006	Steel cylinders under external pressure	NL G+M, static	Medium-high (3D shells, measured geometric imperfections, measured material properties, weld material modelled)

The numerical models in Table 9 have been qualitatively classified by the level of detail implemented: low, medium-low, medium-high and high. The numerical models were penalized

(i.e. assigned a lower score) for simplifications such as axisymmetric behaviour assumptions, idealized geometric imperfections, etc., and rewarded for realistic modeling of geometry, material, boundary conditions, etc. Other factors, such as mesh refinement and the reliability of the experimental data for comparison, were also considered.

A modeling uncertainty factor, X_m, was determined for each of the twenty-five specimens selected from the sources in Table 9 by dividing the critical experimental load, $P_{cr,exp}$ (either external pressure or axial load), by the nonlinear numerical prediction, $P_{cr,nl}$ (see Table 10). The modeling uncertainty factors were subsequently used to calculate the bias and coefficient of variation (COV) for the sample, which represent the systematic and random error, respectively, associated with the numerical solutions. These values are reported in Table 11.

Table 10: Modeling uncertainty factors collected from the literature

Source	Model	Level of Detail	$P_{cr,exp}$ (1)	$P_{cr,nl}$ (1)	X_m (2)
Ross and Johns, 1998	Cylinder 4	Low	9.72E+00	8.41E+00	1.156
Ross and Johns, 1998	Cylinder 5	Low	1.12E+01	1.15E+01	0.975
Ross and Johns, 1998	Cylinder 6	Low	1.32E+01	1.67E+01	0.790
Guggenberger, 1995	Imperfect	Medium-Low	3.60E-03	3.52E-03	1.023
Guggenberger, 1995	Perfect	Medium-Low	4.03E-03	3.87E-03	1.040
Berry *et al.*, 2000	701	Medium-Low	7.14E+01	7.45E+01	0.959
Berry *et al.*, 2000	801	Medium-Low	8.74E+01	9.03E+01	0.968
Berry *et al.*, 2000	901b	Medium-Low	1.17E+02	1.25E+02	0.941
Zhao and Teng, 2004	CCSR-1	Medium-Low	2.30E+02	2.67E+02	0.862
Zhao and Teng, 2004	CCSR-2	Medium-Low	4.10E+02	3.57E+02	1.148
Zhao and Teng, 2004	CCSR-3	Medium-Low	4.34E+02	3.64E+02	1.193
Zhao and Teng, 2004	CCSR-4	Medium-Low	4.42E+02	3.89E+02	1.137
Zhao and Teng, 2004	CCSR-5	Medium-Low	4.77E+02	4.18E+02	1.141
Wullschleger and Meyer-Piening, 2002	Z32	Medium-Low	9.07E+01	1.03E+02	0.885
Wullschleger and Meyer-Piening, 2002	Z33	Medium-Low	1.78E+02	1.45E+02	1.230
Morandi *et al.*, 1996A	Model 2	Medium-High	6.24E+00	6.16E+00	1.013
Morandi *et al.*, 1996A	Model 3	Medium-High	6.49E+00	6.47E+00	1.003
Morandi *et al.*, 1996A	W1	Medium-High	4.50E+00	4.52E+00	0.996
Morandi *et al.*, 1996A	W3	Medium-High	6.22E+00	6.68E+00	0.931
Bisagni, 2000	N/A	Medium-High	1.63E+02	1.87E+02	0.874
Aghajari *et al.*, 2006	A	Medium-High	3.15E-02	3.56E-02	0.885
Aghajari *et al.*, 2006	B	Medium-High	1.10E-02	1.22E-02	0.902
Aghajari *et al.*, 2006	C	Medium-High	3.30E-02	3.62E-02	0.912
Aghajari *et al.*, 2006	D	Medium-High	6.50E-02	6.97E-02	0.933
Arbocz and Starnes Jr, 2002	N/A	High	1.52E+02	1.58E+02	0.965

1. $P_{cr,exp}$ and $P_{cr,nl}$ are the experimental and nonlinear numerical critical load, respectively; they are measured in MPa and kN for external pressure and axial loading, respectively.

2. $X_m = P_{cr,exp}/P_{cr,nl}$

The bias for the entire group, which is close to unity, indicates that, on average, the nonlinear numerical methods used in these studies are successful at predicting the critical load. However, the COV indicates that a large degree of scatter exists in the data. This is to be expected, as the numerical models ranged in their complexity, and no common set of rules or guidelines were used to predict the critical numerical load.

The analyses were further broken down into two groups based on the level of detail in the numerical models: low/medium-low and medium-high/high. Table 11 also summarizes the bias and COV for each of these cases. As expected, the COV for the models with a higher level of detail was much better than for the lower level models. Interestingly, though, the lower level models were, on average, better able to predict the critical experimental loads (i.e. had a bias closer to unity).

Table 11: Bias and COV for nonlinear numerical solutions from the literature

Sample (from Table 10)	Bias	COV
All 25 models	0.994	11.6%
15 models with low and medium-low level of detail	1.030	12.9%
10 models with medium-high and high level of detail	0.941	5.37%

The largely consistent over-prediction of the critical load by the high-level models may suggest a systematic error in the numerical methods; for instance, Aghajari *et al.* (2006) suggest that over-predictions of the critical load in their study were due to constraints associated with the displacement assumptions (i.e. shape functions) in the finite element formulation. These types of error should diminish with a converged mesh, however, and so it is possible that the over-predictions are due to the known inadequacies of the models, such as the over-coarse meshes used in the analyses of Morandi *et al.* (1996A) (this was suggested in the written discussion of the article by J. Arbocz) or a fabrication error in the composite shell, as proposed by Bisagni (2000).

These results were taken from a limited sample size so that it is not possible to make generalizations about the possible limits to the accuracy (i.e. a bias$\rightarrow$1 and COV$\rightarrow$0) of the numerical methods. The near-unity bias of the sample considered here is encouraging, as is the relatively small COV for the high-level models. The numerical results could be further improved by:

- the identification of systematic errors in the high-level analyses,
- specialization for a particular shell structure (i.e. pressure hulls), and
- the development of modeling guidelines to encourage consistent results.

Each of the above tasks is considered in the proposed procedure for implementing numerical methods in pressure hull design, discussed in Section 5.4.

5.4 Design of Pressure Hulls using Computational Modeling

Rationale for Computational Modeling

Structural analysis and design of pressure hulls has traditionally been undertaken using a combination of analytical formulae and simple numerical methods, as described in Section 3. These approaches are based on designing for failure to occur in modes that have been extensively studied experimentally (i.e. interframe collapse), and designing conservatively for less well-understood modes of failure (e.g. overall collapse, stiffener tripping).

The traditional design methods, while having the advantages of being well-established and computationally cheap, have several shortcomings: 1) conservativeness, due to yield-based design and worst-case modeling of structural geometry and imperfections, 2) inflexibility, with regards to non-standard design geometry and loading, secondary structure, and damage, and 3) the statistical properties of the analysis methods have only been thoroughly validated for a single mode of failure (interframe collapse), which makes it difficult to undertake reliability analyses with much confidence, as the modelling error and uncertainty for other modes of failure must be assumed or based on limited experimental correlation.

The use of nonlinear numerical methods, specifically nonlinear finite element analysis (NLFEA), would address the first two deficiencies of the traditional methods by allowing pressure hull designs to be based on limit states, with full geometric complexity, including in-service concerns such as corrosion and collision damage. The traditional pressure hull design methods are compared with NLFEA for a variety of features in Table 12.

Table 12: Comparison of traditional design methods and NLFEA

Area of Comparison	**Traditional Methods**	**NLFEA**
Modeling and computation cost	Cheap	Expensive
Requirement for expertise in analysis method	Low / Medium	Medium / High
Variability of results for different analysts	Low	Analyst dependent
Modeling of structure and geometric imperfections	Conservative	Realistic
Failure criteria	First yield	Limit states

Nonlinear numerical analyses are currently used in pressure hull design and analysis in indirect ways, such as granting “tolerance concessions” to in-service structures, “validating” empirical design methods, identifying failure modes and weak structural features, determining the effects of in-service damage, and for general research purposes (e.g. Creswell and Dow, 1986; Graham *et al.*, 1992; Morandi *et al.*, 1996A; Keron *et al.*, 1997; Lennon and Das, 1997; MacKay *et al.*, 2006).

Despite its widespread informal use and accepted benefits, the direct use of nonlinear numerical methods in the design of pressure hulls is not currently supported by design codes, primarily because the uncertainty regarding the accuracy of the method (i.e. the modelling error and uncertainty) has not, to the author’s knowledge, been quantified. Modeling uncertainty associated with numerical strength predictions for a variety of buckling-critical shells (Table 10 and Table

11) compares favourably with the statistical properties of traditional pressure hull design equations (Table 8). This gives further impetus for the pursuit of full implementation of numerical methods in design codes.

It has been found that accurate predictions of collapse for pressure hulls using nonlinear numerical calculations are dependent on incorporating measured imperfections (Faulkner *et al.*, 1987; Morandi *et al.*, 1996A); furthermore, the use of characteristic, or assumed, imperfections leads to large modeling uncertainties for the numerical methods. As such, it has been suggested that analytical methods be used in the case of unknown imperfections, as they are almost as accurate and have the benefit of low computational cost (Faulkner *et al.*, 1987). This begs the question: is numerical analysis, considering the extra costs involved, advantageous for pressure hull *design*?

The answer to this question is yes, if realistic imperfections can be modeled at the design stage. An alternative to the use of simple characteristic imperfections for design is the use of so-called imperfection databases, which are compilations of large volumes of geometric imperfection data taken from measurements of real structures, and sorted by fabrication method (Arbocz and Starnes Jr, 2002). This method would provide more realistic, and presumably less conservative, imperfection patterns for design, and could only be implemented using numerical methods.

Even if simplistic characteristic imperfections are used for design, the numerical methods offer many advantages over the traditional analytical methods. Faulkner *et al.* (1987) have suggested that traditional design by component (e.g. design of the ring-stiffened cylinder section of a pressure hull) should be complemented by a more thorough treatment of the entire structural system (e.g. entire pressure hull, including conical sections, torispherical domes, and watertight bulkheads). Such an analysis would reduce the uncertainty involved with selecting appropriate boundary conditions and increase the understanding of interactive effects between major structural components. Furthermore, it is often desirable to: 1) assess the effects of in-service damage (MacKay *et al.*, 1996); 2) simulate the fabrication procedure (Lennon and Das, 1997); and 3) incorporate novel design geometry, stiffening options and materials (Graham *et al.*, 1992; Keron *et al.*, 1997); all of which are only possible through the use of numerical methods.

Validation of the Numerical Methods for Pressure Hulls

The incorporation of any structural analysis method into a design code requires the uncertainties associated with the modeling method to be accounted for so that the designer is reasonably assured that the as-built structure will be safe. Of course, the designer must also take into account uncertainties associated with, for instance, construction and loading. For pressure hulls, the modeling uncertainty has traditionally been dealt with by using a lower-bound empirical method or a partial safety factor.

Lower-bound methodology inherently accounts for the statistical uncertainty by use of a knock-down factor that ensures designs are based on the most pessimistic experimental results known. Faulkner *et al.* (1987) discourage the use of lower-bound design equations because they imply that safety factors are not related to strength, as they are inherently included in the lower bound formulation, and because they are not suitable for reliability calculations.

Partial safety factors for deterministic design methods are associated with approximations to the mean, rather than lower-bound, empirical data. The modeling uncertainty is quantified by the partial safety factor, which is generally taken as the maximum scatter from the mean curve.

A third method of quantifying the modeling uncertainty is to establish the partial safety factor by specifying the desired reliability and performing reliability analyses for typical designs. This is the method suggested by Morandi *et al.* (1998) – see Section 5.2.

Whatever type of design methodology is chosen – deterministic or probabilistic – the two parameters describing modeling uncertainty, bias and COV, should be determined, based on a statistically meaningful sample.

Scatter, and sometimes systematic error, is often associated with particular types of failure, and thus establishing a design curve that takes account of failure mode sometimes helps to improve correlation. A common method of establishing a design curve involves plotting the experimental data versus the calculated strengths, with both axes normalized by an analytically determined yield pressure (e.g. mean or lower-bound interframe collapse curves). An empirical equation may then be fit to this data, thus reducing the systematic error. Correlation of the modeling error with basic variables should generally be avoided, especially design curves related to geometry – i.e. slenderness parameters (Faulkner *et al.*, 1987).

If the systematic error is not significant (as indicated by a modelling uncertainty factor that is, on average, close to unity) over the range of structures studied, the bias and COV may be calculated directly without establishing a design curve. Ideally, the modeling error, X_m, should be close to unity over the range of applicability of the strength model and the modeling uncertainty, V_{xm}, should be as low as possible. Faulkner *et al.* (1987) suggest that a bias within ±5% of unity is desirable and that $V_{xm} \leq 13\%$ should be achievable for marine structures (including pressure hulls).

Implementation of Computational Modeling in the Design Process

Faulkner *et al.* (1987) have made several sensible recommendations for the development of improved design codes for the ship and offshore industry. These recommendations, and their implications or applicability for incorporating nonlinear numerical methods in pressure hull design codes are summarized in Table 13.

Based on these recommendations and the discussion of validation above, a procedure has been developed for implementation of numerical methods in pressure hull design codes. The following tasks are being undertaken by DRDC Atlantic, in cooperation with the Netherlands Ministry of Defence and Delft University of Technology:

1. Compile a database of experimental pressure hull collapse tests. This task will include:
    - collecting data from the literature (see Section 5 and Table 15 in Annex A) and obtaining additional detail from the authors when possible;
    - determining the level of detail required for an experiment to be included in the validation procedures (e.g. measured material properties, measured geometric imperfections, etc.); and

- supplementing the data from the literature with additional experiments (MacKay, 2005, 2007A, 2007B).

2. Establish modeling and analysis guidelines based on Sections 4.2 and 4.3, as well as by comparison of numerical and experimental data. Additional research should address:
   - incorporation of the effects of fabrication-induced residual stresses, especially due to cold bending and welding, in the numerical strength calculation;
   - suitable material models for inelastic anisotropic materials (e.g. for extruded tubes, rolled plates, etc);
   - appropriate modeling procedures for shell eccentricities resulting from dome-cylinder transitions, corrosion damage, etc.; and
   - benchmark calibration models.
3. Determine the modeling error and uncertainty associated with the numerical methods. This task will include:
   - establishing criteria for the acceptance of each numerical result (e.g. agreement of numerical and experimental failure mode, location, etc.);
   - ensuring the use of the full range of modeling and analysis options, as set out in the guidelines, by, for instance:
     - random selection of the modeling methods, solution procedures, numerical solver, etc. for each analysis, and/or
     - multiple analysts using various numerical solvers;
   - performing the nonlinear numerical analyses and analyzing the results;
   - assessing the statistical properties of the data, which includes:
     - determining if systematic error exists,
     - locating the source of error and correcting it if possible,
     - determining if a design curve would reduce the unaccounted for error, and
     - calculating the modeling error and uncertainty, with or without a design curve.
4. Propose updates to pressure hull design codes to allow nonlinear numerical strength calculations. For example, implementation in a typical deterministic design procedure would include:
   - calculating the partial safety factor, based on, for example, the maximum scatter in the data or by ensuring a target reliability; and
   - complementing the previously established modeling and analysis guidelines with a design procedure that prescribes geometric imperfections and fabrication-induced residual stresses.

This report, in conjunction with an ongoing pressure hull experimental collapse program (MacKay *et al.*, 2006; MacKay 2007A, 2007B), represents the first stage of this procedure, with modeling guidelines, an experimental database and numerical modeling to follow in the coming months and years.

While the above tasks are listed in order, it is likely that several of them will be undertaken concurrently. Faulkner *et al.* (1987) suggest that experimental data should be used not only to validate the analysis method, but also to identify inaccuracies in the model. This emphasizes the importance of using experimental data when establishing the modeling and analysis guidelines for the numerical methods. The guidelines may be established by minimizing the modeling error and uncertainty by iterating over tasks 2 and 3.

Table 13: Recommendations for the development of structural design codes

Recommendation (Faulkner *et al.*, 1987)	**Implication or Applicability for Numerical Design of Pressure Hulls**
Use a mean, rather than a lower-bound, formulation.	Implementation via partial safety factor for deterministic or probabilistic design methods.
Incorporate analysis methods that cover the widest possible range of variables (i.e. geometry, material, imperfections, etc).	One of the primary benefits of numerical methods is their flexibility.
Base the strength model on structural mechanics and failure theory, rather than empirical curve fitting.	Underlying formulations in numerical methods are physics based and do not depend on empirical parameters.
Use interaction equations for cases of multiple loading.	Not applicable: numerical methods can take all failure modes and loading into account in a single analysis.
Use the simplest appropriate strength model, but not to the detriment of accuracy.	Nonlinear numerical methods are computationally expensive and relatively complex to implement; accuracy should be improved over traditional strength models.
Do not include levels of sophistication in the formulation.	This may be unavoidable, as simpler, more conservative, traditional design methods should still be available, as in the shell structures Eurocode (CEN, 1994).
Include a consistent strength model.	See Section 5.3 for estimates of modeling error and uncertainty for nonlinear numerical methods.
Avoid the following unsafe features: • inclusion of incorrect formulae, • omissions, • use of invalid criteria, • use of incorrect data, and • inclusion of misleading information.	These points must be addressed by a systematic study resulting in modeling and analysis guidelines for nonlinear analyses, and by careful examination and interpretation of the experimental data.

5.5 Discussion of Design Procedures

The author is of the opinion that a thorough comparison of experimentally- and numerically-derived collapse pressures for pressure hulls and related structures is necessary before nonlinear numerical methods can be incorporated into the design procedure. An outline of steps required to

reach this goal has been presented, and an initial list of possible experimental sources is provided in Annex B (Table 15). A verified numerical modeling and analysis procedure could then be incorporated in pressure hull design codes as an additional option for determining strength (i.e. the Eurocode approach that allows for levels of sophistication in the analysis), or as the high-fidelity analysis stage in a hierarchical design method (i.e. as proposed by Arbocz and Starnes Jr, 2002).

A related topic that requires investigation is the treatment of strength-reducing factors, such as geometric imperfections and residual stresses, in a design process using numerical methods. The accuracy of the numerical strength predictions can only be properly quantified if the strength model closely resembles the experimental model in its geometric imperfections, material properties, etc. However, in the design process, the real imperfections cannot be anticipated precisely, so characteristic values must be used.

Appropriate characteristic strength-reducing properties, in general, must be investigated. The use of imperfection data banks (Arbocz and Abramovich, 1979) is an option that could lead to less conservative designs than the use of other less realistic and more pessimistic imperfection assumptions. On the other hand, the significant computational expense of the numerical calculations could be reduced by the use of model reduction in combination with the incorporation of the simpler single-mode geometric imperfections – this may be appropriate for a preliminary design stage. The treatment of residual fabrication stresses must also be covered by the design code. From the perspective of both numerical modeling and design code formulation, the use of effective stress-strain curves or the inclusion of initial stresses would seem to be more practical than direct simulation of pressure hull fabrication.

6 Summary and Future Trends

The classical treatment of pressure hull strength has progressed with regards to two parameters: geometric complexity (i.e. from rings to tubes to ring-stiffened cylinders) and analytical rigor (i.e. from linear-elastic buckling pressures to yield pressures associated with nonlinear growth of non-axisymmetric initial imperfections). Effort continues to be devoted to improving analytical predictions of pressure hull strength, driven by the need for computationally inexpensive strength models for use in reliability analyses or for assessments of in-service damage that can be used with the traditional design methods. By and large, however, the set of design equations and procedures for determining the strength of pressure hulls has changed very little since the introduction of Kendrick's (1979) finite difference solution for overall collapse.

While the basic groundwork for the nonlinear numerical methods were well-established over two decades ago, their application to determining the strength of buckling-critical shell structures did not become widespread until desktop computers became both common and more powerful in the 1990s (see Table 14 and Table 9). The high level of computational expense associated with nonlinear collapse analyses has led to the prevalent use of cheap structural shell elements. It may be assumed that future desktop computers will be powerful enough to allow the use of continuum solid elements for nonlinear calculations. This may seem excessive or unnecessary, but solid modeling would address inconsistencies associated with, for example, branched or offset shells, and with assumptions related to the basic shell theory. For the short-term, however, shell elements will prevail for buckling-critical shell modeling.

A case has been made supporting the implementation of nonlinear finite element analysis in pressure hull design procedures, based on the argument that the numerical methods would address the inherent conservatism and inflexibility of the traditional design methods. Computational modeling would allow strength calculations to be based on the elasto-plastic limit state, rather than first yield criteria, of a complex pressure hull structure, including realistic modeling of geometric imperfections, the effects of fabrication procedures and in-service damage. Furthermore, numerical methods would allow the pressure hull to be designed as a whole, rather than by component, with inherent modeling of the interaction between structural components (e.g. ring-stiffened cylinders, domes and bulkheads) and modes of failure (e.g. interframe and overall collapse).

The traditional analytical methods for buckling-critical shells will likely be retained in novel design codes because of their simplicity and efficiency of use, as well as their value for use in iterative design procedures such as optimization routines and reliability analysis. Numerical modeling is more likely to complement than to replace the analytical methods, as in a hierarchical design procedure.

A way forward for the incorporation of nonlinear numerical methods in pressure hull design procedures has been suggested in this study. The main points are the population of a database of experimental results, the establishment of modeling and analysis guidelines, and the determination of the modeling error and uncertainty associated with the numerical modeling through a structured program of analysis. Additional research is required to address fabrication-induced residual stresses, appropriate inelastic material models, the treatment of shell eccentricities and the prescription of characteristic design imperfections.

The procedure for the implementation of computational modeling in design is being undertaken by DRDC Atlantic, in cooperation with the Netherlands Ministry of Defence and Delft University of Technology. DRDC is carrying out this process for pressure hulls, but it could equally be applied to any class of buckling-critical shell structure.

7 References

Aghajari, S., Abedi, K. and Showkati, H. (2006). Buckling and post-buckling behavior of thin-walled cylindrical steel shells with varying thickness subjected to uniform external pressure. *Thin-Walled Structures*, 44, 904-909.

Arbocz, J. and Abramovich, H. (1979). The initial imperfection data bank at the Delft University of Technology – Part I. (Report LR-290). Delft University of Technology.

Arbocz, J. and Hol, J.M.A.M. (1991). Collapse of axially compressed cylindrical shells with random imperfections. *AIAA Journal*, 29 (12), 2247-2256.

Arbocz, J. and Starnes Jr, J.H. (2002). Future directions and challenges in shell stability analysis. *Thin-Walled Structures*, 40, 729-754.

Arbocz, J. and Starnes, J.H. (2003). A hierarchical high-fidelity analysis procedure for buckling critical structures. (AIAA 2003-1849). In *Proceedings 44th AIAA/ASME/ASCE/AHS Structures, Structural Dynamics and Materials Conference*, Norfolk, Virginia: AIAA.

Arbocz, J. and Starnes, J.H. (2004). On a verified high-fidelity analysis for axially compressed cylindrical shells. (AIAA 2004-1712). *Proceedings 45th AIAA/ASME/ASCE/ AHS/ASC Structures, Structural Dynamics and Materials Conference*, Palm Springs, California: AIAA.

Barlag, S. and Rothert, H. (2002). An idealization concept for the stability analysis of ring-reinforced cylindrical shells under external pressure. *International Journal of Nonlinear Mechanics*, 37, 745-756.

Barlat, F., Maeda, Y., Chung, K., Dick, R.E., Choi, S.-H., Pourboghart, F., Chu, E. and Lege, D.J. (2003). Plane stress yield function for aluminum alloy sheets – Part 1: theory. *International Journal of Plasticity*, 19, 1296-1319.

Bathe K.-J. (1982). Finite Element Procedures in Engineering Analysis. Englewood Cliffs, New Jersey: Prentice Hall, Inc.

Berry, P.A., Rotter, J.M., and Bridge, R.Q. (2000). Compression Tests on Cylinders with Circumferential Weld Depressions. *Journal of Engineering Mechanics*, 126 (4), 405-413.

Bijlaard, S. (1957). *Journal of the Royal Aeronautical Society*, 24 (6), 437.

Bisagni, C. (2000). Numerical analysis and experimental correlation of composite shell buckling and post-buckling. *Composites: Part B*, 31, 655-667.

Boichot, L. and Reynolds, T.E. (1965). Inelastic buckling tests of ring-stiffened cylinders under hydrostatic pressure. (DTMB Report 1992). David Taylor Model Basin.

Bosman, T.N., Pegg, N.G., and Keuning, P.J. (1993). Experimental and Numerical Determination of the Nonlinear Overall Collapse of Imperfect Pressure Hull Compartments. In *Proceedings of*

Warship '93, International Symposium on Naval Submarines 4. Royal Institution of Naval Architects.

Blachut, J. (2002). Buckling of externally pressurized barrelled shells: a comparison of experiment and theory. *International Journal of Pressure Vessels and Piping*, 79, 507-17.

Bresse, M. (1859). Cours de mecaniqué appliquée. Paris.

BSI (1980). BS 5500 British Standard Specification for Unfired Fusion Welded Pressure Vessels, Issue 5. United Kingdom: British Standards Institution.

Bryant, A.R. (1954). Hydrostatic Pressure Buckling of a Ring-Stiffened Tube. (NCRE Report 306). Naval Construction Research Establishment.

Bushnell, D. (1970). Analysis of buckling and vibration of ring-stiffened, segmented shells of revolution. *International Journal of Solids and Structures*, 6, 157-181.

Bushnell, D. (1974). Stress, stability and vibration of complex, branched shells of revolution. *Computers and Structures*, 4, 399-435.

Bushnell, D. (1975). Buckling of elastic-plastic shells of revolution with discrete elastic-plastic ring-stiffeners. *International Journal of Solids and Structures*, 12, 51-66.

Bushnell, D. (1981). Buckling of Shells-Pitfalls for Designers. *AIAA Journal*, 19 (9), 1183-1224.

CEN (1994). European Prestandard ENV 1993-1-6, General Rules – Supplementary Rules for the Strength and Stability of Shell Structures. Brussels: European Committee for Standardization (CEN).

Choong, K.K. and Ramm, E. (1998). Simulation of buckling process of shells by using the finite element method. *Thin-Walled Structures*, 31, 39-72.

Creswell, D.J. (1978). Experimental determination of the elastic collapse pressures of some miniature aluminium stiffened cylinders. (AMTE Report R78643B). Admiralty Marine Technology Establishment.

Creswell, D.J. and Dow, R.S. (1986). The application of nonlinear analysis to ship and submarine structures. In C.S. Smith and J.D. Clarke, (Eds.), *Advances in Marine Structures: Proceedings of an International Conference*, pp. 174-200. Dunfermline, Scotland: Admiralty Research Establishment.

Crisfield, M.A. (1981). A fast incremental/iterative solution procedure that handles "snap-through". *Computers and Structures*, 13, 55-62.

Crisfield, M.A. (1997). Nonlinear Finite Element Analysis of Solids and Structures, Volume 2: Advanced Topics. New York: John Wiley & Sons.

DPA (2001). SSP74 Design of Submarine Structures. United Kingdom: Defence Procurement Agency, Sea Technology Group.

Das, P.K. (1998). Reliability based design of submarine structures. (OMAE98-1303). In *Proceedings of the 17th International Conference on Offshore Mechanics and Arctic Engineering*. Lisbon: ASME.

Dow, D.A. (1965). Buckling and postbuckling tests of ring-stiffened circular cylinders loaded by uniform external pressure. (NASA Technical Note D-3111). National Aeronautics and Space Administration.

ECCS (1988). Buckling of steel shells: European Recommendations. Brussels: European Convention for Constructional Steelwork (ECCS).

Fairbairn, W. (1858). On the resistance of tubes to collapse. *Philosophical Transactions of the Royal Society*, 148, 389-413.

Faulkner, D. (1977). Effects of residual stresses on the ductile strength of plane welded grillages and of ring stiffened cylinders. *Journal of Strain Analysis,* 12 (2), 130-139.

Faulkner, D. (1983). The Collapse Strength and Design of Submarines. In *RINA Symposium on Naval Structures*. London: Royal Institution of Naval Architects.

Faulkner, D., Guedes Soares, C. and Warwick, D.M. (1987). Modelling requirements for structural and assessment. In D. Faulkner, M.J. Cowling and A. Incecik, (Eds.), *Integrity of Offshore Structures – 3*, pp. 25-54. London: Elsevier Applied Science.

Faulkner, D. (1991). Application of reliability theory in submarine design. In C.S. Smith and R.S. Dow, (Eds.), *Advances in Marine Structures 2*, pp. 566-585. New York: Elsevier Applied Science.

Flügge, W. (1932). Die Stabilität der Kreiszylinderschale. *Ingenieur-Archive,* 3, 463-506.

Frieze, P.A. (1994). The Experimental Response of Flat-Bar Stiffeners in Cylinders under External Pressure. *Marine Structures*, 7, 213-230.

Fukuda, N., Yatabe, H., Kawaguchi, S., Watanabe, T., and Masuda, T. (2003). Experimental and analytical study of cold bending process for pipelines. *Journal of Offshore Mechanics and Arctic Engineering*, 125, 153-157.

Goudie, N.M. (1971). Collapse tests of two full-scale OBERON class dome bulkheads. (NCRE Report L12/TG42/71). Naval Construction Research Establishment.

Graham, D., Keron, I., Mitchell, G. and Creswell, D. (1992). DRA structural research on submarines and submersibles. (Paper No. 13). In *Proceedings of the Charles Smith Memorial Conference: Recent Developments in Structural Research*. Dunfermline, Scotland: Defence Research Establishment.

Guggenberger, W. (1995). Buckling and Postbuckling of Imperfect Cylindrical Shells Under External Pressure. *Thin-Walled Structures*, 23, 351-366.

Hibbeler, R.C. (1997). Mechanics of Materials – Third Edition. New Jersey: Prentice Hall.

Holst, J.M.F.G., Rotter, J.M. and Calladine, C.R. (2000). Imperfections and buckling in cylindrical shells with consistent residual stresses. *Journal of Construction Steel Research,* 54, 265-282.

Hübner, A., Albiez, M., Kohler, D. and Saal, H. (2007). Buckling of long steel cylindrical shells subjected to external pressure. *Thin-Walled Structures,* 45, 1-7.

Jansson, M., Nilsson, L. and Simonsson, K. (2005). On constitutive modeling of aluminum alloys for tube hydroforming applications. *International Journal of Plasticity*, 21, 1041-1058.

Jones Jr, R.F., Costello, M.G. and Reynolds, T.E. (1977). Buckling of pressure loaded rings and shells by the finite element method. *Computers and Structures*, 7, 267-274.

Kardestuncer, H. (1987). Basic concepts of the finite-element method. In. H. Kardestuncer (Ed.), *Finite Element Handbook*, pp. 2.75-2.108. Toronto: McGraw-Hill Book Company.

Kendrick, S. (1953A). The buckling under external pressure of circular cylindrical shells with evenly spaced equal strength circular ring frames – Part I. (NCRE Report No. R.211). Naval Construction Research Establishment.

Kendrick, S. (1953B). The buckling under external pressure of circular cylindrical shells with evenly spaced equal strength circular ring frames – Part II. (NCRE Report No. R.243). Naval Construction Research Establishment.

Kendrick, S. (1953C). The buckling under external pressure of circular cylindrical shells with evenly spaced equal strength circular ring frames – Part III. (NCRE Report No. R.244). Naval Construction Research Establishment.

Kendrick, S. (1953D). The deformation under external pressure of nearly circular cylindrical shells with evenly spaced equal strength nearly circular ring frames. (NCRE Report No. R.259). Naval Construction Research Establishment.

Kendrick, S.B. (1955). Analysis of results of static pressure tests of Chatham submarine models. (NCRE Report No. R.218). Naval Construction Research Establishment.

Kendrick, S. (1965). The Buckling under External Pressure of Ring Stiffened Circular Cylinders. *Transactions of the Royal Institution of Naval Architects*, 107, 139-152.

Kendrick, S. (1970). Externally Pressurized Vessels. In S.S. Gill, (Ed.), *The Stress Analysis of Pressure Vessels and Pressure Vessel Components*, pp. 405-511. Toronto: Pergamon Press.

Kendrick, S.B. (1977). Shape imperfections in cylinders and spheres: their importance in design and methods of measurement. *Journal of Strain Analysis*, 12 (2), 117-122.

Kendrick, S. (1979). The Influence of Shape Imperfections and Residual Stress on the Collapse of Stiffened Cylinders. In *Proceedings of the Conference on Significance of Deviations from Design Shape,* 25-35. I. Mech. E.

Kendrick, S. (1982). Design for External Pressure using General Criteria. *International Journal of Mechanical Science*, 24 (4), 209-218.

Kendrick, S. (1985). Ring-Stiffened Cylinders Under External Pressure. In R. Narayanan, (Ed.), *Shell Structures, Stability and Strength*, pp. 57-95. London: Elsevier Applied Science.

Keron, I., Graham, D., Farnworth, J. and Anderson, N. (1997). Recent developments in the analysis and design of submarine structures. (Paper No. 27). In *Proceedings of Advances in Marine Structures 3*. Rosyth, Scotland: DERA.

Knight Jr., N.F., Macy, S.C. and McCleary, S.L. (1995). Assessment of structural analysis technology for static collapse of elastic cylindrical shells. *Finite Elements in Analysis and Design*, 18, 403-431.

Lennon, R.F. and Das, P.K. (1997). The effect of cold forming and welding locked in stress states on the buckling resistance of orthogonally stiffened cylinders. (Paper No. 6). In *Proceedings of Advances in Marine Structures 3*. Rosyth, Scotland: DERA.

Liessem, A., Groß-Weege, J., Marewski, U. and Knauf, G. (2006). Methods for collapse pressure prediction of UOE linepipe. (OMAE2006-92147). In *Proceedings of the 25th International Conference on Offshore Mechanics and Arctic Engineering*. Hamburg, Germany: ASME.

Lin, X. and Teng, J.G. (2003). Iterative Fourier decomposition of imperfection measurements at non-uniformly distributed sampling points. *Thin-Walled Structures*, 31, 901-924.

Lunchick, M.E. (1959). Yield failure of stiffened cylinders under hydrostatic pressure. (DTMB Report 1291). David Taylor Model Basin.

MacKay, J.R. (2005). Design of Pressure Hulls using Nonlinear Finite Element Analysis – PhD Thesis Proposal. (DRDC Atlantic TN 2005-031). Defence Research and Development Canada – Atlantic.

MacKay, J.R. (2007A). Experimental investigation of the strength of damaged pressure hulls – Phase 1. (DRDC Atlantic TM 2006-304). Defence Research and Development Canada – Atlantic.

MacKay, J.R. (2007B). Experimental investigation of the strength of damaged pressure hulls – Phase 2, Summary of experimental results. (DRDC Atlantic TM 2007-013). Defence Research and Development Canada – Atlantic.

MacKay, J.R., Smith, M.J., and Pegg, N.G. (2006). Design of pressure hulls using nonlinear finite element analysis. (OMAE2006-92591). In *Proceedings of the 25th International Conference on Offshore Mechanics and Arctic Engineering*. Hamburg, Germany: ASME.

Miller, C.D. and Kinra, R.K. (1981). External pressure tests of ring-stiffened fabricated steel cylinders. *Journal of Petroleum Technology*, December, 2528-2538.

von Mises, R. (1929). Stodola Festschrilt, pp. 418. Zurich.

Mitchell, G.C. (1986). Overbend prediction for cold-bent beams. *Computers and Structures*, 24 (2), 198-196.

Moaveni S. (2003). Finite Element Analysis – Theory and Application with ANSYS. 2nd ed. Upper Saddle River, New Jersey: Pearson Education, Inc.

Moradi, B. and Parsons, I.D. (1993). A comparison of techniques for computing the buckling loads of stiffened shells. *Computers and Structures*, 46, 505-514.

Morandi, A.C., Das, P.K. and Faulkner, D. (1996A). Finite element analysis and reliability based design or externally pressurized ring stiffened cylinders. *Transactions of the Royal Institution of Naval Architects*, 138, 171-188.

Morandi, A.C., Faulkner, D. and Das, P.K. (1996B). Frame tripping in ring stiffened externally pressurized cylinders. *Marine Structures*, 9, 585-608.

Morandi, A.C., Das, P.K., and Faulkner, D. (1998). Reliability-based design of externally pressurized vessels. *Journal of Offshore Mechanics and Arctic Engineering*, 120, 149-153.

Pegg, N.G. (1989). Experimental determination of interframe buckling of a ring stiffened cylinder. (DREA TM 89/209). Defence Research Establishment Atlantic.

Pegg, N.G. and Smith, D.R. (1987). PRHDEF – Stress and Stability Analysis of Ring Stiffened Submarine Pressure Hulls. (DREA TM 87/213). Defence Research Establishment Atlantic.

Poularikas, A.D. (1999). Fourier series. In A.D. Poularikas, (Ed.), *The Handbook of Formulas and Tables for Signal Processing*. Boca Raton: CRC Press LLC.

Radha, P. and Rajagopalan, K. (2006A). Ultimate Strength of submarine pressure hulls with failure governed by inelastic buckling. *Thin-walled Structures*, 44, 309-313.

Radha, P. and Rajagopalan, K. (2006B). Reliability analysis of submarine pressure hulls with failure governed by inelastic buckling. (OMAE2006-92032). In *Proceedings of the 25th International Conference on Offshore Mechanics and Arctic Engineering*. Hamburg, Germany: ASME.

Ramm, E. and Stegmüller, H. (1982). The displacement finite element method in nonlinear buckling analysis of shells. In E. Ramm, (Ed.), *Buckling of Shells: Proceedings of a State-of-the-Art Colloqium*, pp. 201-235. New York: Springer.

Reid, J.D. (1998). Admissible modeling errors or modeling simplifications. *Finite Elements in Analysis and Design*, 29, 49-63.

Riks, E. (1979). An incremental approach to the solution of snapping and buckling problems. *International Journal of Solids and Structures*, 15, 529-551.

Ross, C.T.F. (1990). Pressure vessels under external pressure: statics and dynamics. New York: Elsevier Science Publishing Co., Inc.

Ross, C.T.F. (1997). Inelastic general instability of ring-stiffened circular cylinders and cones under uniform external pressure. *Structural Engineering and Mechanics*, 5 (2), 193-207.

Ross, C.T.F. and Johns, T. (1998). Plastic axisymmetric collapse of thin-walled circular cylinders and cones under uniform external pressure. *Thin-Walled Structures*, 30 (1-4), 35-54.

Rotter, J.M. (1998). Shell structures: the new European standard and current research needs. *Thin-Walled Structures*, 31, 3-23.

Salerno, V.L. and Levine, B. (1951). (PIBAL Report No. 189). Polytechnic Institute of Brooklyn.

Salerno, V.L. and Pulos, J.G. (1951). Stress Distribution in a Circular Cylindrical Shell Under Hydrostatic Pressure Supported by Equally Spaced Circular Ring Frames – Part 1 – Theory. (PIBAL Report No. 171-A). Polytechnic Institute of Brooklyn.

Şanal, Z. (2000). Nonlinear analysis of pressure vessels: some examples. *International Journal of Pressure Vessels and Piping*, 77, 705-709.

Sarawit, A.T., Kim, Y., Bakker, M.C.M., and Peköz, T. (2003). The finite element method for thin-walled members – applications. *Thin-Walled Structures*, 41, 191-206.

Schmidt, H. (2000). Stability of steel shell structures: General report. *Journal of Construction Steel Research*, 55, 159-181.

Schneider, W. and Brede, A. (2005). Consistent equivalent geometric imperfections for the numerical buckling strength verification of cylindrical shells under uniform external pressure. *Thin-Walled Structures*, 43, 175-188.

Seleim, S.S. and Roorda, J. (1986). Buckling behaviour of ring-stiffened cylinders; experimental study. *Thin-Walled Structures*, 4, 203-222.

Shi, J. (1996). Computing critical points and secondary paths in nonlinear structural stability analysis by the finite element method. *Computers and Structures*, 58 (1), 203-220.

Skallerud, B., Myklebust, L.I. and Haugen, B. (2001). Nonlinear response of shell structures: effects of plasticity modeling and large rotations. *Thin-Walled Structures*, 39, 463-482.

Slankard, R.C. and Nash, W.A. (1953). *Tests of the elastic stability of a ring-stiffened cylindrical shell, model BR-5 (λ = 1.705), subjected to hydrostatic pressure*. Report 822. David Taylor Model Basin.

Slankard, R.C. (1955). Tests of the elastic stability of a ring-stiffened cylindrical shell, model BR-4 (λ = 1.103), subjected to hydrostatic pressure. (DTMB Report 876). David Taylor Model Basin.

Smith, M.J. and MacKay, J.R. (2004). Overall elasto-plastic collapse of submarine pressure hull compartments. (DRDC Atlantic TM 2004-243). Defence Research and Development Canada – Atlantic.

Smith, M.J. and MacKay, J.R. (2005). Overall elasto-plastic collapse of ring stiffened cylinders with corrosion damage. *Transactions of the Royal Institution of Naval Architects Part 1A – International Journal of Maritime Engineering*.

Sridharan, S. and Alberts, J. (1997). Numerical modeling of buckling of ring-stiffened cylinders. *AIAA Journal*, 35 (1), 187-195.

Teng, G.J. (1996). Buckling of thin shells: recent advancs and trends. *Applied Mechanics Review*, 49 (4), 263-274.

Thoft-Christensen, P. and Baker, M.J. (1982). Structural Reliability Theory and Its Applications. New York: Springer-Verlag.

Timoshenko, S.P. and Gere, J.M. (1961). Theory of Elastic Stability. New York: McGraw-Hill, Inc.

Wilson, L.B. (1956A). The deformation under uniform pressure of a circular cylindrical shell supported by equally spaced circular ring frames, Part I – Asymptotic method. (NCRE Report No. R.337A). Naval Construction Research Establishment.

Wilson, L.B. (1956B). The deformation under uniform pressure of a circular cylindrical shell supported by equally spaced circular ring frames, Part II – Fourier series method. (NCRE Report No. R.337B). Naval Construction Research Establishment.

Wilson, L.B. (1956C). The deformation under uniform pressure of a circular cylindrical shell supported by equally spaced circular ring frames, Part III – General discussion. (NCRE Report No. R.337C). Naval Construction Research Establishment.

Windenburg, D.F. and Trilling, C. (1934). Collapse by Instability of Thin Cylindrical Shells under External Pressure. (TMB Report No. 385). David Taylor Model Basin.

Wullschleger, L. and Meyer-Piening, H.-R. (2002). Buckling of geometrically imperfect cylindrical shells – definition of a buckling load. *International Journal of Non-Linear Mechanics*, 37, 645-657.

Yamamoto, Y., Homma, Y., Oshima, K., Mishiro, Y., Terada, H., Yoshikawa, T., Morihana, H., Yamauchi, Y. and Takenaka, M. (1989). General instability of ring-stiffened cylindrical shells under external pressure. *Marine Structures*, 2, 133-149.

Zhao, Y. and Teng, J.G. (2004). Buckling experiments on steel silo transition junctions II: Finite element modeling. *Journal of Construction Steel Research*, 60, 1803-1823.

This page intentionally left blank.

Annex A NLFEA of Buckling-Critical Shells

Table 14: Nonlinear numerical analyses of buckling-critical shells reported in the literature

Study	Shell Description	Solution Strategy	Elements
Creswell and Dow, 1986	Ring-stiffened steel cylinders under external pressure	NL G+M, static	4-node flat plates
Guggenberger, 1995	Polymer cylinders with dent under external pressure	NL G, static	8- or 9-node shells
Morandi *et al.*, 1996A	Ring-stiffened steel cylinders under external pressure	NL G+M, static (including checks for bifurcation)	4- and 8-node shells
Lennon and Das, 1997	Ring- and stringer-stiffened steel cylinders under axial compression and external pressure	NL G+M, static	8-node shells
Choong and Ramm, 1998	Various shells	NL G, static up to collapse, transient buckling response	8-node shells
Ross and Johns, 1998	Plastic axisymmetric collapse of ring-stiffened steel cylinders and cones under external pressure	NL G+M, static	Axisymmetric shells
Berry *et al.*, 2000	Axially compressed steel cylinders with circumferential weld depressions	NL G+M, static (including checks for bifurcation)	Axisymmetric shells
Bisagni, 2000	Axially compressed composite cylinders	NL G, static and transient	4-node shells
Holst *et al.*, 2000	Axially compressed steel cylinders with residual stresses	NL G, static	4-node shells
Şanal, 2000	Steel cylinders under external pressure	NL G+M	4-node solids (2D)
Arbocz and Starnes Jr, 2002	Axially compressed composite cylinders	NL G+M, static up to collapse, transient buckling response, static in post-buckling	8-node shells
Barlag and Rothert, 2002	Ring-stiffened steel cylinders under external pressure	NL G+M, Static	8-node shells
Wullschleger and Meyer-Piening, 2002	Axially compressed composite cylinders	NL G, static (including checks for bifurcation)	4-node shells
Zhao and Teng, 2004	Steel silo transition junctions	1) NL G+M, static (including checks for bifurcation) 2) NL G+M, static	1) Axisymmetric shells 2) 3- and 4-node shells
Schneider and Brede, 2005	Steel cylinders under external pressure	NL G+M, static	N/A (shells?)
Aghajari *et al.*, 2006	Steel cylinders under external pressure	NL G+M, static	4-node shells
Radha and Rajagopalan, 2006A	Ring-stiffened steel cylinders under external pressure	NL G+M	4-node shells

Annex B Experimental Studies

Table 15: Experimental studies on the collapse of pressure hulls and related structures

Source	Geometry and Loading	Material and Fabrication	Failure Mode
Fairbairn, 1858	Wrought iron and steel cylindrical tubes under external pressure	Fabricated steel, cold bent and riveted, no ring-stiffeners	Lobar collapse
Slankard and Nash, 1953	Ring-stiffened steel cylinder under external pressure	Fabricated steel, cold rolled shell and cut stiffeners, external rectangular section ring-stiffeners	Interframe collapse
Kendrick, 1955	Ring-stiffened steel cylinders (89) under external pressure	Fabricated steel, cold rolled shell and stiffener flanges, cut stiffener webs, internal (74) and external (15) T-section ring-stiffeners	Interframe (63), overall (4) and mixed inteframe-overall (22) collapse
Slankard, 1955	Ring-stiffened steel cylinder under external pressure	Fabricated steel, cold rolled shell and cut stiffeners, external rectangular section ring-stiffeners	Interframe collapse
Lunchick, 1959	Ring-stiffened steel cylinders (7) under external pressure	Fabricated steel, external rectangular section ring-stiffeners	Axisymmetric shell collapse
Boichot and Reynolds, 1965	Ring-stiffened aluminium cylinders (69) under external pressure	Machined aluminium, external rectangular section ring-stiffeners	Overall collapse (47), overall elastic buckling (3), axisymmetric shell collapse (18) and interframe collapse (1)
Dow, 1965	Ring-stiffener aluminium cylinders (10) under external pressure	Aluminium sheet construction, Z-section ring-stiffeners	Interframe buckling followed by overall collapse (10)
Goudie, 1971	Steel torispherical domes	Spun steel domes	Elasto-plastic collapse
Creswell, 1978	Ring-stiffened aluminium cylinders (4) under external pressure	Machined aluminium, external rectangular section ring-stiffeners	Overall elastic buckling
Miller and Kinra, 1981	Ring-stiffened cylinders (20) under external / lateral pressure	Fabricated steel, external (17) and internal (3) rectangular section ring-stiffeners	Overall (6) and interframe (14) elasto-plastic collapse
Pegg, 1989	Ring-stiffened aluminium cylinder (1) under external pressure	Machined aluminium, external rectangular section ring-stiffeners	Interframe elastic buckling
Seleim and Roorda, 1986	Ring-stiffened cylinders (10) under lateral pressure (no axial load)	Machined aluminium, external rectangular section ring-stiffeners	Overall (5) and interframe (5) elastic buckling

Table 15: Experimental studies… continued

Source	Geometry and Loading	Material and Fabrication	Failure Mode
Yamamoto *et al.*, 1989	Ring-stiffened cylinders (6) under external pressure	Machined steel (4) and fabricated steel – cold rolled shell and cut stiffeners (2), external rectangular section ring-stiffeners	Overall elasto-plastic collapse
Bosman *et al.*, 1993	Ring-stiffened cylinders (5) under external pressure	Machined aluminium, external rectangular-section (5), simulated decks (2)	Overall collapse
Frieze, 1994	Ring-stiffened cylinders (2) under external pressure	Welded steel, cold rolled shell and cut external rectangular section ring-stiffeners	Stiffener tripping
Ross, 1997	Ring-stiffened cylinders (3) and cones (3) under external pressure	Machined steel, external rectangular section ring-stiffeners	Overall elasto-plastic collapse
Ross and Johns, 1998	Ring-stiffened cylinders (3) and cones (2) under external pressure	Machined steel, external rectangular section ring-stiffeners	Axisymmetric shell collapse
Blachut, 2002	"Barrelled" steel cylindrical shells (6) under external pressure	Machined mild steel, no ring-stiffeners	Lobar and axisymmetric collapse
Aghajari *et al.*, 2006	Cylindrical shells (4) under external pressure	Fabricated steel, cold rolled and welded, variable shell thickness over length, no ring-stiffeners	Lobar buckling
Liessem *et al.*, 2006	Cylindrical steel tubes (6) under external pressure	Fabricated steel, cold formed and welded, no ring-stiffeners	Lobar collapse
Hübner *et al.*, 2007	Cylindrical steel tubes (6) under external pressure	Welded steel, no ring-stiffeners	Lobar collapse
MacKay, 2007A	Ring-stiffened cylinders (6) under external pressure	Machined aluminium, external T-section (5) and rectangular section (1) ring-stiffeners	Overall (3) and interframe (3) elasto-plastic collapse
MacKay, 2007B	Ring-stiffened cylinders (6) and cylindrical shell (1) under external pressure	Machined aluminium, external (2) and internal (4) T-section ring-stiffeners, no ring-stiffeners (1)	Overall (5) and interframe (1) elasto-plastic collapse, elastic lobar buckling (1)

This page intentionally left blank.

List of Symbols and Acronyms

Symbols

a	mean radius of shell plating
a_f	radius to extreme fibre of frame flange $r-h-(d+h_f)$ for internal frames $r+d+h_f$ for external frames
a_{gc}	radius to neutral axis of combined frame and effective breadth of plate
a_{gf}	radius to centre of gravity of frame $r-h-x_f$ for internal frames $r+x_f$ for external frames
a_1	radius to the toe of the frame
a'	$\dfrac{\left(rL_f-\dfrac{A_f\sigma_{yf}a_f}{P_{fy}a_{gf}}\right)}{L_f h}$
a_n	sine amplitude for mode *n*, for a one-dimensional Fourier series
A	$\dfrac{a^2}{a_f{}^2}A_f$
A_f	cross sectional area of frame
A_{mn}, B_{mn}, C_{mn}, D_{mn}	
b	width of faying flange
b'	$-\left(\sigma_{yp}+a'P_{cr,o}+\left(n^2-1\right)\dfrac{EC_0e_p}{a^2}\right)$
b_0	average measured radius

b_n	cosine amplitude for mode *n*, for a one-dimensional Fourier series
c'	$\sigma_{yp} P_{cr,o}$
C_0	maximum amplitude of applied OOC
C_{0mn}	maximum amplitude of geometric imperfection for axial mode *m* and circumferential mode *n*
d	depth of frame web
e_f	distance from the extreme fibre of the frame flange to the neutral axis of the frame and effective breadth of plating $h + d + h_f - e_p$
e_p	distance from the outside of the shell plating to the neutral axis of the frame and effective breadth of plating $\frac{\left[\frac{h^2}{2} L_e + \left(h + \frac{d}{2}\right) d h_w + \left(h + d + \frac{h_f}{2}\right) f h_f\right]}{h L_e + d h_w + f h_f}$
E	Young's modulus
f	width of frame flange
f_h	Hill's anisotropic yield function
f_m	von Mises' isotropic yield function
f_t	Tresca's isotropic yield function
$\{f\}$	right-hand-side (force) vector
f_1	web slenderness parameter
f_2	flange slenderness parameter
f_3	frame inertia parameter
G	shear modulus

G $$\frac{-2\left[\sinh\frac{\alpha L}{2}\cos\frac{\alpha L}{2}+\cosh\frac{\alpha L}{2}\sin\frac{\alpha L}{2}\right]}{\sinh\alpha L+\sin\alpha L}$$

h thickness of shell plating

h_f thickness of frame flange

h_w thickness of frame web

H $$\frac{-2\left\{\left(1+\sqrt{\frac{3\mu^2}{1-\mu^2}}\right)\sinh\frac{\alpha L}{2}\cos\frac{\alpha L}{2}+\left(1-\sqrt{\frac{3\mu^2}{1-\mu^2}}\right)\cosh\frac{\alpha L}{2}\sin\frac{\alpha L}{2}\right\}}{\sinh\alpha L+\sin\alpha L}$$

I flexural moment of inertia

I_0 ring-stiffener section polar moment of inertia, relative to the toe of the web

I_c moment of inertia of the combined frame and effective breadth of plating

$$\frac{h^3L_e}{12}+\frac{h_wd^3}{12}+\frac{{h_f}^3}{12}+hL_e\left(e_p-\frac{h}{2}\right)^2$$
$$+h_wd\left(e_p-h-\frac{d}{2}\right)^2+h_ff\left(e_f-\frac{h_f}{2}\right)^2$$

I_z moment of inertia of the frame about its symmetric axis

J St. Venant's torsional constant; for a T-section ring-stiffener:

$$\frac{f{h_f}^3+d{h_w}^3}{3}$$

k_{0n} rotational spring constraint at the shell-stiffener intersection

$$\frac{Eh^3}{3\left(1-\mu^2\right)L}\left[1+\left(\frac{nL}{\pi a}\right)^2\right]^2$$

$[K]$ stiffness matrix

$[K_0]$ linear-elastic stiffness matrix

$[K_L]$ displacement stiffness matrix

$[K_t]$	tangent stiffness matrix
$[K_\sigma]$	stress stiffness matrix
L	unsupported length of shell between stiffeners $L_f - h_w$
L_B	length between rigid bulkhead supports
L_e	effective length of shell between stiffeners
L_f	stiffener spacing
m	axial wave number
n	circumferential wave number
N	$\frac{\cosh \alpha L - \cos \alpha L}{\sinh \alpha L + \sin \alpha L}$
N	also variously, the number of ring-stiffeners in a pressure hull compartment, OOC measurements about the cylinder circumference, and possible eigenvalues
p_f	probability of failure
P	external applied pressure
P_B	Bresse overall buckling pressure
P_{c2}	"boiler" pressure; external pressure at which the circumferential stress of a cylindrical shell of infinite length equals the yield stress
P_{c3}	external pressure at which the circumferential stress at the outside of the plating midway between frames, σ_3, equals the yield stress
P_{c4}	semi-empirical collapse pressure for the design of ring-stiffened cylinders (not currently in use)
P_{c5}	external pressure at which the mean circumferential stress in the plating midway between frames, σ_5, equals the yield stress
P_{c6}	external pressure at which the mean stress in the plating reaches the Von Mises yield criterion

P_{c7}	external pressure at which the longitudinal stress on the inside of the plating, adjacent to the frame, σ_7, equals the yield stress
P_{ci}	interframe collapse pressure for design
P_{co}	overall collapse pressure for design
P_{cr}	elastic buckling pressure for a ring-stiffened cylinder, as derived by Kendrick (1953A)
$P_{cr,exp}$	experimentally-derived collapse load
$P_{cr,nl}$	nonlinear numerically-derived collapse load
$P_{cr,o}$	Critical overall elastic buckling pressure
P_d	design pressure
P_{fy}	external pressure causing yield in the frame flange of an ideal circular ring-stiffened cylinder
P_{m1}	von Mises interframe elastic buckling pressure; iterated Kendrick solution
P_N	Bryant overall buckling pressure
P_P	external pressure causing overall collapse of a ring-stiffened cylinder, precipitated by shell yielding
$P_{y(n)}$	external pressure causing overall collapse of a ring-stiffened cylinder, precipitated by frame yielding
q_{cr}	critical elastic buckling load of a pressure loaded ring (units are force/length)
r	outer radius of shell plating
R	$\frac{\sinh \alpha L - \sin \alpha L}{\sinh \alpha L + \sin \alpha L}$
R	variously the reliability of a structure or the resistance of a structure
R_{sf}	residual stress multiplication factor
$R(\theta)$	measured radius as circumferential angle θ

S	loads on a structure
u	axial displacement (cylindrical coordinates)
$\{u\}$	displacement vector
v	tangential displacement (cylindrical coordinates)
w	radial displacement (cylindrical coordinates)
w_0	initial geometric imperfection
x	axial or longitudinal cylindrical coordinate
x_f	distance from adjacent edge of shell plating to centre of gravity of frame
	$\frac{d^2 h_w + f h_f (2d + h_f)}{2(d h_w + f h_f)}$
X	$\frac{Eh}{2a^2(1-\mu^2)}\left\{\left(n^2-1\right)+\mu\left(\frac{\pi a}{L}\right)^2\right\}e_{ps}$
X_m	modeling uncertainty factor
y	tangential cylindrical coordinate
z	radial cylindrical coordinate
Z	performance function in a reliability analysis
α	$\sqrt[4]{\frac{3(1-\mu^2)}{a^2 h^2}}$
β	$\frac{2hN}{\alpha(A+hh_w)}$
β	reliability index
δ_p	mid-bay shell distortion due to welding
ε_y	yield strain

γ $\dfrac{A\left(1-\dfrac{\mu}{2}\right)}{(A+hh_w)(1+\beta)}$

η factor defining the heat affected zone due to welding

Γ warping constant; for T-section ring-stiffeners:
$\Gamma_1+\Gamma_2$

Γ_1 longitudinal warping constant; for T-section ring-stiffeners:
$I_z\left(d+h_f/2\right)^2$

Γ_2 transverse warping constant; for T-section ring-stiffeners:
$\left(f^3h_f{}^3/4+d^3h_w{}^3\right)/36$

μ Poison's ratio

$\{\phi\}$ eigenvector

θ circumferential angle

σ_1, σ_2, σ_3 principal stresses

σ_f Direct stress in the stiffener flange

σ_{fb} stress in the stiffener flange due to bending

σ_{fT} total stress in the stiffener flange due to direct and bending stresses

σ_{r1},σ_{r2} residual stresses due to cold bending of a plate

σ_{rc}, σ_{rc1}, σ_{rc2} compressive residual stresses due to welding

σ_{rf} tensile residual stress in flange due to welding

σ_{sb} springback stress occurring during cold bending of a plate

σ_t tripping stress for a ring-stiffener

σ_y yield stressl

σ_{yf} yield stress of ring-stiffener (frame) material

σ_{yp}	yield stress of shell material
σ_3	circumferential stress at the outside of the plating midway between frames of a ring-stiffened cylinder
σ_6	von Mises equivalent stress
σ_5	mean circumferential stress in the plating midway between frames of a ring-stiffened cylinder
σ_7	longitudinal stress on the inside of the plating, adjacent to the frame of a ring-stiffened cylinder
λ	eigenvalue
ξ	ratio of ring-stiffener tripping stress to tripping pressure: $\frac{\sigma_t}{P_t} = \frac{\sigma_{yf} a_f}{P_{fy} a_{gf}}$

Acronyms

BS5500	British Standard Specification for Unfired Fusion Welded Pressure Vessels
COV	coefficient of variation
DND	Department of National Defence
DRDC	Defence Research and Development Canada
ECCS	European Convention for Constructional Steelwork
FE	finite element
FEA	finite element analysis
FS	factor of safety
kN	kiloNewton
mm	millimetre
MPa	megaPascal
NLFEA	nonlinear finite element analysis

OOC	out-of-circularity
PSF	partial safety factor
SSP74	Sea Systems Publication No. 74, Design of Submarine Structures

Distribution list

Document No.: DRDC Atlantic TM 2007-188

LIST PART 1 – Internal Distribution by Centre:

4 Author (2 paper copies, 2 CDs)
2 DRDC Atlantic Library File Copies (1 paper copy, 1 CD)
3 DRDC Atlantic Library (spares)

9 TOTAL LIST PART I

LIST PART II: External Distribution within Canada by DRDKIM

1 NDHQ/DRDKIM 3
2 NDHQ/DMSS 2
2 NDHQ/DMEPM(SM) 4-2

5 TOTAL LIST PART II

LIST PART III: External Distribution outside Canada by DRDKIM

1 Prof. Fred van Keulen
Structural Optimization and Computational Mechanics Group
Department of Precision and Microsystems Engineering
Delft University of Technology
Office 8b-3-8
Mekelweg 2
2628 CD Delft
THE NETHERLANDS

1 Mr. Theo Bosman
Centre for Mechanical and Maritime Structures (CMC)
Structures and Safety
Business Unit of TNO Built Environment and Geosciences
P.O. Box 49
2600 AA Delft
THE NETHELANDS

2 TOTAL LIST PART III

16 TOTAL COPIES (3 paper copies, 13 CDs)

This page intentionally left blank.

DOCUMENT CONTROL DATA

(Security classification of title, body of abstract and indexing annotation must be entered when the overall document is classified)

1. ORIGINATOR (The name and address of the organization preparing the document. Organizations for whom the document was prepared, e.g. Centre sponsoring a contractor's report, or tasking agency, are entered in section 8.)

Defence R&D Canada – Atlantic
9 Grove Street
P.O. Box 1012
Dartmouth, Nova Scotia B2Y 3Z7

2. SECURITY CLASSIFICATION (Overall security classification of the document including special warning terms if applicable.)

3. TITLE (The complete document title as indicated on the title page. Its classification should be indicated by the appropriate abbreviation (S, C, R or U) in parentheses after the title.)

Structural Analysis and Design of Pressure Hulls: the State of the Art and Future Trends:

4. AUTHORS (last name, followed by initials – ranks, titles, etc. not to be used)

MacKay, J.R.

5. DATE OF PUBLICATION (Month and year of publication of document.)	6a. NO. OF PAGES (Total containing information, including Annexes, Appendices, etc.)	6b. NO. OF REFS (Total cited in document.)
October 2007	98	114

7. DESCRIPTIVE NOTES (The category of the document, e.g. technical report, technical note or memorandum. If appropriate, enter the type of report, e.g. interim, progress, summary, annual or final. Give the inclusive dates when a specific reporting period is covered.)

Technical Memorandum

8. SPONSORING ACTIVITY (The name of the department project office or laboratory sponsoring the research and development – include address.)

Defence R&D Canada – Atlantic
9 Grove Street
P.O. Box 1012
Dartmouth, Nova Scotia B2Y 3Z7

9a. PROJECT OR GRANT NO. (If appropriate, the applicable research and development project or grant number under which the document was written. Please specify whether project or grant.)	9b. CONTRACT NO. (If appropriate, the applicable number under which the document was written.)

10a. ORIGINATOR'S DOCUMENT NUMBER (The official document number by which the document is identified by the originating activity. This number must be unique to this document.)	10b. OTHER DOCUMENT NO(s). (Any other numbers which may be assigned this document either by the originator or by the sponsor.)
DRDC Atlantic TM 2007-188	

11. DOCUMENT AVAILABILITY (Any limitations on further dissemination of the document, other than those imposed by security classification.)

(X) Unlimited distribution
( ) Defence departments and defence contractors; further distribution only as approved
( ) Defence departments and Canadian defence contractors; further distribution only as approved
( ) Government departments and agencies; further distribution only as approved
( ) Defence departments; further distribution only as approved
( ) Other (please specify):

12. DOCUMENT ANNOUNCEMENT (Any limitation to the bibliographic announcement of this document. This will normally correspond to the Document Availability (11). However, where further distribution (beyond the audience specified in (11) is possible, a wider announcement audience may be selected.))

13. ABSTRACT (A brief and factual summary of the document. It may also appear elsewhere in the body of the document itself. It is highly desirable that the abstract of classified documents be unclassified. Each paragraph of the abstract shall begin with an indication of the security classification of the information in the paragraph (unless the document itself is unclassified) represented as (S), (C), (R), or (U). It is not necessary to include here abstracts in both official languages unless the text is bilingual.)

Pressure hulls are the main load bearing structures of naval submarines, commercial and research submersibles, and autonomous underwater vehicles (AUVs). The many similarities between pressure hull, offshore, aerospace and some civil engineering structures mean that advances in one group are often applicable to the others, and thus this document is sometimes concerned with the entire collection of thin-walled curved structures designed for instability, referred to hereafter as "buckling-critical shells." The state-of-the-art of pressure hull structural analysis and design is established in this document by: 1) explaining the nature of structural strength, and associated weaknesses, in pressure hulls; 2) summarizing traditional and contemporary structural analysis and design methods for pressure hulls; 3) identifying trends with respect to numerical modeling of buckling-critical shell structures; and 4) reviewing novel design procedures for buckling-critical shell structures. It is suggested that the layered conservatism of the traditional design approach could be improved by the use of nonlinear numerical methods for strength predictions, and a way forward is suggested that would allow pressure hull design procedures to incorporate these methods.

Error! Reference source **not found.**

14. KEYWORDS, DESCRIPTORS or IDENTIFIERS (Technically meaningful terms or short phrases that characterize a document and could be helpful in cataloguing the document. They should be selected so that no security classification is required. Identifiers, such as equipment model designation, trade name, military project code name, geographic location may also be included. If possible keywords should be selected from a published thesaurus, e.g. Thesaurus of Engineering and Scientific Terms (TEST) and that thesaurus identified. If it is not possible to select indexing terms which are Unclassified, the classification of each should be indicated as with the title.)

submarine, pressure hull, buckling, collapse, ring-stiffened cylinder, finite element analysis

This page intentionally left blank.

Defence R&D Canada

Canada's leader in defence
and National Security
Science and Technology

R & D pour la défense Canada

Chef de file au Canada en matière
de science et de technologie pour
la défense et la sécurité nationale

www.drdc-rddc.gc.ca